Cavity QED with a Large Mode Volume High Finesse Cavity

An Experimental Challenge

Dissertation
zur Erlangung des Doktorgrades
des Fachbereichs Physik
der Universität Hamburg

vorgelegt von
Leif Malik Lindholdt
aus Nuuk (Dänemark)

Hamburg 2009

Gutachter der Dissertation	: Prof. Dr. A. Hemmerich : Prof. Dr. W. Neuhauser
Gutachter der Disputation	: Prof. Dr. A. Hemmerich : Prof. Dr. K. Sengstock
Vorsitzender des Prüfungsausschusses	: Prof. Dr. W. Hansen
Vorsitzender des Promotionsausschusses	: Prof. Dr. R. Klanner

Summary

This thesis deals with the interaction between a cold quantum gas and the photons of a high finesse cavity mode. The regime of strong coupling was first explored by measuring the normal mode splitting of a ring cavity mode. In the last decade many interesting scenarios, like cavity Doppler cooling, cavity sideband cooling and self organization of atoms were predicted theoretically. Demonstrating these effects with a large number of atoms at extreme low temperatures require a cavity with a very high finesse and a large mode volume.

Thus an experimental apparatus was built that allows overlapping a BEC of a few 10^5 rubidium atoms with a cavity mode with a large mode volume. To explore the regime of strong coupling a moderate detuning from the atomic resonance and a cavity with a finesse of more than 400000 was chosen. The cavity has an adjustable length and can be adjusted to be nearly spherical. With a cavity to free space scattering ratio up to 20 cavity Doppler cooling, cavity sideband cooling and self organization of atoms should be accessible. The relevant quantities for these scenarios are calculated and the feasibility of a experimental realisation is discussed.

Zusammenfassung

Diese Arbeit behandelt die Wechselwirkung zwischen einem kalten Quantengas und den Photonen einer Mode eines Hochfinesse-Resonators. Das Regime der starken Kopplung wurde zunaächst anhand der Modenaufspaltung in einem Ringresonator untersucht. Im vergangenen Jahrzehnt wurden viele interessante Szenarien, wie Resonator-Dopplerkühlung, Resonator-Seitenbandkühlung und Selbstorganisation von Atomen theoretisch vorhergesagt. Um diese Effekte mit einer grossen Anzahl von Atomen bei extrem niedrigen Temperaturen experimentell zu demonstrieren, braucht man einen Resonator mit einer sehr grossen Finesse und einem grossen Modenvolumen.

Daher wurde eine Apparatur aufgebaut, die es erlaubt ein BEC, das aus einigen 10^5 Atomen besteht, mit einer Resonatormode mit grossem Modenvolumen zu überlagern. Um in das Regime der starken Kopplung zu gelangen, wurde eine moderate Verstimmung von der Atomresonanz und ein Resonator mit einer Finesse von mehr als 400000 verwendet. Der Resonator ist längenverstellbar und kann so eingestellt werden, dass er fast sphärisch ist. Mit einem Verhältnis aus Streuung in den freien Raum zu Streuung in die Resonatormode von 20, sollte es möglich sein Resonator-Dopplerkühlung, Resonator-Seitenbandkühlung und Selbstorganisation zu erreichen. Die entscheidenden physikalischen Grössen für diese Szenarien werden berechnet und die experimentelle Realsierbarkeit wird diskutiert.

1 Introduction

Optics is the study of properties of light and its interaction with matter. Among the many research fields in optics this thesis focuses on the study of a single radiation mode interacting with an atomic sample. A resonator can be used to enhance the scattering probability of an atom at certain frequencies and suppress it at other frequencies. If this frequency selection is sufficiently good, an atom inside a resonator only interacts with a single radiation mode.

The development of the single atom maser (micromaser) in the 1980s allowed a detailed study of the interaction between a single highly excited atom and a single radiation mode in the microwave regime [1,2]. The study of single atoms interacting with a single resonant radiation mode has expanded to the optical domain, and of particular interest for the topics discussed in this thesis can be mentioned cavity cooling of a single atom [3].

A different regime to explore is the interaction between a resonator mode and a dilute atomic gas. The atomic samples created in a magnetic optical trap have such a high density that many atoms overlap well with a resonator mode. An early experimental observation was made in 1995 with an atomic sample from a magnetic optical trap overlapped with a resonator mode [4]. Due to the relative low finesse (~100) the radiation mode had to be resonant with an atomic transition to observe an interaction between the radiation mode and the atomic sample.

In the end of the 1990s it became technically possible to create mirrors with only a few ppm losses per reflection. Thus it became possible to reach the strongly coupled regime with a resonator mode far detuned from an atomic resonance (the dispersive regime) and an atomic sample of a few million atoms. In the strongly coupled regime the scattering of photons by atoms into a resonator mode dominates over all other scattering processes. The dynamics between a cold atomic sample extracted from a magnetic optical trap and a far detuned resonator mode was first investigated with ring-cavities and interesting phenomena as collective atom recoil lasing (CARL) [5], optical bistability [] and the normal mode splitting of a resonator mode in the dispersive regime [65] have been observed. The measurement of the normal mode splitting is discussed in this thesis.

In the last few years efforts have been made to study the interaction between a Bose-Einstein condensate and a resonator mode [6,7,8]. In a Bose-Einstein condensate all atoms are in the ground state and thus all the atoms have the same wavefunction. This is analogous to a laser beam where all the photons have the same state, and an atomic beam extracted from a Bose-Einstein is referred to as an atom laser. The interaction of a Bose-Einstein condensate and a resonator mode can be used for non-demolition measurement on the Bose-Einstein condensate [92], or to cool excitations of a Bose-Einstein condensate.

The experimental apparatus

To explore the interaction between a Bose-Einstein condensate and a resonator mode, an experimental apparatus was built as part of this thesis, and this experimental apparatus allows a Bose-Einstein condensate to be overlapped with a resonator mode of a high finesse cavity.

What sets the cavity presented in this thesis apart from other experiments with high-finesse cavities and a Bose-Einstein condensate is a small linewidth of a few kHz. The small linewidth makes the resonator ideally suited for cavity cooling near the recoil limit.

Cavity cooling

A cooling scheme using a resonator mode is known as cavity cooling. The principle in cavity cooling is the same as the one for laser cooling on an atomic resonance, the atom absorbs a photon with less energy than the one it on average emits. For far detuned light, the number of spontaneous emissions by the atoms can be small, and thus the probability for the atom to change its internal state during the time period where the atom is cooled by the light can also be made small. The fact that the internal state of the atom can remain unchanged in the cooling process is a potential major advance of cavity cooling over laser cooling on an atomic transition, and in principle every particle that is polarizable can be cooled with cavity cooling. Another advantage of not having resonant photons in the cooling process is the fact that the maximum density is not limited by an internal light pressure of resonant photons as it is the case in a magnetic optical trap.

In laser cooling the steady state temperature depends on the linewidth of the cooling transition and the linewidths of the atomic transitions, typically used in laser cooling, are a few MHz and this corresponds to a temperature of 100 μK. The linewidth of a resonator mode can be made arbitrarily small in theory and for a large open cavity with a length of a few centimetres a linewidth of a few kHz is technically achievable. With a steady state temperature near the recoil limit it would be possible to cool an atomic sample to a Bose-Einstein condensate without the loss of atoms as in evaporative cooling.

The advantages of using a cavity resonance instead of an atomic resonance for laser cooling are: in principle every polarizable particle can be cooled, practical no density limitation and the possibility to cool an atomic sample to the recoil temperature without any loss of atoms.

Two different scenarios for cavity cooling are considered in this thesis, Doppler cooling and sideband cooling. Doppler cooling uses free atoms, and it is similar to Doppler cooling on an atomic resonance. Cavity sideband cooling is for bound atoms in a harmonic potential.

Self-organization of an atomic sample

In [51] an organization process (self-organization) is discussed in which an initial even atomic distribution is changed to a Bragg grating structure with the periodicity of the wavelength of an illuminating laser beam. In this type of distribution all photons emitted by the atoms will constructively interfere with each other, and this will significantly increase the scattering rate into the cavity mode. As a scattering event into the cavity mode typically is a cooling process, the ordering of atoms into a distribution with periodicity of one wavelength promises to be a method which could significantly improve cavity cooling.

In [53] experimental evidence of such a process has been observed. When the atom/cavity interaction is in the strongly coupled regime the illuminating light and light field in the cavity mode are predicted to destructively interfere with similar amplitudes [55]. In this case the fluorescence of atoms is strongly suppressed. In the limit of weak coupling the self-organization process will strongly enhance scattering into the cavity mode and therefore significantly increase the cooling rate. In the strong coupled regime it is be possible to hold atoms at very low intensity. Due to the low scattering rate in this configuration, the atoms can be held at very low temperatures.

Measurement of the normal mode splitting with a far detuned probe

The results of the measurements of the normal mode splitting in the strongly coupled regime with a far detuned probe beam are presented in this thesis [94]. The experimental apparatus used for this measurement is the previous cavity experiment in the group [65,71]. The experimental apparatus consisted of a ring cavity where a cold atomic sample could be loaded into the modes of a ring cavity from a MOT. With this experimental apparatus optical bistability was observed [9], however, it was not possible to observe cavity cooling with this experimental set-up. The primary reason for this is believed to be that the scattering rate into the cavity mode was comparable to the scattering rate into free space. Thus, one of the criteria for the design of the experimental apparatus presented in this thesis was to have a high ratio of the scattering rate into the cavity modes compared to the scattering rate into free space.

Collective side band cooling

An interesting variation of the cavity cooling scenario is the possibility to use a second cavity mode instead of a detuned laser beam to a cavity resonance to create a dissipative process. In [61] the possibility to use the normal mode splitting for a cooling scheme is discussed (collective sideband cooling). The normal mode splitting has previously been measured with a near-resonant probe beam [62,63], however, one of the major advantages of cavity cooling is the possibility to use far detuned light. Thus the measurement of the normal mode splitting with a far detuned probe beam gives important insight for the possibility to implement a cooling cavity scheme based on the normal mode splitting.

Structure of the thesis

Chapter 2 consists of an introduction to the theoretical aspects of creating a BEC from a dilute vapour gas at room temperature. The subjects discussed are: the properties of Rb_{87}, a brief introduction to optical molasse and magnetic optical traps, magnetic traps with emphasis on aspects relevant for evaporative cooling, the parameters relevant for optimising evaporative cooling, the atomic distribution in a harmonic trap, and how a thermal gas and a BEC can be distinguished in a free expansion and in the end of the chapter the formulas to calculate the density of an atomic sample from an absorption image are presented.

Chapter 3 consists of an introduction to the theory of resonators, and it serves to understand the next chapter about cavity/atom interaction. The subjects are: the electrical field of a cavity mode, design criteria for the cavity mirrors for high in-coupling, power enhancement of an in-coupled beam and the enhancement of the scattering of an atom into a cavity mode.

In chapter 4 the interaction between atoms and a cavity mode is discussed. A theoretical discussion of the three scenarios with a detuned laser beam to a cavity mode is given. The three scenarios are: self-organization, cavity Doppler cooling and cavity sideband cooling. The subjects are: the threshold power for the self-organization process is estimated and the cooling and heating rates for cavity cooling of bound atoms (sideband cooling) and free atoms (cavity Doppler cooling) with the cavity presented in this thesis are estimated. Instead of using a detuned laser beam to a cavity mode to create a dissipative process, two modes of the cavity can be used. Two possibilities are considered: a zero order Gaussian mode and a higher Gaussian mode of the cavity, and the normal mode splitting in the strongly coupled regime. The results of the measurement of the normal mode splitting with a far detuned probe beam are also discussed.

In chapter 5 the experimental procedures and methods used in the experiment are discussed. The subjects are: Pound-Drever-Hall technique for stabilization on atomic and cavity resonances, the atomic source for cold Rb_{87}, the second MOT for recapturing the atoms in the experimental chamber, the transfer from the second MOT into a magnetic trap and transport to the magnetic trap used for evaporative cooling (the QUIC trap), the two imaging system for respectively imaging the atoms in second MOT and atomic sample in the QUIC trap and a stabilization system for having a laser beam detuned from a cavity resonance with a fixed detuning (the AOM lock).

In chapter 6 the steps in the creation of a BEC are characterized: The compressed MOT phase, the optical molasses, the transfer into the magnetic trap from the optical molasse, the transport to the QUIC trap, the evaporative cooling to the condensation temperature of the BEC and the identification of a BEC by the free expansion of the BEC and the bimodal density distribution.

In chapter 7 future perspectives of the experiment are discussed. The feasibility for realizing the three theoretically scenarios presented in chapter 4 with the experimental apparatus is discussed.

2 Theoretical basis

This chapter gives an overview of the theoretically concepts, which are relevant for cooling a thermal dilute gas to a Bose-Einstein condensate. Bose-Einstein condensation can be understood as a "pure" quantum mechanical statistical phenomenon as it can happen even in the absence of any interaction between atoms in an atomic gas.

An atom obeys either Bose-Einstein statistics or Fermi-Dirac statistics. A Bose gas is understood as a gas, which consists of one element from the periodic table that obeys Bose-Einstein statistics. For a Bose gas at a certain temperature, the population in the ground state changes dramatically. This is known as the temperature of Bose-Einstein condensation. Below the condensation temperature, the fraction of atoms in the ground state is much larger than the population in any other state.

The width of the probability distribution of an atom is described by the de Broglie wavelength (λ_{dB}). At the condensation temperature the average distance between atoms become comparable to the de Broglie wavelengths of the atoms in the gas [10]. The assumption that it is possible to distinguish between two atoms of the same element is no longer valid when the probability distribution of the atoms overlap. In the classical limit, the de Broglie wavelength is much smaller than the average distance between the atoms in the gas, and in this limit the atoms in the gas can be described as distinguishable billiard balls. The fact that the quantum mechanical principle of indistinguishability of identical atoms becomes important for the atomic distribution of a gas at a certain temperature is basis for the quantum mechanical phenomenon known as Bose-Einstein condensation.

Bose-Einstein was first suggested by Einstein in 1925 [11] and it was first experimentally demonstrated in 1995 [12,13]. The experimental method used in these experiments to cool a thermal dilute gas to a Bose-Einstein condensate can be summarized as follows: firstly the atoms are cooled in the magnetic optical trap (MOT) and then, secondly the atoms are transferred into a magnetic trap, where the atoms are cooled by evaporative cooling to Bose-Einstein condensation. Review papers describing this process can be found in [10,14].

In chapter 2.1 atomic properties for Rb_{87} relevant for laser cooling and evaporative cooling are described. Chapter 2.2 gives an introduction to magnetic optical trapping, and in chapter 2.3 magnetic trapping of neutral atoms is discussed. In chapter 2.4 an overview of evaporative cooling is given, and in chapter 2.5 the distribution of the atomic sample in a harmonic trap is discussed. Lastly, in chapter 2.6 the equations to calculate the atomic density from an absorption image are given.

2.1 Atomic properties of Rb87

It is necessary to consider several factors when choosing an element to create a BEC with a method that first captures the atoms in a MOT, and then transfers the atoms into a magnetic trap for evaporative cooling to the BEC limit.

The operation of a MOT is much simpler for an atom, which has a cycling transition than one without such a transition. A cycling transition is understood as a transition, in which an atom continuously can cycle between one excited state and one ground state without having the possibility to decay or be excited to a third state. While no atom has a transition fulfilling exactly the conditions for being a cycling transition, the alkali metals all have transitions that can be approximated as such. Another factor to consider is the availability of laser light at the frequencies of the relevant transitions.

The efficiency of evaporative cooling for an atom depends on the ratio between elastic and inelastic collisions of the atom. In elastic collisions the internal states of the atoms involved are not changed, while that is the case of inelastic collisions. Elastic collisions redistribute the kinetic energy of the atoms.

The cooling and the repump transitions of Rb_{87}

A compendium of data of Rb_{87} can be found in [98]. The level scheme for Rb_{87} can be seen in Figure 1. The transition from the ground state $\left|5S_{1/2}, F = 2\right\rangle$ to the excited state $\left|5P_{3/2}, F = 3\right\rangle$ can be approximated as a cycling transition, and it will be referred to as the cooling transition. The frequency difference between the cooling transition and the transition from $\left|5S_{1/2}, F = 2\right\rangle$ to $\left|5P_{3/2}, F = 2\right\rangle$ is 267 MHz. If the frequency of the illuminating light is resonant with the cooling transition, then the ratio of the probability for a Rb_{87} to be excited to the state $\left|5P_{3/2}, F = 3\right\rangle$ compared to the probability to be excited to the state $\left|5P_{3/2}, F = 2\right\rangle$ is 8000, if the saturation broadening of the atomic transitions is not considered. In the state $\left|5P_{3/2}, F = 2\right\rangle$ the atom can both decay to the state $\left|5S_{1/2}, F = 2\right\rangle$ with the probability 5/8 and it can decay to the state $\left|5S_{1/2}, F = 1\right\rangle$ with the probability 3/8. In the state $\left|5S_{1/2}, F = 1\right\rangle$ an atom will be far off resonant compared to the cooling transition (6.8 GHz) and in order for the atom to be cooled on the cooling transition again, it must be pumped back to the state $\left|5S_{1/2}, F = 2\right\rangle$. A laser resonant on the transition from $\left|5S_{1/2}, F = 1\right\rangle$ to $\left|5P_{3/2}, F = 2\right\rangle$ can pump the atoms back to the state $\left|5S_{1/2}, F = 2\right\rangle$. The fact that only one extra single laser beam is needed to pump the atoms back to the ground state of the cooling transition is an advantage shared by all the Alkali metals.

The wavelength of the D2 line at 780 nm is easily generated by commercially available diode lasers. The vapour pressure of Rb at room temperature is high (melting point 39.3 °C) [98]. Due to this a Rb vapour cell at room temperature of a few cm length can generate a good absorption signal.

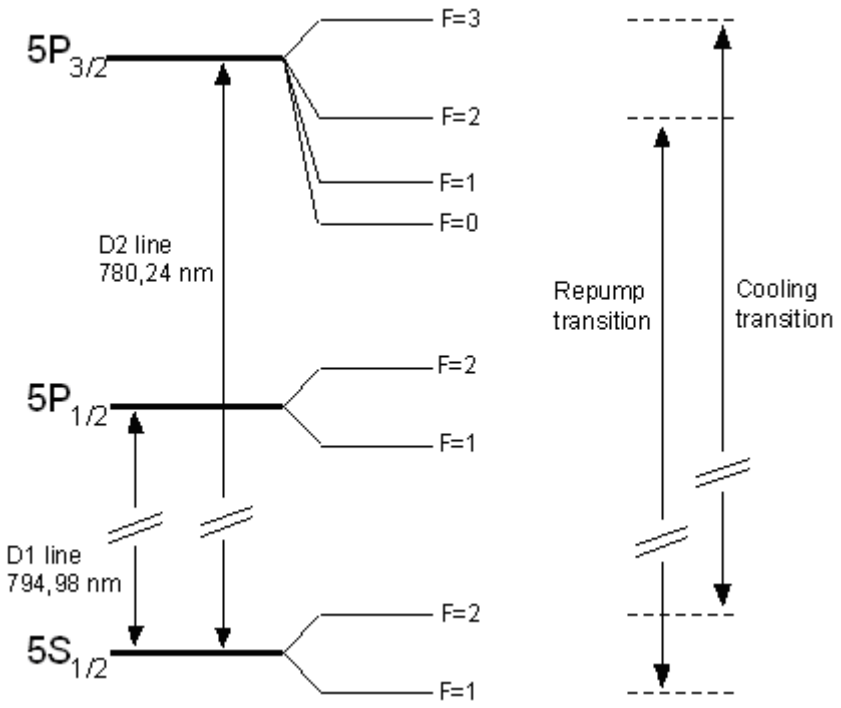

Figure 1: The hyperfine structure of Rb_{87}.

Losses in a magnetic trap due to the magnetic dipole-dipole interaction

Two atoms both in the state $|F, m = F\rangle$, can decay to states with a lower m number through the magnetic dipole-dipole interaction [15]. For the standard quantification axis of the magnetic field, the states with positive m number can only be trapped magnetically at the minimum of the magnetic field (see 2.3), and therefore the magnetic dipole-dipole interaction gives a loss rate of atoms from an atomic sample confined in a magnetic trap.

For Rb and heavier Alkali metals the spin-orbit interaction has to be considered and this gives rise to a second order interaction similar to those of the magnetic dipole-dipole interaction. For Rb, the spin-orbit interaction has the opposite sign of the magnetic dipole-dipole interaction, but a smaller amplitude [15, 16]. For caesium the spin-orbit interaction has the same sign as for Rb, however it has an amplitude that is much larger than the magnetic dipole–dipole interaction. Due to the high two-body inelastic scattering rate of Caesium, it has not been possible to evaporatively cool it in a magnetic trap to a BEC.

Choice of isotope of Rb

Rb has two naturally occurring isotopes: Rb_{85} and Rb_{87}. The scattering length (a) describes low energy scattering. For positive scattering lengths interaction is repulsive, and for negative scattering lengths the interaction is attractive. Rb_{87} has a positive scattering length, while the scattering length of Rb_{85} is negative. If the scattering length is negative, there can only be a certain number of atoms in a BEC before it will collapse due to attractive interaction [17].

3-body recombination

For the formation of a molecule at least three atoms have to be involved in the scattering process as one atom must carry the extra energy away. The 3-body recombination rate for Rb_{87} is in [18] calculated to be a factor 50 smaller than the ones for Li_7 and Na_{23}. The atoms in a molecule are not trapped in the magnetic trap, and thus the 3-body recombination leads to loss at high densities.

Rb_{87} was chosen as the element to condensate to a BEC due to its simple level structure, positive scattering length, a low two-body inelastic scattering rate and a low 3-body recombination rate.

2.2 Magnetic optical trap

The magnetic optical trap (MOT) is a highly effective method of cooling and trapping an atomic sample. In a MOT it is possible to capture up to 10^{10} atoms at temperatures of a few tens of μK, and with densities up to 10^{12} atoms/cm^3 from a room temperature background gas. In this chapter the key concepts are introduced. A good introduction to laser cooling and MOT theory can be found in [50].

Controlling the motion of an atom with light forces

The absorption process of a photon from a laser beam gives the atom a momentum transfer in the propagation direction of the laser beam. Spontaneous emissions are in a random direction, and the net momentum transfer averaged over many spontaneous emissions is zero. Hence, the absorptions from a laser beam and spontaneous emissions give a directional momentum transfer over time. This force on an atom can be used to control the motion of an atom.

Magnetic optical trap (MOT)

A three dimensional MOT consists of three pairs of counter propagating laser beams. The 3 pairs of laser beams are red-detuned to an atomic resonance, and their propagation directions are perpendicular to each other. An atom moving in a direction opposite to the propagation direction of one of the six laser beams will be more resonant with that laser beam than the others. This is the well known Doppler Effect. As the atom is more likely to absorb photons from the laser beams propagating in the opposite direction of its velocity, the net momentum transfer due to absorptions from the laser beams will be in the opposite direction of the velocity of the atom. In other words the absorption processes act as a friction force on the atom.

By adding a magnetic field gradient the energy of Zeeman levels become position dependent, and this position dependency combined with a particular polarization of the 6 laser beams can be used to create a confining potential for an atom. The resonant photons emitted by the atoms captured in the MOT creates an internal pressure, and this limits the maximum obtainable density to ~10^{12} atoms/cm^3 [19,20]. An atomic sample held in a MOT with a density limited by the internal light pressure is said to be in the density limited regime.

The Doppler temperature

The illuminating light also heats the atoms through random recoils, and the steady state temperature expected is the Doppler temperature. The temperature corresponding to one recoil created by a spontaneous emission of a photon is the minimum obtainable temperature, and it is known as the recoil temperature.

Sub-Doppler cooling

It is possible to cool to substantially lower temperatures than the ones indicated by the Doppler temperature. This is known as sub-Doppler cooling, and the type of sub-Doppler cooling used in this experiment is known as σ^+, σ^- polarization gradient cooling [21]. This type of cooling relies on the different transition probabilities between the different Zeeman levels and to enable this type of cooling the Zeeman levels have to be degenerate.

Therefore, it is often advantageous to have a short period of σ^+, σ^- polarization gradient cooling after a sufficient number of atoms have been captured in the MOT to increase the phase space density. The magnetic field is quickly switched off and the laser beams are further detuned. The practical implementation of this step is described in chapter 5.3.

2.3 Magnetic traps

The phase space density of an atomic sample in a MOT is typically a factor 10^6 lower than the phase space density needed to reach the transition to BEC. For the last step the atomic sample can be transferred to a magnetic trap or dipole trap for evaporative cooling. The advantage of a magnetic trap compared to a dipole trap is that in a magnetic trap forced evaporation can be used without changing the confinement for the atoms that remain in the trap. The disadvantage of capturing the atoms in a magnetic trap compared to a dipole trap is the losses due to inelastic collisions and 3-body recombination, which do not occur in a dipole trap.

Magnetic trapping of neutral atoms

The potential energy of a neutral atom in a magnetic field is given by:

$$U(\vec{r}) = -\vec{\mu} \cdot \vec{B}(\vec{r}) \tag{1}$$

where $\vec{\mu}$ is the magnetic moment of the atom and $\vec{B}(\vec{r})$ is the B-field. The energy shift of the states $|F = 2, I = 3/2, J = 1/2, m\rangle$ due to an external magnetic field can be calculated according to the Breit-Rabi formula in the limit where the energy shift due to the magnetic field is small compared to the hyperfine splitting [22,98]:

$$\Delta E_{F=2,J=1/2,I,m_F} = g_F \mu_B B m_F + \frac{\Delta E_{hfs}}{2}\sqrt{1 + \frac{4 m_F x}{2I+1} + x^2} \tag{2}$$

where ΔE_{hfs} is the hyperfine splitting, $x = \frac{(g_j - g_I)\mu_B B}{\Delta E_{hfs}}$, g_I is the g-factor for the nucleus, g_J is the g-factor for the electron, g_F is the Lande factor and m_F is an integer from – 2 to +2. The quantification axis for the m states is in the direction of the magnetic field. The values for the g-factors for Rb_{87} can be found in [98]. At a low magnetic field the second term in equation 2 is much smaller than the first term and in this case the potential seen by the atoms in the ground state $\left|5S_{1/2}, F = 2, m_F\right\rangle$ is:

$$U(\vec{r}) = g_F \mu_B m_F B(\vec{r}) \tag{3}$$

Depending on the sign of g_F, the states with positive m number will either experience a force towards low field (low field seeker) or high magnetic field (high field seeker). In [23] it is proven that no magnetic maximum can exist in free space, and thus only low field seeker states can be captured in an inhomogeneous magnetic field.

Majorana spin flips

It is possible for an atom in a given Zeeman level to undergo a non-adiabatic crossing into another Zeeman level. The smaller the energy gab between the two levels is, the larger the probability is for a non-adiabatic crossing to occur is. This type of non-adiabatic crossing is known as Majorana spin flips. The probability for a non-adiabatic crossing at the minimum energy difference can be estimated as $P = e^{-2\pi\Gamma_{lz}}$ where Γ_{lz} is the Laundau-Zener parameter and it is given by [24,25]:

$$\Gamma_{lz} = \frac{\Delta E_{\min}^2}{4\hbar \frac{dE}{dt}} \approx \frac{g_F \mu_B B_{\min}^2}{4\hbar m_F B' v} \tag{4}$$

where B_{min} is the magnetic field at the minimum of the trapping region. $\frac{dE}{dt}$ can be estimated as: $\frac{dE}{dt} = \frac{dE}{dr}\frac{dr}{dt} \approx B'v$, where B' is the gradient of the magnetic field and v is the velocity of the atom. For $\Gamma_{lz} >> 1$ the probability for an atom to undergo a non-adiabatic crossing to an other Zeeman state is small.

The life time associated with Majorana spin flips (τ_0) in a linear trap $B(\vec{r}) = B'\left|\vec{r}\right|$ only depends on the width of the atomic sample, and it is given by [26]: $\tau_0 = \sigma_{FWHM}^2 \frac{3{,}77\,10^2}{4}(s/mm^2)$, where σ_{FWHM} is the full width half maximum of the atomic sample.

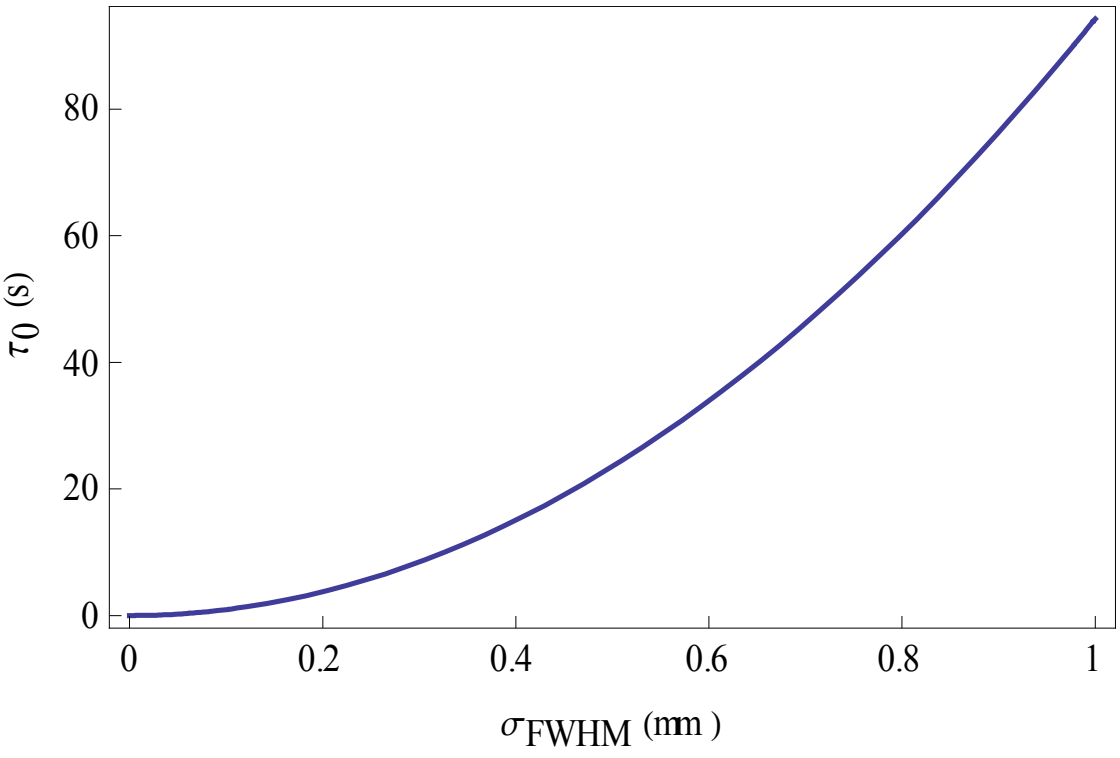

Figure 2: The lifetime associated with Majorana spin flips in a linear trap as a function of the fullwidth half maximum of the atomic sample (σ_{FWHM}).

The magnetic field configuration in the Ioffe-quadrupole trap

To increase the lifetime of the atomic sample at small widths one can capture the atomic sample at a minimum with $|B| \neq 0$. In [27] it is shown that if the field along the z-axis is of the form: $B_Z(z) = B_0 + \frac{B''}{2} z^2$ and the leading term along the x and y axis is linear and symmetric on these two axis, the Maxwell equations give the following field configuration:

$$B(x,y,z) = B_0 \begin{pmatrix} 0 \\ 0 \\ 1 \end{pmatrix} + B' \begin{pmatrix} x \\ -y \\ 0 \end{pmatrix} + \frac{B''}{2} \begin{pmatrix} -xz \\ -yz \\ z^2 - \tfrac{1}{2}\left(x^2 + y^2\right) \end{pmatrix} \tag{5}$$

where B' and B'' are set to real numbers greater than zero. The trap configuration from equation 5 is called the Ioffe-quadrupole trap.

For $\rho = \sqrt{x^2 + y^2} << B_0/B'$ the amplitude of the magnetic field can be approximated with [10]:

$$|B(\rho, z)| = \frac{1}{2}\left(B''_{radial}\rho^2 + B''z^2\right) + B_0 \tag{6}$$

where $B''_{radial} = \frac{B'^2}{B_0} - \frac{B''}{2}$. A displacement along the z-axis term $\frac{-B''}{2}xz$ destructively interfere with the term $B'x$ and this lowers the radial confinement along the x-axis. The point on the z-axis ($Z_{no\ trap}$) with no confinement on the x-axis is [10]:

$$Z_{no\ trap} = \pm\left(\frac{B'}{B''} - \frac{B_0}{2B'}\right) \tag{7}$$

$Z_{no\ trap}$ limits the size of an atomic sample, which can be captured in the magnetic trap given by equation 5. For a negative B_0 there exist two minima with B = 0. For B_0 approaching zero the two minima move towards each other and coincide at $B_0 = 0$. For B_0 greater than zero there is an local minima with a B-field greater than zero on the z-axis. In chapter 5.5 it is explained, how to generate a field configuration that closely resembles the one given in equation 5.

Adiabatic heating due to compression

The volume occupied by an atomic sample depends on the trap geometry. A generalized trapping potential can be written as:

$$U(x, y, z) = \varepsilon_x\left|\frac{x}{a_x}\right|^{s_x} + \varepsilon_y\left|\frac{y}{a_y}\right|^{s_y} + \varepsilon_z\left|\frac{z}{a_z}\right|^{s_z} \tag{8}$$

In [28] it is proven that the volume scales with the temperature as $V \sim T^{\xi}$, where $\xi = \frac{1}{s_x} + \frac{1}{s_y} + \frac{1}{s_z}$. The linear trap has $\xi = 3$, the harmonic trap has $\xi = 3/2$ and the Ioffe-quadrupole trap at high temperatures $\left(k_B T >> \mu_B B_0\right)$ has $\xi = 5/2$.

If an atomic sample is compressed or expanded adiabatically (no energy transfer in the process), the phase space density of the atomic sample does not change. The phase space density (ϖ) is defined as the number of atoms inside a cube with the length equal to the de Broglie wavelength, and it is given by [15]:

$$\varpi = n\left(\frac{2\pi\hbar^2}{mk_B T}\right)^{3/2} \tag{9}$$

From equation 8 it follows that if the potential U is changed with a factor β, the volume for a fixed temperature is changed with a factor $\beta^{-\xi}$ if the atoms are assumed not to interact (ideal gas). From the assumption of an adiabatic compression the temperature change and the density change are respectively: $\beta^{\frac{2\xi}{3+2\xi}}$ and $\beta^{\frac{4\xi}{3+2\xi}}$ [10]. The criterion for adiabaticity is: $\frac{d\omega_{trap}}{dt} << \omega_{trap}^2$.

2.4 Evaporative cooling

The principle in evaporative cooling is that atoms, which have a higher kinetic energy than the average kinetic energy in the atomic sample, are removed. After having lost a group of relative hot atoms, the remaining atoms will rethermalize to a lower temperature after some time due to collisions between the atoms. Good introductions to evaporative cooling can be found in [29,30].

The parameter α describing the efficiency of evaporative cooling

The average energy of the remaining atoms can be estimate from [15]:

$$\bar{\varepsilon} + d\bar{\varepsilon} = \frac{E + (1+\alpha)\bar{\varepsilon}dN}{N + dN} \tag{10}$$

where $\bar{\varepsilon}$ is the average energy of an atom before evaporation, $d\bar{\varepsilon}$ is the energy change due to evaporation, E is the energy of the entire atomic sample before evaporation, N is the number of atoms in the atomic sample before evaporation, dN is the number of atoms lost in the evaporation (dN < 0) and $(1+\alpha)\bar{\varepsilon}$ is the average energy of the atoms removed in the evaporation. By assuming that dN and dε are small compared to respectively N and $\bar{\varepsilon}$, equation 10 can be approximated as:

$$\frac{d\ln(\bar{\varepsilon})}{d\ln(N)} = \alpha \tag{11}$$

According to the Virial theorem, the average kinetic energy of an atom held in a power law potential is proportional to the average potential energy. Due to this $\bar{\varepsilon}$ can be substituted with the temperature T in equation 11.

$$\frac{d\ln(T)}{d\ln(N)} = \alpha \tag{12}$$

If α is independent of N, the relation between T and N is: $\frac{T}{T_0} = \left(\frac{N}{N_0}\right)^{\alpha}$ where T_0 is the temperature, and N_0 is the atom number before evaporation. α is a good figure of merit to describe how effective a given evaporation run has been.

In [30] it is calculated how the different thermodynamic variables relevant for evaporation cooling scales compared to N and α.

The thermodynamic variable X scales as: $\frac{X}{X_0} = \left(\frac{N}{N_0}\right)^q$ and the exponent q is given in Table 1.

Thermodynamic variable (X)	**q**
N	1
T	α
Volume	$\xi\alpha$
Density	$1-\xi\alpha$
Phase space density	$1-\alpha(\xi+3/2)$
Collision rate	$1-\alpha(\xi-1/2)$

Table 1: Evaporation parameters dependence on the atom number [30].

If the exponent q is larger than one for the collision rate, the number of collisions increases during the evaporation, which is called runaway evaporation. From Table 1 it is clear that a high value of ξ is desirable as it gives a greater increase in phase space density for a fixed α and atom loss. For this reason a linear trap is a very suitable trap for evaporation as long as losses due to Majorana spin flips are not important.

Simple model for evaporative cooling

In a simple model of evaporative cooling one can assume that all atoms with energies above a certain limit U_i are removed instantly from the trap. Collisions between the atoms remaining in the trap redistribute energy and create atoms with energies above U_i. The probability for an atom to acquire an energy above U_i through collisions depends on the temperature of the atomic sample in a given potential. By calculating the time for the number of collisions for the sample to thermalize, and the fraction above U_i for a thermalized sample, the number of atoms removed due to acquiring energies above U_i from collisions can be estimated. An average of 2.7 collisions are needed for thermalization [31]. The fraction above U_i for a thermalized sample with the temperature T is: $1 - e^{-\frac{U_i}{k_B T}}$.

By choosing U_i a compromise has to be found between the cooling rate and the average energy of the atoms removed from the trap. If only the atoms can escape the trap by obtaining energies larger than U_i through collisions, a high U_i compared to $k_B T$ means a high α but a low cooling rate.

An atomic sample held in a magnetic trap has a certain lifetime associated with other loss processes than the one used for evaporation. Collisions with a background gas, inelastic collisions and 3-body recombinations are among the loss processes, which limit the lifetime of an atomic sample in a magnetic trap. The average energy of the atoms removed by these loss processes affects the value of α. By assuming that all other loss processes than the one

used for evaporation can be described by a lifetime independent of N and T (τ_{loss}) and assuming all evaporated atoms have the energy U_i, an expression for α can be written [15]:

$$\alpha = \frac{\frac{U_i}{(3/2+\xi)k_B T} - 1}{1 + \frac{\tau_{el}}{\tau_{loss}} \frac{\sqrt{2}k_B T}{U_i} e^{\frac{U_i}{k_B T}}} \tag{13}$$

where τ_{el} is the collisions time for elastic collisions and it is given by:

$$\frac{1}{t_{el}} = n(0)\sigma_{col} v_{rel} \tag{14}$$

where n(0) is the density in the centre of the trap, σ_{col} is the collision cross section and v_{rel} is the mean relative velocity of the atoms in the atomic sample $4\sqrt{\frac{k_B T}{\pi m}}$ [15]. If the temperature of the atoms is low enough for the scattering to be assumed to be pure s-wave scattering, then: $\sigma_{col} = 8\pi a^2$. The maximum value of α for a given ratio of (τ_{loss} /τ_{el}) for a linear trap (ξ=3) is plotted in Figure 3.

The run-away regime for a linear magnetic trap

For a trap with ξ = 3, α must be greater than 2/5 for collision rate not to decrease during the evaporation according to Table 1 (the runaway regime). According to Figure 3 this means the collision time between the atoms have to be a factor 1500 shorter than the lifetime of the atomic sample. In [14] a ratio of 100 between the collision rate and the loss rate is suggested as a rule of thumb as a condition for runaway evaporation.

Typical values for an sample transferred from a MOT to a magnetic trap are of the order: $n(0) = 10^{11}$ atoms/cm^3, T = 100 μK and scattering lengths for the ground states of Rb_{87} are around 100 a_0 [15,32]. a_0 is the Bohr radius. This gives a value of $\tau_{el} \approx 50$ ms and this means the lifetime of the atomic sample in the trap have to be greater than 75 s for the evaporation to be in the run away regime in a trap with ξ = 3.

Forced evaporation with a radio frequency field

In a magnetic trap the low field seeking states can be removed from the trap by inducing transitions into untrapped states. This can be done by an oscillating magnetic field with a frequency ψ_0. The spin of a photon is $\hbar$, and thus a scattering event of one radio frequency photon can change the m-number of a trapped atom by 1. The probability for such a transition is largest, if the energy of the radio frequency photon is equal to the energy difference between two adjacent Zeeman levels (Δm=1).

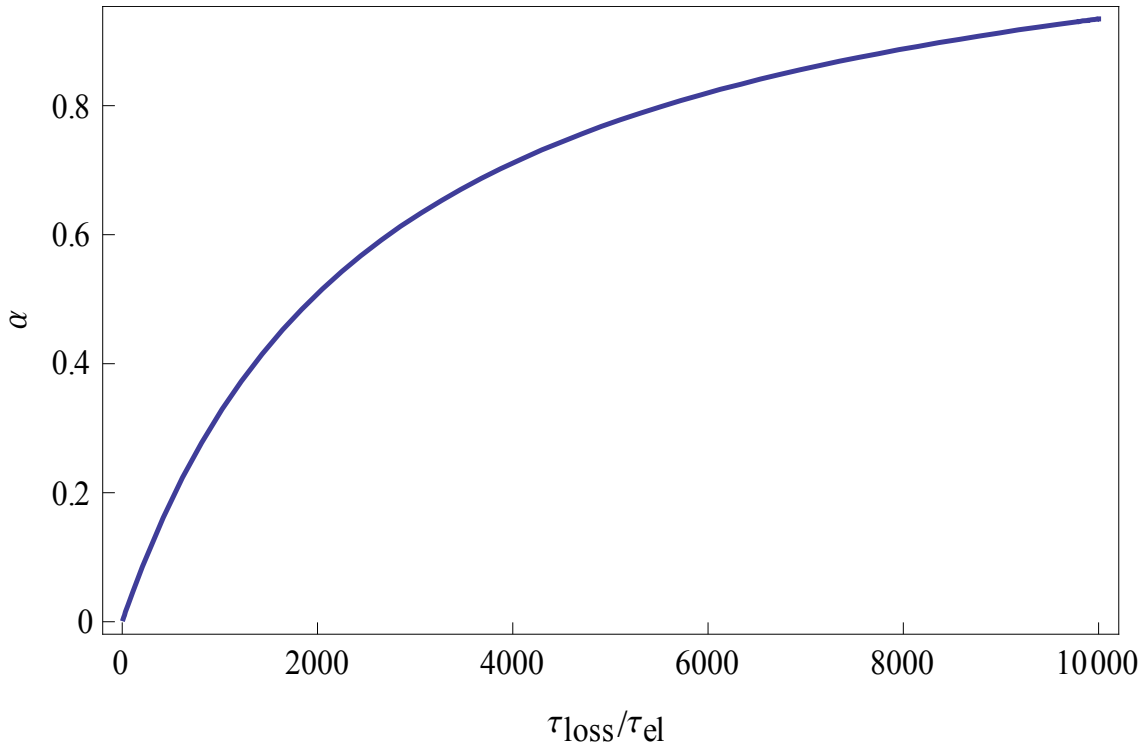

Figure 3: The maximum value of α for a given ratio of (τ_{loss} /τ_{el}) for a linear trap (ξ=3).

The potential energy of the atoms where the transition probability is the largest to an adjacent Zeeman level, is:

$$U_i = \hbar\Psi_0 - \mu_B g_F B_0 \qquad (15)$$

Hence, by varying ψ_0 one can selectively remove atoms with a certain potential energy. The orbit of an atom with a higher total energy than U_i has some probability to cross the region, where the potential energy is U_i. If this probability is high, the trap is said to have "sufficient" ergodicity and the assumption that all atoms with total energies above U_i will be removed is good. Collisions between the atoms in the trap change the orbits of the atoms, and this typically ensures the criterion for "sufficient" ergodicity. In [33] the effect of non-ergodicity is discussed.

A second assumption is that atoms with energies above U_i are instantly removed from the trap. This is a good assumption if the removed atoms do not collide with atoms remaining in the trap. A necessary condition for this is that the collisional free path length of an atom in the gas is much longer than the length of the sample (the Knudsen regime).

A limiting factor in evaporative cooling is incomplete evaporation due to the quadratic Zeeman term (see equation 2). Due to the quadratic Zeeman term the energy difference between two adjacent Zeeman levels is no longer independent of m and an atom in the state with m = 2 cannot therefore any longer at same position cascade down to an untrapped state at the same position at a fixed radio frequency. This effect becomes important at magnetic fields around 20 Gauss, and it is discussed in [34,35].

Losses in a magnetic trap due to 3-body recombination of Rb_{87}

At high densities tree-body recombination losses become important and the lifetime associated with 3 body losses scales as:

$$\frac{1}{\tau_{3body}} = -Ln^2 \tag{16}$$

In [36] the 3-body recombination rate (L) for Rb_{87} is measured to be 4.3 10^{-29} cm^6/s for a thermal gas. The 3 body recombination rate is a factor six times lower for a pure condensate [15,36].

The phase density of an atomic sample close to the transition temperature to BEC is close to one. Assuming the transition temperature is 500 nK, the density of the atomic sample at the transition is 5 10^{13} atoms/cm^3 and the lifetime associated with 3-body losses is then 10 sec.

2.5 A dilute Bose gas in a harmonic potential

The general form of the atomic distribution depends on the potential and the temperature of the atomic sample. At temperatures where the kinetic energy is much larger than the energy due to interaction between the atoms, the atomic sample can be treated as an ideal gas (no interaction). This approximation is typically good for an atomic sample with a temperature much larger than the transition temperature for a BEC for the atomic sample (a thermal cloud). At low enough temperature the interaction energy becomes much larger than the kinetic energy, and the kinetic energy can be neglected.

This approximation is typically good for a pure BEC, and it is known as the Thomas-Fermi approximation. It is relative simple to find the atomic distribution with the ideal gas or the Thomas-Fermi approximation. It is, however, not simple to solve the atomic distribution around the transition temperature to a BEC (t_c). A simple way to describe the atomic distribution around t_c is to assume that the atomic sample consists of two separate samples: a pure BEC and a thermal cloud.

The spatial distribution of a thermal atomic cloud in a power law potential

The occupation number $\langle n_k \rangle$ for a Bose-distribution is at the temperature T:

$$\langle n_k \rangle = \frac{1}{e^{\frac{\varepsilon_k - \mu}{k_B T}} - 1} = \sum_{l=1}^{\infty} e^{-\frac{l(\varepsilon_k - \mu)}{k_B T}} \tag{17}$$

where ε_k is the energy of the energy level k and μ is the chemical potential. The chemical potential is decided through the atom number N:

$$N = \sum_k \langle n_k \rangle \tag{18}$$

If the level spacing between the energy levels in the magnetic trap is much smaller than k_BT, the number of atoms in the excited state can be written as:

$$N - N_0 = \int_0^{\infty} \frac{1}{e^{\frac{\varepsilon_k - \mu}{k_B T}} - 1} \rho(\varepsilon) d\varepsilon \tag{19}$$

where N_0 is the number of atoms in the ground state, $\rho(\varepsilon)$ is the density of states, and it is given by [28]:

$$\rho(\varepsilon) = \frac{2\pi(2M)^{3/2}}{h^3} \int_{V_\varepsilon} \sqrt{\varepsilon - U(r)} dr^3 \tag{20}$$

where V_ε is the volume, where r fulfils the following condition: $\varepsilon - U(r) \geq 0$. The density of the atoms in the excited states in a power law trap is [28]:

$$n_{th}(r) = \frac{1}{\lambda_{dB}^3} g_{3/2}(z(r)) \tag{21}$$

where $z(r) = e^{\frac{\mu - U(r)}{k_B T}}$ and the Bose function is: $g_j(z) = \sum_{i=1}^{\infty} \frac{z^i}{i^j}$. For a thermal cloud in the Ioffe-quadrupole trap at low temperatures ($k_BT << B_0\mu_B$) the trap is harmonic $U(r) = \frac{1}{2} m\left(\omega_x^2 x^2 + \omega_y^2 y^2 + \omega_z^2 z^2\right)$ (see chapter 2.2).

The spatial distribution of a freely expanding thermal cloud

The density profile during a free expansion of an atomic sample, which has been captured in a harmonic potential is given by [10]:

$$n_{tof}(r,t) = \frac{1}{\lambda_{dB}^3} \left(\prod_{q=x,y,z} \frac{1}{\omega_q^2 t^2 + 1} \right) g_{3/2} \left(e^{\left(\mu - \frac{m}{2} \sum_{q=x,y,z} q^2 \left(\frac{\omega_q^2}{\omega_q^2 t^2 + 1} \right) \right) / (k_B T)} \right) \tag{22}$$

If $Z << 1$ the following approximation can be made for the Bose function $g_{3/2}(Z) \approx Z$. In the classical limit $\mu << 0$, and the density can be approximated as:

$$n_{tof}(r,t) \approx \frac{N - N_0}{\pi^{3/2} \prod_{q=x,y,z} q_{1/e}(t)} e^{\sum_{q=x,y,z} \left(\frac{q}{q_{1/e}(t)} \right)^2} \tag{23}$$

where $q_{1/e}(t)$ is the 1/e radius and it is given by:

$$q_{1/e}(t) = \sqrt{\frac{2k_B T}{m} t^2 + \frac{2k_B T}{\omega_q^2 m}} = \sqrt{v^2 t^2 + q_0^2} \tag{24}$$

where v is the velocity and q_0 is the 1/e radius at t = 0 of the atomic sample. The expansion of an atomic sample released from a non-harmonic potential is different from equation 24, however for expansions times, where the atomic sample has expanded to a size significantly larger than the original size, the expansion behaviour described by equation 24 is typically a good approximation.

The spatial distribution of a pure BEC with the Thomas-Fermi distribution

For a pure BEC, all atoms are in the same single-particle state and the many body particle function of the entire sample $\psi(r)$ is simply a product of the same single particle wave function. $\psi(r)$ is described by the Gross-Pitaevskii equation. An introduction for the solutions of the Gross-Pitaevskii equation for trapped bosons can be found in [15,37]. The Gross-Pitaevskii equation is:

$$i\hbar \frac{d\psi(r)}{dt} = -\frac{\hbar^2}{2m}\nabla^2\psi(r) + U(r)\psi(r) + U_0|\psi(r)|^2 \tag{25}$$

where U_0 is the interaction energy due to two-body collisions $\left(U_0 = 4\pi\hbar^2 a/m\right)$. The interaction term $\left(U_0|\psi(r)|^2\right)$ can be identified as the chemical potential (μ).

In the Thomas-Fermi approximation the kinetic energy term is set to zero and the steady state distribution becomes [10]:

$$n_{TF}(r) = \frac{15}{8\pi}\frac{N_0}{x_0 y_0 z_0}\left(1 - \left(\frac{x}{x_0}\right)^2 - \left(\frac{y}{y_0}\right)^2 - \left(\frac{z}{z_0}\right)^2\right) \text{ for } q \le q_0 \ (q = x, y, z) \tag{26}$$

where $q_0 = \sqrt{\frac{2\mu}{m\omega_q^2}}$ and q = (x,y,z). For $q > q_0$ $n_{TF}(r) = 0$. The Thomas-Fermi approach is applicable when $\psi(r)$ varies slowly in space. For large BECs this is typically the case, but near the surface of the BEC the Thomas-Fermi approximation fails.

The spatial distribution of a freely expanding BEC

The expansion of the cloud from a cigar-shaped trap ($\omega_\rho = \omega_x = \omega_y >> \omega_z$) is [38]:

$$\rho(t) = \rho_0\sqrt{1 + \omega_\rho^2 t^2} \tag{27}$$

$$z(t) = \rho_0 \left(\frac{\omega_\rho}{\omega_z} + \frac{\omega_z}{\omega_\rho} \left((\omega_\rho t) \mathrm{ArcTan}(\omega_\rho t) - \ln \sqrt{1 + (\omega_\rho t)^2} \right) \right) \tag{28}$$

The atomic distribution of a partly condensed cloud can be approximated by a distribution for the BEC with N_0 atoms given by equation 26, and a thermal cloud with $N\text{-}N_0$ atoms given by equation 21. The resulting atomic distribution is bimodal and the bimodality can be observed in the atomic distribution after a sufficient time of expansion depending on the trap parameters. Bimodality of the atomic distribution is a clear proof of a BEC.

It is possible for a non-condensed cloud to be in the regime where the Thomas-Fermi approach is valid. A necessary condition for the Thomas-Fermi approximation to be valid is:

$$E_{kin} = \left| \frac{3}{2} k_B T \right| << \left| U_0 |\psi(r)|^2 \right| = \left| \frac{4\pi\hbar^2 a}{m} \right| n \tag{29}$$

If the phase density is assumed to be 1, the temperature has to be greater than 300 μK for equation 29 to be valid. Then the density is then of the order 10^{17} atoms/cm^3. Such an atomic sample cannot be experimentally realized with the present apparatus. A BEC has a phase space density of typically 10^7, and thus the temperatures and densities, at which equation 29 is valid, are much lower than for a non-condensed cloud. In practice, if an atomic sample has an expansion following equation 27 and equation 28, it can be taken as a clear proof of a BEC.

The column density of thermal cloud and a BEC

The column density along an imaging axis is much easier to measure directly than the density. Defining the imaging axis to be the y-axis and integrating the atomic distributions from y = -∞ to y = ∞, column densities for a thermal gas and a Bose-Einstein condensate are [10]:

$$\tilde{n}_{th}(x,z) = \frac{\tilde{n}_{th}(0)}{g_2(1)} g_2 \left(e^{1 - \left(\frac{x}{x_{th,0}}\right)^2 - \left(\frac{z}{z_{th,0}}\right)^2} \right) \approx \tilde{n}_{th}(0) e^{1 - \left(\frac{x}{x_{th,0}}\right)^2 - \left(\frac{z}{z_{th,0}}\right)^2} \tag{30}$$

$$\tilde{n}_{TF}(x,z) = \tilde{n}_{TF}(0) \left(1 - \left(\frac{x}{x_{TF,0}} \right)^2 - \left(\frac{z}{z_{TF,0}} \right)^2 \right) \text{ for } q < q_{TF,0} \ (q = x, z) \tag{31}$$

where $\tilde{n}_{th}(0)$ and $\tilde{n}_{TF}(0)$ are the column densities respectively for a thermal gas and for a gas in the Thomas-Fermi limit at x = z = 0. $x_{TF,0} = \rho_0$ and $z_{TF,0} = \rho_0 \frac{\omega_\rho}{\omega_z}$.

2.6 Absorption imaging

The only feasible method to measure the density distribution of an atomic gas with up to 10^{10} atoms is with optical methods. The simplest method to imagine the atomic sample is by illuminating it with light, and measure the absorption as a function of the displacement from the centre of the sample. From this method, the column density of the sample can be measured. By comparing the light intensity with and without atoms on a CCD chip, the optical density can be estimated. Among the systematic errors in this measurement is the dark signal on the CCD chip, the saturation effect of the illuminating light on the atomic sample, the resolution of the CCD chip, off-resonant light and scattering light on the CCD chip due to absorption of the illuminating light from the atomic sample. By accounting for these errors a measure for the column density can be found and the temperature can be estimated by measuring the column density at various expansion times (Time of flight (TOF)).

Beer's law

For the absorption imaging a laser beam is used as the spectrum is close to monochromatic, and it has a well-defined propagation direction. The optical density (OD) of an atomic sample at a given position in the plane perpendicular to the propagation direction of the laser beam is defined by Beer's law, and it is given by:

$$I(x,z) = I_0(x,z)e^{-OD} \tag{32}$$

where I(x,z) is the intensity on the CCD chip if the laser beam had passed through an atomic sample, and $I_0(x,z)$ is the intensity on the CCD chip in the absence of an atomic sample.

The measured optical density

The measured value for the optical density is given by:

$$OD_{measure} = \ln\left(\frac{I_0 - I_{dark}}{I - I_{dark}}\right) \tag{33}$$

where I_{dark} is the intensity measured on the CCD chip in the absence of any illuminating light (the dark signal).

Correction factors for the measured optical density

The resolution of the CCD chip and the scattered light due to absorption set an upper limit on the maximum measurable optical density (OD_{sat}). The correction for optical density due to a maximum measurable optical density is given by [14]:

$$OD_{mod} = \ln\frac{1 - e^{-OD_{sat}}}{e^{-OD_{measure}} - e^{-OD_{sat}}} \tag{34}$$

To obtain the most reliable value of the optical density it is preferable that $OD_{measure} < OD_{sat}/2$, so that the correction factor is not big. The illuminating light saturates the atoms and this lowers the measure absorption.

The actual OD can be estimated from [14]:

$$OD_{actual} = OD_{mod} + \left(1 - e^{-OD_{mod}}\right)\frac{I}{I_S} \tag{35}$$

where I_S is the saturation intensity. In the limit of no saturation the optical density is given by [10]:

$$OD(x,z) = \tilde{n}(x,z)\sigma_0 \frac{1}{1+\left(\frac{2\delta}{\gamma}\right)^2} \tag{36}$$

where $\tilde{n}$ is the column density, σ_0 is the absorption cross section and γ is the natural linewidth of the imaging transition.

3 Cavity theory

In this chapter a review of the important concepts needed to understand the next chapter regarding cavity/atom interaction. In [39] an introduction to the classical theory of Gaussian beams and cavities are given. Chapter 3.1 gives the characteristics of Gaussian beams. Chapters 3.2 to 3.4 describe how one can most optimal couple light into a high finesse cavity. Chapter 3.5 discusses how a cavity can change the emission spectrum of an atom.

3.1 Gaussian beams

A Gaussian beam is a good approximation for the beam generated by a laser. The electrical field of a Gaussian beam is given by equation 37 [39].

$$E(x,y,z,t) = \left(a\frac{w_0}{w(z)} e^{i(kz-\tan^{-1}(z/z_0))} e^{ik\frac{x^2+y^2}{2R(z)}} e^{-\frac{x^2+y^2}{w(z)^2}} \right) e^{i\omega t} \tag{37}$$

$$w(z) = w_0\sqrt{1+\frac{z^2}{z_0^2}} \tag{38}$$

$$R(z) = z + \frac{z_0^2}{z} \tag{39}$$

where E(x,y,z,t) is the electrical field of the beam at the position (x,y,z) and at the time t, $a = \frac{2P}{\pi w_0^2}$, P is the power of the Gaussian beam, z_0 is the Rayleigh range, k is the wave number ($2\pi/\lambda$), λ is the wavelength of the light, w_0 is the waist of the laser beam at the focus, w(z) is the waist at the position z and R(z) is the radius of curvature of the laser beam at the position z. The Rayleigh length and the waist w_0 have the following relation [39]:

$$z_0 = \pi\frac{{w_0}^2}{\lambda} \tag{40}$$

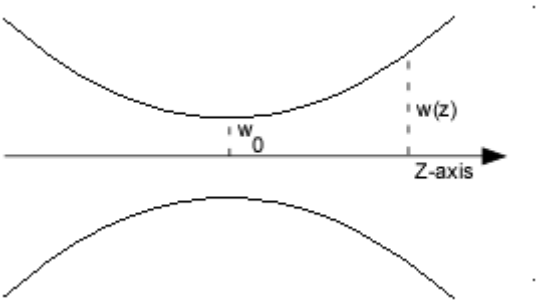

Figure 4: A Gaussian beam along its axis of propagation.

The Gaussian beam as described by equation 37 is a TEM_{00} mode. The TEM_{mn} mode has m zero crossings on the x-axis and n zero crossings on the y-axis.

3.2 Cavity stability

The cavities described in this thesis are all standing wave cavities. For the photons inside the cavity to have a high storage time, the cavity must be stable.

Figure 5: The arrow shows a stable path for a light ray inside a spherical resonator. The beam is reflected upon itself on each of the two mirrors and thus can stay an infinite number of reflections inside the resonator, if it is not transmitted through or scattered on the mirrors.

That a cavity is stable means that it is possible for a light ray originating anywhere on the surface of one of the mirrors to stay inside the cavity for an infinite number of reflections on the two mirrors.

Ray optics

The constraints on the radius of curvature of the two mirrors and the length of the cavity for it to be stable can be calculated with ray optics. In ray optics, a ray is described by a 2-dimensional column vector $\vec{r} = \begin{pmatrix} r \\ r' \end{pmatrix}$ where r is the lateral displacement and r' is the angle (see Figure 6).

Each optical element is described by a 2x2 matrix. Ray matrix for a spherical mirror is given by M_1 and free propagation is given by M_2. R is the curvature of the mirror and d is the distance travelled by the ray [39].

$$M_1 = \begin{pmatrix} 1 & 0 \\ \frac{-2}{R} & 1 \end{pmatrix} \qquad M_2 = \begin{pmatrix} 1 & d \\ 0 & 1 \end{pmatrix}$$

To calculate the new vector for a ray after an optical element, the relevant matrix is multiplied with the vector for the ray $(M\vec{r})$. For an optical system consisting of more than one element, the matrixes for the different elements can be multiplied together to create one matrix for the entire system. The resulting matrix is of the type: $\begin{pmatrix} A & B \\ C & D \end{pmatrix}$ and is called an ABCD matrix.

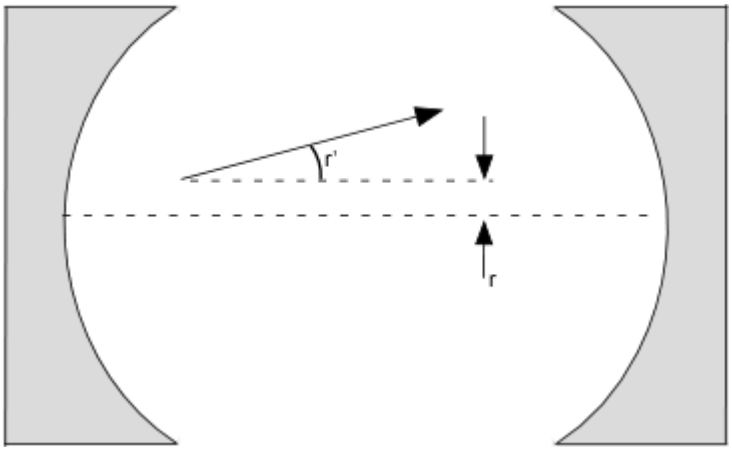

Figure 6: Illustration of parameters used in ray optics.

If all entries in the matrix $M_N = (M_2M_1M_2M_1)^N$ corresponding to N round trip in the cavity are finite for N going towards infinity, the cavity is said to be stable. The constraints on the allowed values of the radius of the curvature of the mirrors (R_i) and the length of the cavity (L) if the cavity has to be stable are given by [39]:

$$0 \le \left(1 - \frac{L}{R_1}\right)\left(1 - \frac{L}{R_2}\right) \le 1 \tag{41}$$

The shape of a Gaussian beam depends on two parameters at a given location along the propagation direction: the waist and the radius of the curvature. Thus, the shape of a Gaussian beam can therefore also be described by a 2D-column vector. The two entries in vector are chosen to depend on the waist and the curvature in such a way that the matrixes for various optical elements are the same as for a ray. By demanding that there must exist a Gaussian beam, which has the same waist and radius of curvature after one round trip, the same constraints on L and R_i as the one given in equation 41 can be derived for the cavity to be stable.

A more intuitive way of calculating the stability conditions for a Gaussian beam is to demand that the radius of curvature of the Gaussian beam at the position of a reflecting mirror is the same as the one of the mirror.

The stability conditions for a Gaussian beam

From the condition in the previous paragraph, one can calculate the position of the focus and the waist at the focus. The waist at the focus is given by [39]:

$$w_0 = \sqrt{\frac{\lambda L}{\pi}} \sqrt[4]{\left(\frac{g_1 g_2 (1 - g_1 g_2)}{(g_1 + g_2 - 2 g_1 g_2)^2}\right)} \tag{42}$$

where $g_i = 1-L/R_i$. The Rayleigh length corresponding to the waist given by equation 42 can be calculated from equation 40. For a cavity consisting of two identical mirrors, the focus is at the centre of the cavity (equal distance to both mirrors).

If a Gaussian beam has the same phase after one round trip, it will constructively interfere with itself. This is fulfilled for the following frequencies [39].

$$f_q = \frac{c}{2L}\left(q + \frac{1}{\pi}\cos^{-1}\left(\sqrt{g_1 g_2}\right)\right) \tag{43}$$

where c is the speed of light, q is a natural number, and q gives the frequencies of the longitudinal modes of the cavity. FSR = c/(2L) is the free spectral range, and it is the frequency difference between two longitudinal modes. If a Gaussian beam fulfils the constraint in equation 43, the beam is said to be resonant with the cavity.

3.3 Cavity incoupling

This chapter is describing, how to couple light into a cavity through one of the mirrors. The mirror consists of a plane side of glass without a coating, which has a few percent reflection and a curved side with a highly reflecting coating. The reflection from the plan side is neglected due to its much higher transmission than the coated side. In the following discussion a Gaussian beam that fulfils the conditions for being a stable mode of the cavity is considered.

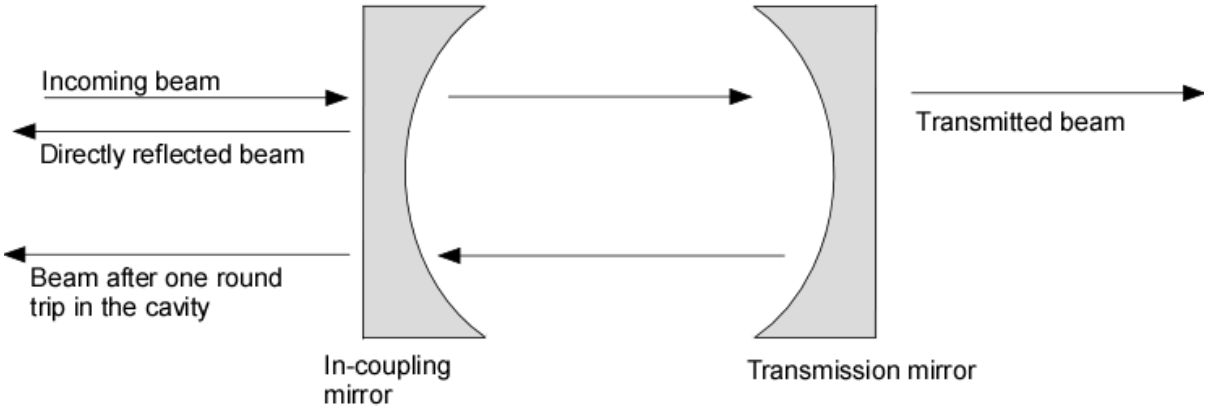

Figure 7: illustration of different electrical field arising when a laser beam is sent to the incoupling mirror of a cavity.

One part of the incoming Gaussian beam will be directly reflected at the mirror coating of the incoupling mirror, and the other part of the beam is transmitted into the cavity. A part of the beam, which was transmitted into the cavity, will be transmitted through the incoupling mirror after one round trip in the cavity. This beam will have the same parameters as the directly reflected beam except for the phase. The beam, which has made one roundtrip in the cavity, has the same phase as the incoming beam, while the phase of the directly reflected beam has obtained a phase of π in the reflection. Hence, the beam transmitted through the

incoupling mirror by the light inside the cavity and the directly reflected beam destructively interfere. This is seen as a reduction of the intensity of the light reflected by the cavity. At the incoupling mirror, there are only two options: either the light is reflected or transmitted through the incoupling mirror. Thus a reduction in the reflected light must mean an increase in the light transmitted into the cavity.

The minimum ratio of the intensity of the reflected light to the intensity of the incoming light is given by [40]:

$$\frac{I_R}{I_{IN}} = 1 - \frac{4\chi_1\chi_2}{(\chi_1 + \chi_2 + \chi_0)^2} \tag{44}$$

where χ_1 is the transmission coefficient of the incoupling mirror, χ_2 is the transmission coefficient of the second mirror, χ_0 is the sum of loss processes not including the transmission losses through the two mirrors (for a cavity in vacuum χ_0 is the sum of the absorption losses and the diffuse scattering losses on the two mirrors), I_R is the reflected intensity and I_{IN} is the incoming intensity on the incoupling mirror. The light of the incoming beam is assumed to be resonant with the cavity and equation 44 is only valid in the limit, where χ_0, χ_1, $\chi_2 << 1$ (low loss cavity). If $\chi_1 = \chi_0 + \chi_2$ the reflected intensity has its minimum. In this case the cavity is said to be impedance matched. From equation 44 one can calculate the maximum possible incoupling for a given cavity.

In an experiment the incoming beam will to some degree deviate from the TEM_{00} mode of the cavity. In this case the incoming beam will be a superposition of TEM_{00} and higher order Gaussian modes of the cavity [41]. The higher order Gaussian modes will usually not fulfil the phase condition, that they have the same phase as incoming beam at the incoupling mirror after one round trip in the cavity, at the same frequency as the TEM_{00} mode has. Modes that do not fulfil the frequency conditions will be directly reflected, and this is seen as less incoupling. The maximum incoupling in a cavity is a measure for how good the incoming beam matches the TEM_{00} mode of the cavity, and how well the cavity is impedance matched.

3.4 Cavity enhancement

In the previous chapter it was shown that it is possible to transmit a significant part of a Gaussian beam into a resonator mode assuming that the Gaussian beam has the right parameters for the cavity in question. For ultra low internal losses, the intensity of the light cycling in the cavity is much larger than the intensity of the incoming beam.

The intensity of the electrical field inside the cavity compared to the intensity of the incoming beam on resonance and for a low loss cavity can be estimated from [40]:

$$\frac{I_{cavity}}{I_{IN}} = \frac{4\chi_1}{(\chi_1 + \chi_2 + \chi_0)^2} = A \tag{45}$$

When the cavity is impedance matched the enhancement is $1/\chi_1$. The transmission through the cavity as a function of the frequency (ω) is given by [40]:

$$\frac{I_T(\omega)}{I_{IN}(\omega)} = \frac{T_{Max}}{1 + \left(\frac{2F}{\pi}\right)^2 Sin^2\left(\frac{\omega}{2FSR}\right)} \tag{46}$$

where $I_T(\omega)$ is the transmitted intensity for a Gaussian beam with the frequency (ω), T_{max} is transmission on resonance, FSR is the free spectral range and F is the finesse of the cavity. The finesse is defined as:

$$\frac{I_T\left(\frac{FSR}{2F}\right)}{T_{Max}} \equiv \frac{1}{2} \tag{47}$$

The line width of the cavity ($\Delta\nu$) is defined as the full width half maximum of the resonance profile ($\Delta\nu$=FSR/F). The finesse can also be expressed in terms of the internal losses [40]:

$$F = \frac{2\pi}{\chi_1 + \chi_2 + \chi_0} \tag{48}$$

Equation 48 shows that for low losses the finesse is high and this in turn means a small line width. When a photon can undergo many round trips in the cavity before it escapes from the cavity, the phase it can pick up per round trip must also be small in order for it to constructively interfere with the incoming beam. The total losses per round in the cavity can be measured by switching the incoming beam off and the light inside the cavity will then decay exponentially with the time constant: $T = \frac{2L}{c}(\chi_1 + \chi_2 + \chi_0)$.

3.5 Scattering enhancement

The fact, that an optical resonator can change the spontaneous scattering rate of an atom was first suggested by E. M. Purcell [42]. Spontaneous emission can be understood as stimulated emission by the ground states of the quantified electrical field (also called the vacuum modes) [43]. Vacuum modes that fulfil the conditions for being a stable mode of the cavity have their electrical field enhanced inside the cavity, and this gives a higher rate of emission into these modes.

The scattering rate of a single localized dipole inside a cavity, where only one stable mode is considered, can be estimated with Fermi Golden Rule [44]:

$$\frac{1}{\tau_{cavity}} = \frac{2\pi}{\hbar}\rho(\omega)\left|\langle 1|\vec{d}\,\vec{\varepsilon}(\vec{r})|0\rangle\right|^2 \tag{49}$$

where τ_{cavity} is the decay time of the excited atom into the resonator mode, $\rho(\omega)$ is the density of photon modes at the frequency ω (which is the frequency of the emitted photon), $\vec{d}$ is the dipole operator, $\vec{\varepsilon}$ is the electrical field operator, $\vec{r}$ is the location of the dipole, $|1\rangle$ is the state with one photon in the cavity mode and $\langle 0|$ is the vacuum state of the cavity mode.

The electrical operator corresponding to the classical electrical field given in equation 37 for the cavity mode is [44]:

$$\vec{\varepsilon}(\vec{r},t) = i\varepsilon_{max}E(\vec{r},t)\vec{p}(\vec{r})\hat{a} + h.c. \tag{50}$$

where $E(\vec{r},t)$ is the electrical field of the standing wave in the cavity where each propagation direction of the standing wave is given by equation 37 with a = 1 and $\pm k$, $\vec{p}(\vec{r})$ is the local polarization field vector (normalized to 1), $\hat{a}$ is the annihilation operator for a photon in the cavity mode and ε_{max} is a measure for the maximum field per photon in the cavity mode.

ε_{max} can be estimated by calculating the energy of the vacuum mode $|n=0\rangle$ in the resonator and assuming that this energy is equal to the total energy of the vacuum mode $\frac{\hbar\omega}{2}$ [45].

$$\varepsilon_{max} = \sqrt{\frac{\hbar\omega}{2\varepsilon_0 V_{eff}}} \tag{51}$$

where V_{eff} is the effective volume of the cavity mode [44]:

$$V_{eff} = \int |E(\vec{r})|^2 d\vec{r} \tag{52}$$

V_{eff} corresponding to the electrical field given in equation 37 is [46]:

$$V_{eff} = \frac{\pi L w_0^{\,2}}{2} \tag{53}$$

The mode density of the empty cavity is [43,44]:

$$\rho_{cav}(\omega) = \frac{2Q}{\pi\,FSR}\frac{\Delta\upsilon^2}{\Delta\upsilon^2 + (\omega - \upsilon_c)^2} \tag{54}$$

where υ_c is the resonance frequency and Q is the cavity quality factor $\left(\frac{4\pi L}{\lambda_c}\frac{1}{\chi_1 + \chi_2 + \chi_0}\right)$ [40]. The ratio between the scattering rate into the cavity mode and the scattering rate into free space is when the emitted light into the cavity mode is resonant with the cavity and the excited atom is the centre of the cavity mode [44,46]:

$$\eta_c = \frac{\tau_{free}}{\tau_{cavity}} = \frac{3Q\lambda_c^{\,3}}{4\pi^2 V_{eff}} = \frac{12A}{k^2 w_0^2} \tag{55}$$

where $1/\tau_{free}$ is the scattering rate into free space [47] and λ_c is the wavelength of the resonant cavity mode. The last equality in equation 55 is only valid for an impedance matched cavity. In the cavity cooling scenarios a scattering into the cavity mode is typically a cooling mechanism, while a scattering into free space is a heating mechanism. Thus η_c is a good figure of merit for a cavity to evaluate it s usefulness for cavity cooling.

4 Cavity/atom interaction

In this chapter, the subject is the interaction between atoms with a position inside the cavity mode and the light in the cavity mode. The simplest interaction between atoms in the cavity mode and the cavity mode is the dipole force on atoms from light in the cavity mode, and this is discussed in chapter 4.1. In chapter 4.2 is explained how a cavity mode can be used to cool atoms, which are not spatially confined (cavity Doppler cooling). Chapter 4.3 discusses self-ordering of initial free atoms, and in chapter 4.4 side band cooling of atoms in the Lamb-Dicke regime is discussed. In chapter 4.5 cavity cooling with two cavity modes is discussed and in chapter 4.6 the measurement of the normal splitting with a far detuned probe beam is discussed.

4.1 Optical dipole trap

Using optical dipole forces to capture neutral atoms is a standard method to tightly confine an atomic sample spatially with a long storage time. An introduction to far red-detuned optical dipole traps is given in [48]. Chapter 3 described how a strong electrical field can be build up in a cavity mode. The electrical field in a cavity mode can create a spatial confining potential for an atom if the frequency of the cavity mode is red-detuned to an atomic resonance.

The potential energy of a neutral atom in a light field

In the case where the cavity mode is far red-detuned from an atomic resonance, the potential is given by [48]:

$$U_{dip}(\vec{r}) = \frac{3\pi c^2}{2\omega_0^3}\frac{\gamma}{\Delta} I_{cavity}(\vec{r}) \tag{56}$$

where γ is the linewidth of the atomic transition, Δ is the detuning from the atomic resonance ($\Delta < 0$ for red-detuning) and $I_{cavity}(\vec{r})$ is the intensity of the electrical field in the cavity mode. By adding the two directions of the cavity mode together (see equation 37) and taking into account the cavity enhancement, $I_{cavity}(\vec{r})$ can be estimated near the focus as (i):

$$I_{Cavity}(x,y,z) = b_{in} A \frac{2P}{\pi w_0^2} \mathrm{Sin}^2(kz) e^{-2\frac{x^2+y^2}{w_0^2}} \tag{57}$$

where b_{in} is the fraction of the incoming beam, which is transmitted into the cavity mode.

---

i $\left|k\left(x^2+y^2\right)^2\right| << \left|2R(z)\right|$ and $\left|z\right| << \left|z_0\right|$

The potential energy of a neutral atom in a Gaussian standing wave in the harmonic approximation

The second order Taylor expansion of equation 56 is:

$$U_{dip}(\vec{r}) = U + \frac{1}{2}m\Omega_x{}^2x^2 + \frac{1}{2}m\Omega_y{}^2y^2 + \frac{1}{2}m\Omega_z{}^2z^2 \tag{58}$$

where $U = Ab_{in}\frac{2P}{\pi w_0^2}\frac{3\pi c^2}{2\omega_0^3}\frac{\gamma}{\Delta}$, m is the mass of the atom, $\Omega_z = k\sqrt{\frac{2U}{m}}$ and $\Omega_y = \Omega_x = \frac{2}{w_0}\sqrt{\frac{U}{m}}$. The potential given by equation 58 is the one for the linear harmonic oscillator and each dimension can be treated separately. The eigenstates of the linear harmonic oscillator in one dimension can be written as [49]:

$$|n\rangle = \psi_n(x) = \frac{1}{\sqrt{2^{-n}n!}}\sqrt[4]{\left(\frac{m\Omega}{\hbar\pi}\right)}e^{-\frac{m\Omega}{2\pi}}H_n\left(\sqrt{\frac{m\Omega}{\hbar}}x\right) \tag{59}$$

where n is an integer ($n \geq 0$) and H_n is the Hermite polynomial of the order n. The eigenstates $|n\rangle$ can be understood as different vibrational levels in the harmonic oscillator and the energy of each state is given by [49]:

$$E_n = \hbar\Omega_z(1/2 + n) \tag{60}$$

Correction term of the energy of the vibrational levels

In the harmonic oscillator the energy difference between the vibrational level $|n+1\rangle$ and the vibrational level $|n\rangle$ does not depend upon n, however, this is only true as long the higher order terms in the Taylor expansion are not considered. The extra potential terms in the fourth order Taylor expansion are:

$$U'(x,y,z) \equiv U\left(\frac{1}{2w_0^4}\left(x^4 + y^4\right) + \frac{k^4}{3}z^4\right) \tag{61}$$

The shifting of the energy (ΔE_n) of the eigenstate $|n\rangle$ can be estimated by treating $U'(x,y,z)$ as a perturbation.

The first order approximation for the energy shift ($\Delta E_{z,n}$) on the z-axis for $|n_z\rangle$ is [49]:

$$\Delta E_{z,n} = U\frac{k^4}{3}\langle n_z|z^4|n_z\rangle = Uk^4 z_0^4(2n^2+2n+1) = \frac{(2n^2+2n+1)\hbar^2k^2}{8m} \tag{62}$$

where $z_0 = \sqrt{\frac{\hbar}{2m\Omega_z}}$. The energy difference $(\Delta E_{n+1,n})$ between the states $|n+1\rangle$ and $|n\rangle$ is:

$$\Delta E_{n+1,n} = \hbar\Omega_z + (1+n)\frac{\hbar^2k^2}{2m} \tag{63}$$

Heating of neutral atoms in a dipole trap due to scattering

An atom captured in the dipole trap by the cavity mode will scatter light from the cavity mode into free space. The random recoils heat the atom and the heating rate is given by [48]:

$$P_{heat} = 2\frac{\hbar^2k^2}{m}I_{free}(\vec{r},\Delta) = \frac{\hbar^2k^2}{2m}\frac{s_0(\vec{r})\gamma^3}{\gamma^2(1+s_0(\vec{r}))+4\Delta^2} \tag{64}$$

where $s_0(\vec{r}) = \frac{I_{cavity}(\vec{r})}{I_0}$, $I_{free}(\vec{r},\Delta)$ is the free space scattering rate and I_0 is the saturation intensity of the atom. The trap depth of a bound atom in the dipole trap can be estimated by:

$$T = \frac{2U}{3k_B} \tag{65}$$

4.2 Cavity Doppler cooling

A cooling scheme for free atoms has been suggested in [46]. The basic set-up is sketched in Figure 8. A mono-chromatic pump beam illuminates atoms inside the cavity mode from the side of the cavity, and an atom can scatter a photon from the pump beam into the cavity mode.

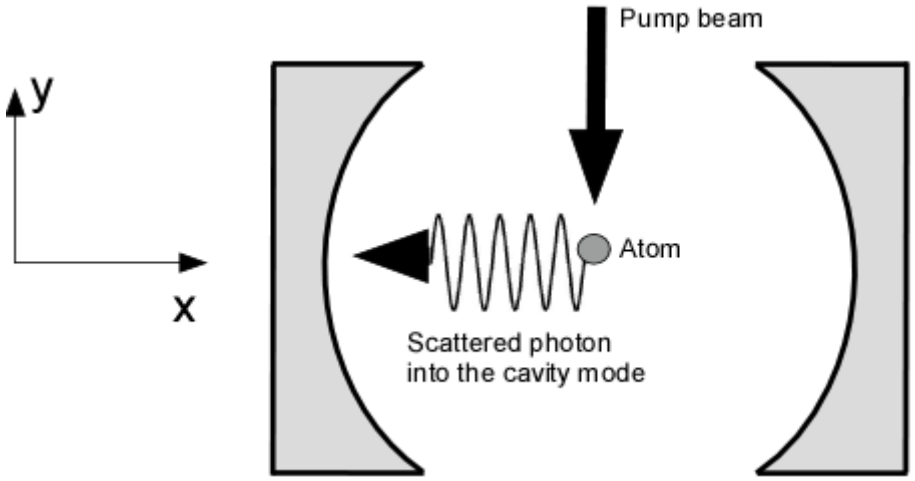

Figure 8: Outline of the cooling scheme. The pump light illuminates the atoms from the side and the atoms can scatter light into the cavity mode. If the pump beam is red-detuned from a cavity resonance, the scattering process from the pump beam into the cavity mode is a dissipative process.

The friction force

Momentum conservation for the scattering process demands:

$$p_2 + \hbar k_s = p_1 + \hbar k_p \tag{66}$$

where p_1 is the momentum of the atom before the scattering event, p_2 is the momentum after the scattering event, $\hbar k_p$ is the momentum of a photon in the pump beam and $\hbar k_s$ is the momentum of a photon in the cavity mode. The energy of an atom after a scattering event can be written as:

$$\begin{aligned} E_2 = \frac{{p_2}^2}{2m} = E_1 + \frac{2p_1\hbar(k_p - k_s)}{2m} + \frac{\hbar^2(k_p - k_s)^2}{2m} = \\ E_1 + v\hbar(k_p - k_s) + \frac{\hbar^2(k_p - k_s)^2}{2m} = E_1 - \hbar\Delta \end{aligned} \tag{67}$$

where v is the velocity of the atom. From energy conservation it follows that the energy difference between a photon from the pump beam and a photon which has been

scattered into cavity is $\hbar\Delta$. If Δ is positive the process of scattering photons from the pump beam into the cavity mode is dissipative.

The momentum transfer of the process of scattering from the pump beam into the cavity mode is the vector $\Delta p = \hbar(k_p - k_s)$, and since both beams affect the direction of the momentum transfer, it is a called a two photon process.

The pump beam is retro-reflected, and the k-vectors for the two directions are: $\pm k_y$. The k-vectors for the two directions for the cavity mode is: $\pm k_x$. Scattering of light from the pump beam with $+k_y$ to the cavity direction with $+k_x$ is called the ++ scattering event.

The frequency of the emitted photon by one of the four scattering events can be calculated from equation 67 by inserting the appropriate k vectors for the scattering event considered. The detuning of the emitted light into a cavity mode in terms of the detuning of the pump light to the cavity mode (δ) for one of the four scattering events is [46]:

$$\delta_{\pm\pm} = -(\pm k_x \mp k_y)\cdot v + \delta - \frac{\hbar k^2}{m} = -(\pm k_x \mp k_y)\cdot v + \delta' \qquad (68)$$

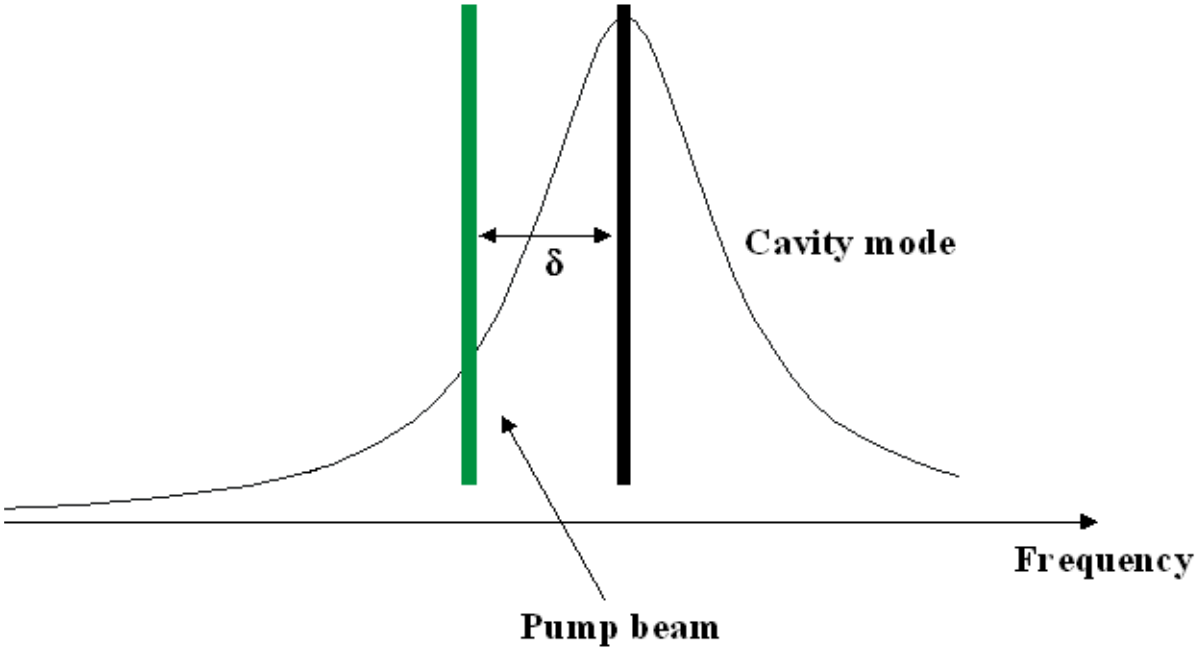

Figure 9: Detuning of the pump beam (δ) to a cavity mode.

Only one cavity mode is considered, and it is assumed that the intensity in the cavity mode is too small to affect the distribution of the atoms inside the cavity mode. The atoms are assumed to be positioned at the focus of the cavity mode.

With the detuning of the emitted photon to the cavity mode known from equation 68, the scattering rate can be calculated from equation 49. The scattering of photons from a pump beam into one of the directions of the cavity mode is a series of discrete momentum changes, where the time interval between two scatterings from the same pump beam into the same direction of the cavity mode is τ_{cavity}.

If instead the series of discrete momentum changes is assumed to be a continues momentum change over time, it is possible to write this as a continues force on an atom in the cavity mode:

$$\begin{aligned} f = &\Gamma\left(\omega+\Delta_{+k_x,+k_y}\right)\hbar\left(k_x-k_y\right)+\Gamma\left(\omega+\Delta_{+k_x,-k_y}\right)\hbar\left(k_x+k_y\right)+ \\ &\Gamma\left(\omega+\Delta_{-k_x,+k_y}\right)\hbar\left(+k_x-k_y\right)+\Gamma\left(\omega+\Delta_{-k_x,-k_y}\right)\hbar\left(-k_x+k_y\right) \end{aligned} \tag{69}$$

where $\Gamma(\omega)$ is the scattering rate from one of the pump beams into one direction of the cavity mode, and where ω is the frequency of the emitted photon. If ω is equal to the frequency of the cavity mode, the scattering rate into one direction of the cavity mode is $\Gamma(\omega)=\frac{\eta_c\Gamma_{free}(\omega)}{2}=\eta_0\Gamma_{free}(\omega)$. $\Gamma_{free}(\omega)$ is the spontaneous emission rate into free space due to scattering from one of the pump beams. The factor ½ is due to the fact that only scattering into one direction of the cavity mode is considered. If the pump beam is detuned relative to the cavity resonance, the scattering is lowered by the factor $1/\left(1+\left(\frac{\omega-\upsilon_c}{\Delta\upsilon}\right)^2\right)$, (see equation 54).

As only one mode of the cavity is considered, it is more obvious to write the frequency ω in terms of the detuning to the cavity mode considered. The scattering rate from scattering one of pump beams into one direction of the cavity mode is [46]:

$$\Gamma(\delta_{\pm\pm}) = \eta_0\frac{\Gamma_{free}}{1+\left(\delta_{\pm\pm}/\Delta\upsilon\right)^2} \tag{70}$$

By inserting the expression for the scattering rate into equation 69, the force along the vectors (k_x-k_y) and (k_x-k_y) can be calculated [46]:

$$f=\hbar\left(k_x-k_y\right)\Gamma_{free}\eta_0\frac{4\delta\delta\Delta\upsilon^2\left(k_x-k_y\right)\cdot v}{\left(\Delta\upsilon^2+\delta_{++}^2\right)\left(\Delta\upsilon^2+\delta_{--}^2\right)}+\hbar\left(k_x+k_y\right)\Gamma_{free}\eta_0\frac{4\delta\delta\Delta\upsilon^2\left(k_x+k_y\right)\cdot v}{\left(\Delta\upsilon^2+\delta_{+-}^2\right)\left(\Delta\upsilon^2+\delta_{-+}^2\right)} \tag{71}$$

If δ' (see equation 68 for the defnition) is negative, the force on an atom along the vectors ($k_x \pm k_y$) will be opposite of the projection of the velocity of the atom on these vectors. In other words f for negative δ' is a friction force.

In Figur 10 the friction force along the k-vector ($+k_x$-k_y) is plotted as a function of the Doppler shift when $\delta' = -\Delta\nu$ is shown. k is the length of the k-vectors ($+k_x \pm k_y$). The capture velocity is defined as the velocity where the friction force has the largest amplitude.

Capture velocity

From equation 71, the capture velocity along the k-vector ($k_x \pm k_y$) can be calculated:

$$v_{capture} = \frac{\Delta\upsilon}{k}\sqrt{\frac{2}{3}\sqrt{1+\left(\frac{\delta'}{\Delta\upsilon}\right)^2+\left(\frac{\delta'}{\Delta\upsilon}\right)^4}+\frac{1}{3}\left(\frac{\delta'}{\Delta\upsilon}\right)^2-\frac{1}{3}} \approx \frac{\delta'}{k} \qquad (72)$$

where the approximation is valid when $\delta'/\Delta\nu >> 1$.

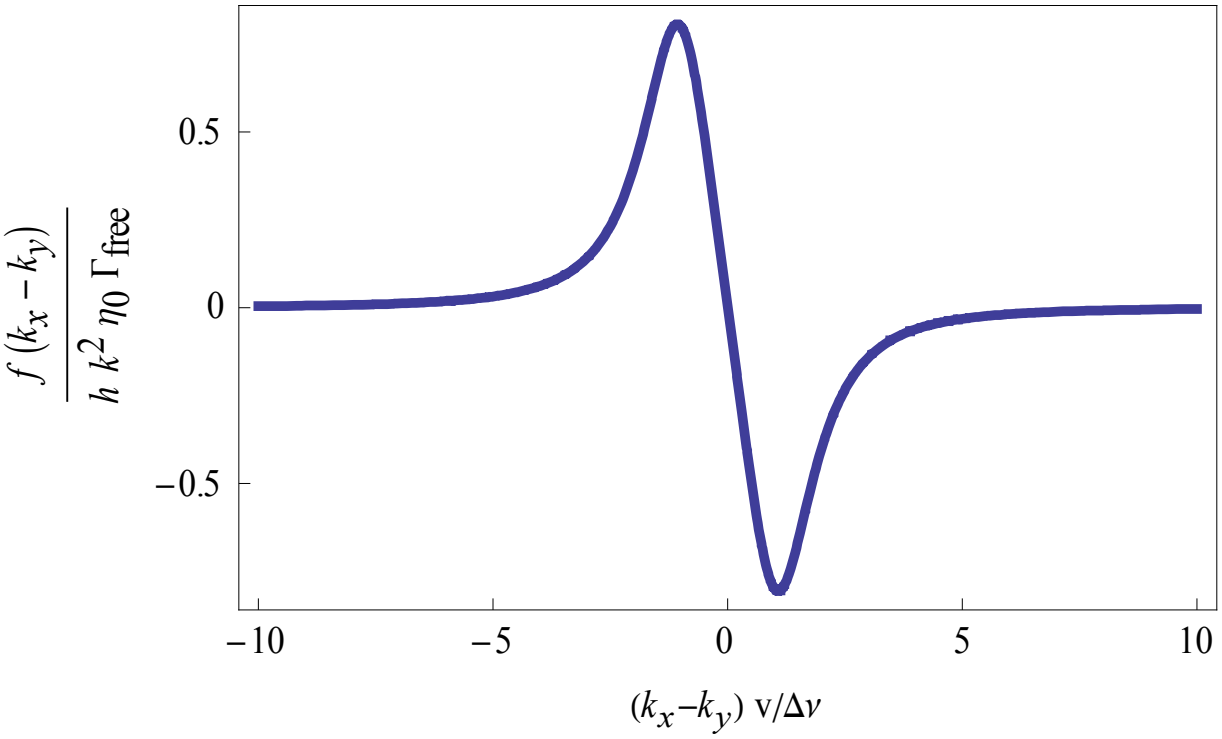

Figure 10: The friction force on an atom in the cavity mode as a function of projection of the velocity of atom on the k-vector (k_x-k_y) . The detuning (δ') is Δν.

Heating rate due to random recoils

The friction force given in equation 71 states that it should be possible to cool an atomic sample to the absolute zero. This unphysical result is due to the assumption that the force on atoms is acting continuously on the atoms and not in a series of discrete momentum kicks. The heating rate due to the discrete nature of momentum changes can be estimated by calculating the heating rate for an atom at T = 0 (e.g. the Doppler shift is set to zero).

The energy change for one scattering event for an atom with v = 0 according to equation 67 is: $\frac{\hbar^2\left(k_p - k_s\right)^2}{2m}$. If the frequency difference between the pump beams and the cavity mode is small, the energy change can be approximated to: $\frac{\hbar^2 k_p{}^2}{m}$. The scattering rate for the four possibilities are the same for v = 0 and is given by equation 70.

The heating rate from scattering from the pump beams into the two directions of the cavity mode is:

$$\gamma_{heating,cavity} = 4\frac{\hbar^2 k_p{}^2}{m}\Gamma(\delta') = 4\eta_0\frac{\hbar^2 k_p{}^2}{m}\frac{\Gamma_{free}}{1+\left(\delta'/\Delta\upsilon\right)^2} \tag{73}$$

The cooling rate due to scattering from the pump beams into free space is the same as the heating rate for standard Doppler cooling. The absorption of a photon from a pump beam and the spontaneous emission can be treated as two different momentum changes and the momentum change for each process is: $\frac{\hbar^2 k_p{}^2}{2m}$.

The heating due to scattering from both pump beams into free space is:

$$\gamma_{heating,free} = 4\frac{\hbar^2 k_p{}^2}{2m}\Gamma_{free} \tag{74}$$

The total heating rate at T = 0 due to the pump laser beams is:

$$\gamma_{heating} = 2\Gamma_{free}\frac{\hbar^2 k_p{}^2}{m}\left(\frac{2\eta_0}{1+\left(\delta'/\Delta\upsilon\right)^2}+1\right) \tag{75}$$

The Doppler temperature

The kinetic energy of an atom in steady state can be estimated by setting the cooling rate for an atom with the velocity v $\left(f\cdot v\right)$ equal to the heating rate at T = 0.

$$\left|f\cdot v\right| = \hbar\Gamma_{free}\eta_0\frac{4\left|\delta'\right|\Delta\upsilon^2 k^2 v^2}{\left(\Delta\upsilon^2+\delta_{++}^2\right)\left(\Delta\upsilon^2+\delta_{--}^2\right)} = \gamma_{heating} = 2\Gamma_{free}\frac{\hbar^2 k_p{}^2}{m}\left(\frac{2\eta_0}{1+\left(\delta'/\Delta\upsilon\right)^2}+1\right)\Leftrightarrow$$

$$\frac{1}{2}mv^2 = \frac{\Gamma_{free}\hbar^2 k_p{}^2\left(\frac{2\eta_0}{1+\left(\delta'/\Delta\Delta\right)^2}+1\right)}{\hbar\Gamma_{free}\eta_0\frac{4\left|\delta'\right|\Delta\upsilon^2 2k_p{}^2}{\left(\Delta\upsilon^2+\delta_{++}^2\right)\left(\Delta\upsilon^2+\delta_{--}^2\right)}} \approx \frac{\hbar\left(\Delta\upsilon^2+\delta_{++}{}^2\right)\left(\Delta\upsilon^2+\delta_{--}{}^2\right)}{2\left|\delta'\right|\Delta\upsilon^2}\frac{1}{1+\left(\delta'/\Delta\upsilon\right)^2} \approx$$

$$\frac{\hbar\Delta\upsilon}{2}\left(\frac{\Delta\upsilon}{\left|\delta'\right|}+\frac{\left|\delta'\right|}{\Delta\upsilon}\right) \tag{76}$$

In the first approximation in equation 76 it is assumed that $\gamma_{\text{heating, cavity}} >> \gamma_{\text{heating, free}}$. In the second approximation in equation 76 it is assumed that $|\delta'| >> k|v|$. With these approximations the minimum kinetic energy has its minimum when $|\delta'| = \Delta\upsilon$ and the kinetic energy for the atom in this case is $\hbar\Delta\upsilon$.

The Doppler temperature is defined as:

$$T_{\text{Doppler,cavity}} = \frac{\hbar\Delta\upsilon}{k_B} \tag{77}$$

The Doppler temperature gives an estimation of which temperatures that can be reached with cavity cooling.

Advantages of cavity cooling

In standard Doppler cooling on an atomic transition the Doppler temperature is [50]:

$$T_{\text{Doppler,atomic transition}} = \frac{\hbar\gamma}{2k_B} \tag{78}$$

where γ is the linewidth of the atomic transition of the cooling transition. The linewidths of the cooling transitions used in standard Doppler cooling are typically several MHz [50] and the corresponding Doppler temperatures are around 100 μK. The cavity linewidth is decided by the finesse and the length of the cavity, and it is possible for large open cavities to have a linewidth of a few kHz. From the comparison of the Doppler temperature for standard Doppler cooling and the one possible in cavity cooling one can expect, that an atom can be cooled to a much lower temperature with cavity cooling than with the standard Doppler cooling and this is one of the major advantages of cavity cooling.

Another advantage of cavity cooling compared to standard Doppler cooling is that in cavity cooling the detuning of the pump beams can be chosen to be far away from any atomic transition. This means that the scattering of light from the pump beams into the cavity mode does not change the internal state of the atom significantly. This avoids the problem of the atom decaying to a dark state for the cooling light as in a MOT. The only demand for an atom or a molecule to be cooled by cavity cooling is that $\Gamma_{\text{free}}(\omega) > 0$. If the atom or molecule can be polarized, there will always be frequencies ω where the free space scattering rate is not zero.

If the pump beams are far detuned from any atomic transition, cavity cooling does not have the same density limitation as standard Doppler cooling has. The scattered photons from the pump beams into free space are also far detuned and the internal pressure these photons create on an atomic sample is much smaller than if these photons had been resonant.

Relevant experimental parameters for the cavity

Parameter	Value
Cavity Doppler temperature	500 nK
Capture velocity (v_c) with $\delta' = \Delta\nu$.	7.8 mm/s
Capture temperature $\frac{mv_c^2}{2k_b}$	320 nK
Recoil temperature at 780	370 nK
Cooling rate	3 μK/ms

Table 2: The cooling rate for the cavity presented in this thesis is calculated with a detuning of one linewidth relative to a cavity mode, the velocity of the atom is the capture velocity, an atomic detuning of 5 GHz and a pump intensity of 10^7 mW/cm^2.

4.3 Self-organization of atoms in a cavity

In the derivation of the cooling force in the previous sub-chapter, the electrical field that can build up inside the cavity due to scattering from the pump beams into the cavity mode was neglected, and this omits a very important aspect of the cavity. The field inside the cavity is a standing wave and if the cavity mode is red-detuned to an atomic transition, the potential minimums are at the anti-nodes of the standing wave. For a sufficiently strong electrical field in the cavity mode, this will force a periodic ordering of the atoms along the propagation direction of the cavity mode.

The periodicity of the atomic distribution depends on the interaction between the atoms in the cavity mode, the pump beam and the cavity mode. In [51] it is shown that for a certain choice of the parameters of the cavity mode and the pump beam, a threshold of the intensity of the pump beam exists above which the periodicity of the steady state atomic distribution inside the cavity mode is λ where λ is the wavelength of the cavity mode. In this thesis, self-organization is understood as the process by which the atomic distribution goes from an initially even one to a one with a periodicity of λ.

When the atoms are ordered λ apart, the photons emitted by the atoms into the cavity mode are all constructively interfering and this greatly enhances scattering [52]. In [53] a factor 2000 difference in the emission intensity from the atoms into the cavity mode above a certain threshold intensity of the pump beam was observed.

The equations describing the interaction between a cavity mode and an atom

The theory of self-organization is discussed in [51,54,55,56,57,58], and in these papers the Heisenberg-Langevin approach is used to describe the interaction between the atoms, a cavity mode and the vacuum modes. A text book introduction to the Heisenberg-Langevin approach can be found in [43]. The electrical field in the cavity mode is assumed to be classical, while the atom is treated as a two level quantum system (semi-classical model). In the limit of a large detuning of the pump light from an atomic transition compared to the linewidth of the atomic transition, the excited state can be adiabatically eliminated.

From these assumptions the following equations can be written as [51]:

$$\frac{d\alpha}{dt} = i\left(\delta - U_0 \sum_j Cos^2(k_p z_j)\right)\alpha - \left(\kappa + \Gamma_0 \sum_j Cos^2(k_p z_j)\right)\alpha - \eta_{eff} \sum_j Cos(k_p z_j) + \xi_\alpha \qquad (79)$$

$$\frac{dp_j}{dt} = -\hbar U_0\left(|\alpha|^2 - \frac{1}{2}\right)\frac{d}{dz}\left(\mathrm{Cos}^2(k_p z_j)\right) - i\hbar\left(\eta^*_{\hat{e}ff}\alpha - \eta_{eff}\alpha^*\right)\frac{d}{dz}\left(\mathrm{Cos}(k_p z_j)\right) + \xi_j \qquad (80)$$

where α is the number of photons in the cavity mode. p_j is the momentum of the atom with the number j (j = 1,2,…,N), z_j is the position of the atom with the number j on the propagation direction of the cavity mode, $U_0 = \frac{g^2\Delta_A}{\Delta_A^2 + \gamma^2}$ is the frequency shift of the cavity mode due to one atom in the cavity mode, $\Gamma_0 = \frac{g^2\gamma}{\Delta_A^2 + \gamma^2}$ is the scattering rate from one atom in the cavity mode into free space, $\eta_{eff} = \frac{\eta g}{\gamma - i\Delta_A}$ is the effective pumping rate, η is the pumping rate, Δ_A is the atomic detuning of the pump beam, g is the coupling strength between an atom and the cavity mode $\left(g = d\sqrt{\frac{\omega_c}{2\hbar\varepsilon V_{eff}}}\right)$, d is the atomic dipole moment, κ is the decay rate of the electrical field of the cavity mode, and ξ are the noise terms due to scattering into free space. A discussion of the derivation of the equations for $\frac{d\alpha}{dt}$ and $\frac{dp_j}{dt}$ can be found in [54,56].

The potential energy of the atoms in the cavity in the mean-field approximation

The self-organization can be understood by the conservative terms in equation 80. In [57] the assumption is made that the cavity field instantly adjusts to the position of the atoms (mean-field approximation). From this assumption, the potential seen by an atom in the cavity mode is:

$$V(z) = U_2 \cos^2(k_p z) + U_1 \cos(k_p z) \qquad (81)$$

where $U_2 = N^2\hbar I_0 U_0 \sum_j \mathrm{Cos}^2(k_p z_j)$, $U_1 = 2N\hbar I_0\left(\delta - NU_0 \sum_j \mathrm{Cos}^2(k_p z_j)\right)\sum_j \mathrm{Cos}(k_p z_j)$ and $I_0 = \frac{|\eta_{eff}|^2}{(\kappa + N\Gamma_0)^2 + (\delta - NU_0)^2}$ is the maximum number of scattered photons into the cavity mode for an atom. If the distribution is not completely even, then $U_1 \neq 0$. If both U_2 and $U_1 < 0$ then $U_2 \cos^2(kz)$ and $U_1 \cos(kz)$ have the same sign for $kz = 2n\pi$ and opposite

sign for kz = (2n+1)π. If the detuning is chosen such that $\delta - NU_0 \sum_j \mathrm{Cos}^2(k_p z_j) < 0$ the sign of U_1 is the opposite of the sign of $\sum_j \mathrm{Cos}(k_p z_j)$. For U_1 to be negative $\sum_j \mathrm{Cos}(k_p z_j)$ must be greater than zero, which means that the atoms must be closer to the points with $\frac{2\pi n}{k}$ compared to the points with $\frac{2\pi(n+1)}{k}$ in order to obtain a sum that is greater than zero.

If there are initially more atoms close to even sites (2n) than at the uneven sites (2n+1), this imbalance creates a stronger confinement at even sites and a weaker confinement at the uneven sites. This imbalance in confinement leads to more atoms at the even sites than at the uneven sites and this in turn creates a greater difference in the confinement between the even and uneven sites. The process that an uneven distribution creates an uneven confinement which then amplifies the difference in the distribution between the even and uneven sites is the physical mechanics for self-organization process.

Threshold power of the pump beam for the self-organization

Thermal fluctuations counteract the self-organization process, and only at a certain intensity of the pump beam, the self-organization process can occur. The depth of the potential of the standing wave of the cavity mode is given by U. In order to confine the atoms at the anti-nodes the following must be true $U > k_b T$ where T is the temperature of the atomic sample in the dipole trap. From this condition, the power in the cavity mode can be estimated to be (P_{cavity}):

$$U > k_b T \Leftrightarrow P_{cavity} > \frac{w_0^2 \omega_c^3 k_b T}{3c^2} \frac{\Delta_a}{\gamma} \tag{82}$$

In steady state the energy scattered from the pump beam into the cavity mode must be equal to the decay of the cavity field.

The cavity field can decay through two methods: loss process at the mirrors (transmission or scattering loss) or by light scattered from the cavity mode into free space by atoms in the cavity mode.

$$h\omega_c \eta_c \Gamma_{pump} N = P_{cavity} \chi + h\omega_c N \Gamma_{cavity} \tag{83}$$

where Γ_{pump} is the scattering rate into the cavity mode due to the pump beam, $\chi = \chi_0 + \chi_1 + \chi_2$ is the total losses at the mirrors, N is the number of atoms in the cavity mode and Γ_{cavity} is the scattering rate from the cavity mode into free space. In the limit of large atomic detuning compared to the natural linewidth and a low saturation, equation 83 can be written as:

$$I_{pump} = I_{sat} \frac{P_{cavity}\left(\chi + \frac{h\omega_c N \gamma^2}{\pi w_0^2 \Delta^2 I_{sat}}\right)}{h\omega_c \eta_c N} \frac{\Delta_a^{\,2}}{\gamma^3} > I_{sat} \frac{w_0^2 k^2 k_b T\left(\chi + \frac{h\omega_c N \gamma^2}{\pi w_0^2 \Delta^2 I_{sat}}\right)}{3h\eta_c N} \frac{\Delta_a^{\,3}}{\gamma^4} \tag{84}$$

where I_{sat} is the saturation intensity.

The power needed for self-organization according to equation 84 has to be greater than 10 $\mu W/cm^2$ with an atomic detuning of 30 nm, a temperature of 1 μK of the atomic sample in the cavity mode, an atom number of 10^5 and the cavity parameters can be found in Table 11. When the atoms self-organize into an atomic distribution with a periodicity of λ, one can expect the scattering rate to increase and thus the threshold for self-organization should therefore be lower than the one predicted from equation 84.

The superradiant and the strongly coupled regime for a self-organized sample

In [55] the dependence of I_{cavity} on the cavity decay rate, the atomic detuning and the atom number is discussed. The power of the pump beam is assumed to be above the threshold for the self-organization, and the atomic sample is assumed to have self-organized into a distribution with the periodicity of λ. With the same assumption as the ones for equation 84, I_{cavity} can be written as:

$$I_{cavity} \sim \frac{N^2}{\left(4\delta^2 + N^2 s^2 4\Delta_a^2 + \kappa^2 + Ns(2\gamma\kappa - 8\delta\kappa)\right)} \tag{85}$$

where $s = \frac{g^2}{\Delta_a^2}$. From Figure 11 two different regimes can be identified. When $N << N_0$, the coupling between the atomic distribution and the cavity mode is weak and the dependence of the intensity in the cavity mode on the atom number is N^2 (superradiance). When the atom number is above N_0 the coupling between the atomic distribution and cavity mode is strong. The intensity of the cavity mode becomes independent of the atom number N in the strong coupling regime because the reason is that the atoms are sitting in the dark. The cavity field and the pump field are of the same order of magnitude in the strongly coupled regime and they destructively interfere [55,58].

The dependence of the N_0 is given by:

$$N_0 = \frac{4\delta^2 + \kappa^2}{s(4\delta\Delta_a - \gamma\kappa)} \tag{86}$$

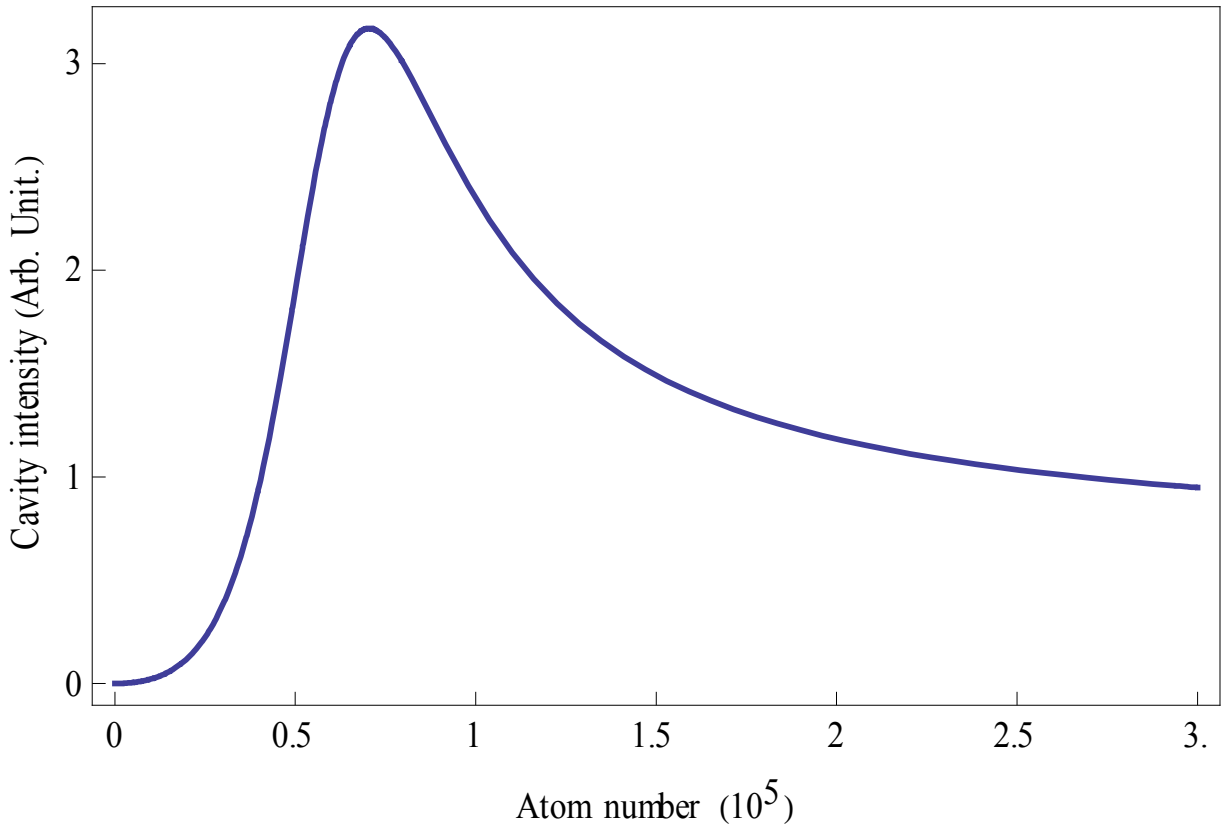

Figure 11: Photon number in the cavity mode in steady state with the atoms illuminated by a pump beam from the side. The atomic sample is assumed to have self-organized into a distribution with a periodicity of λ (see equation 85). The values for the cavity can be found in Table 11, and the atomic detuning (Δ_a) is set to 30 nm. The peak intensity in the cavity mode is at $N_0 = 6\ 10^4$.

The transmitted power through out-coupling mirror in the limit of large N

When $N >> N_0$ the pump beam and the cavity mode have the same intensity at the position of the atoms as they cancel each other in the centre of the cavity mode. From this condition the power in the cavity mode can be calculated as the intensity in the cavity mode in the centre is the same as the one of the pump beam. By multiplying the transmission coefficient (χ_2) of the out-coupling mirror (see Figure 7) with the power in the power in the cavity mode, the power of the transmitted beam through that mirror can be estimated. I_p is the intensity of the pump beam and P_t is the power of the beam transmitted through the out coupling mirror:

$$P_t = \chi_2 \frac{\pi}{2} I_p w_0^2 \tag{87}$$

An intensity of the pump beam of 10^5 W/cm^2, a waist of 30 μm and δ_2 = 1 ppm gives an estimate for P_t of 1 nW.

Cancelling the potential variation along the propagation direction of the cavity mode

In chapter 5.10 it is explained how to keep a fixed detuning of the pump beam to a cavity mode. To achieve this technically it is necessary to have a laser beam resonantly locked to a cavity mode. The in-coupled beam will create a standing wave inside the cavity. For the self-organization process to occur, the depth of the potential of the standing wave due to the directly in-coupled light must be comparable to or smaller than the kinetic energy of the atoms.

If the potential wells are much deeper than the kinetic energy, the atoms are locked into an atomic distribution with a periodicity of $\lambda/2$ with a very low probability to tunnel from one lattice site to the next.

From the potential depth (U_0) given in equation 56, the in-coupled power (P) must be 10 pW for an atomic detuning of 30 nm and in-coupled ratio of 1 (b_{in}) in order to be equal to the recoil temperature of Rb_{87}.

A method to suppress the potential along the cavity axis is to couple a second laser beam into the cavity through a mirror with a frequency difference of one free spectral range ($\Delta q=1$, see equation 43) compared to the cavity mode, which the first laser beam is locked to.

The wavelength of the first laser beam is given by: $q\lambda_1 = 2L$ and the wavelength of the second laser beam is given by: $(q+1)\lambda_2 = 2L$. As the width of the BEC is of the order 100 μm along the propagation direction of the cavity mode and the Rayleigh length (z_0) of the cavity mode is 3 mm, the intensity can be assumed to be constant over the atomic sample near the waist of the cavity mode. Thus, the intensity of the electrical field of both cavity modes near the waist ($z \approx L/2$) is:

$$\begin{aligned} I(z,t) &= \left|E_1 \mathrm{Sin}(k_1 z) e^{i\omega_1 t} + E_2 \mathrm{Sin}(k_2 z) e^{i\omega_{21} t}\right|^2 = \left|E_1 \mathrm{Sin}(k_1 z) + E_2 \mathrm{Sin}(k_2 z) e^{i\Delta\omega t}\right|^2 = \\ & E_1^2 \mathrm{Sin}^2(k_1 z) + E_2^2 \mathrm{Sin}^2(k_2 z) + 2\mathrm{Sin}(k_1 z)\mathrm{Sin}(k_2 z)\mathrm{Cos}(\Delta\omega t) \end{aligned} \tag{88}$$

$\Delta\omega$ is one free spectral range (3 GHz) and it is much faster than all other timescales relevant in the self-organization process. Therefore, the intensity can be averaged over one oscillation period ($2\pi/\Delta\omega$), and the last term in equation 88 has a time average of zero.

$$\begin{aligned} I(z) &= E_1^2 \mathrm{Sin}^2(k_1 z) + E_2^2 \mathrm{Sin}^2(k_2 z) = E_1^2 \mathrm{Sin}^2\left(\frac{n\pi}{L}x\right) + E_2^2 \mathrm{Sin}^2\left(\frac{n\pi}{L}x + \frac{\pi}{L}x\right) \\ &\approx E_1^2 \mathrm{Sin}^2\left(\frac{n\pi}{L}x\right) + E_2^2 \mathrm{Cos}^2\left(\frac{n\pi}{L}x\right)\mathrm{Sin}^2\left(\frac{\pi}{L}x\right) \approx E_1^2 \mathrm{Sin}^2\left(\frac{n\pi}{L}x\right) + E_2^2 \mathrm{Cos}^2\left(\frac{n\pi}{L}x\right)\left(1 - \left(\frac{n\pi}{L}x\right)^2\right) \\ &= E_1^2 \mathrm{Sin}^2\left(\frac{n\pi}{L}x\right) + E_2^2 \mathrm{Cos}^2\left(\frac{n\pi}{L}x\right) - \left(\frac{n\pi}{L}x\right)^2 E_2^2 \mathrm{Cos}^2\left(\frac{n\pi}{L}x\right) \end{aligned} \tag{89}$$

For $E_2 = E_1$ the potential variation along the propagation direction near the waist is suppressed by a factor $a = \left(\frac{\pi}{L}x\right)^2 \approx 4\,10^{-6}$ for $x = 100\,\mu\mathrm{m}$ compared to the situation without a

second laser beam coupled in. Depending on the achievable stability of the two laser intensities it is possible to stabilize with a much higher power than the 10 pW, and there is still no lattice along the propagation direction of the cavity mode at the position of the BEC. In the directions perpendicular to the propagation direction of the cavity mode, the confinement near the waist is the same as for only one laser beam coupled in.

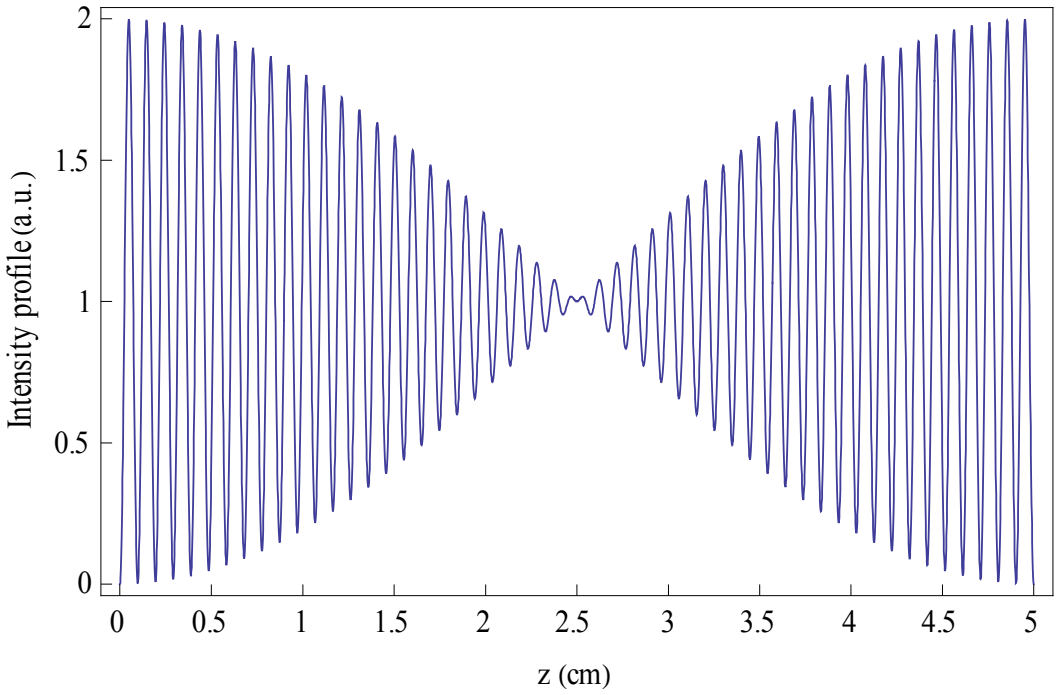

Figure 12: Intensity profile inside the cavity along the propagation direction of the cavity mode. The length of the cavity is set to 5 cm. The intensities of both laser beams are equal.

Relevant parameters for self-organization

Parameter	Value
Threshold intensity for self-organization	10 μW/cm2
Number of atoms for strong coupling at 30 nm detuning from an atomic resonance (N0)	$6\ 10^4$
Expected transmitted power through outcoupling mirror with pump intensity of 105 mW/cm2 (Pt)	1 nW

Table 3: The atomic detuning is 30 nm.

4.4 Cavity sideband cooling

Atoms tightly bond in a harmonic trap can be cooled by illuminating them with a pump beam. The pump beam can induce transitions from one vibrational state of the atom to another state. The symmetry between the probability for a transition from the initial state to a vibrational state with more energy (heating transition), and the probability for the transition from the initial state to a vibrational state with less energy (cooling transition) can be broken by the cavity. This asymmetry can be used to cool an atom by making the cooling transition more likely than the heating transitions.

Emission spectrum of a bound atom

Laser cooling of bound atoms is described in [59,60]. The electrical field of the radiation from an atom in the cavity mode into one of the directions of the cavity mode is: $\vec{E}(z,t) = \vec{E}_0 \mathrm{Sin}(k_p z - \omega t)$ where $\vec{E}_0$ is the maximum electrical field along the propagation direction of the cavity mode and ω is the frequency of the emitted light for an atom at rest with respect to the cavity.

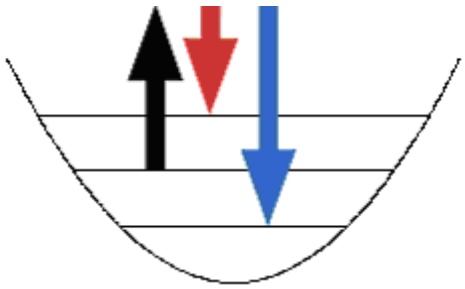

Figure 13: Sideband cooling of bound atoms in a harmonic potential. The cavity breaks the symmetry between scattering events, which heat an atom (red arrow), and the scattering events that cool an atom (blue arrow).

The oscillation of a bound atom in a harmonic trap is: $z(t) = z_a \mathrm{Sin}(\Omega_z t + \varphi_z)$ where Ω_z is the oscillation frequency for the harmonic trap, z_a is the amplitude of the oscillation and φ_z is the phase, which can be set to zero since only one atom is being considered. Then the electrical field emitted by the atom is: $\vec{E}(t) = \vec{E}_0 \mathrm{Sin}(k_p z_a \mathrm{Sin}(\Omega_z t) - \omega t)$. The electrical field $\vec{E}(t)$ can be expanded as: $\vec{E}(t) = \sum_{j=-\infty}^{\infty} J_j^2(k_p z_a) \mathrm{Sin}((\omega + j\Omega_z)t)$, where j is an integer and $J_j(k_p z_a)$ is the Bessel function of the first kind [59]. If $k_p z_a << 1$ (the Lamb Dicke Limit) is valid, the amplitude of the sidebands $\omega \pm \Omega$ is much larger than the amplitude of the sidebands, where $|j| \geq 2$.

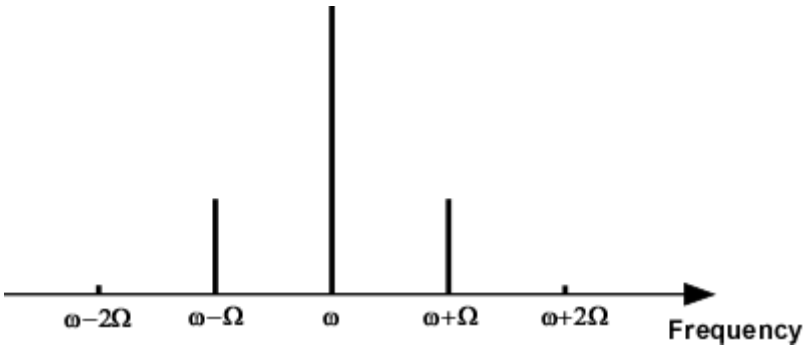

Figure 14: The amplitudes of the sidebands for $k_p z_a = 1$.

The cooling rate for a single sideband for an atom in the classical limit

The cooling (heating) rate for scattering from the pump beam into the sideband ω+jΩ is [59]:

$$\frac{dE}{dt} = -\hbar j\Omega_z I_w(\delta_j) J_j^2(k_p z_a) \tag{90}$$

where $\delta_j = \delta - \frac{\hbar k_p^2}{m} - j\Omega_z$, δ is the frequency difference between the pump beam and the cavity mode, $I_w(\delta_j)$ is the scattering rate into the cavity mode at the detuning δ_j and $J_j^2(k_p z_a)\eta_0 \frac{\Gamma_{free}}{1+(\delta_j/\Delta\upsilon)^2}$ is the scattering rate from the pump beam into one direction of the cavity mode with the frequency (ω+jΩ). As in cavity Doppler cooling the random recoils heat the atom and each recoil heats an atom at rest with $\frac{\hbar^2 k_p^2}{m}$.

The total cooling (heating) rate is:

$$\frac{dE}{dt} = \left(\frac{\hbar^2 k_p^2}{m} - \hbar j\Omega_x\right) J_j^2(k_p z_a)\eta_0 \frac{\Gamma_{free}}{1+(\delta_j/\Delta\upsilon)^2} \tag{91}$$

equation 91 is only valid when the energy of the atom is high compared to the energy of the ground state $\left(\frac{1}{2}\hbar\Omega_z\right)$.

The cooling rate for a single sideband for an atom quantum mechanically

To calculate the cooling (heating) rate at low temperatures the scattering rate from one vibrational state to another has to be calculated by quantum mechanics.

The eigenstate with the energy E_n of the atom in the harmonic trap, and N photons in the cavity mode with the frequency (ω+jΩ) is written as $|n,N\rangle$. If the atom is at the focus, and the only field along the propagation direction is considered (y = x = 0), the electrical field for one direction of the cavity mode can be approximated to $E(z,t) = i\varepsilon_{max} e^{i(kz+\omega t)}\hat{a} + h.c.$ (see equation 50).

The scattering rate for the transition from the state $|n',1\rangle$ to the state $|n,0\rangle$ is given by Fermi Golden Rule:

$$\frac{1}{\tau_{\omega+j\Omega}} = \frac{2\pi}{\hbar}\rho(\omega)\left|\langle n',1|E(z,t)|n,0\rangle\right|^2 = \frac{2\pi}{\hbar}\rho(\omega+j\Omega)\left|\langle n'|e^{-i(kz+\omega t)}|n\rangle\right|^2\left|\langle 0|i\varepsilon_{max}\hat{a}\ |1\rangle\right|^2$$
$$= \left|\langle n|e^{ikz}|n'\rangle\right|^2 \frac{1}{\tau_{cavity}(\omega+j\Omega)} \qquad (92)$$

where $\frac{1}{\tau_{cavity}(\omega+j\Omega)}$ is the scattering rate from the pump beam into one direction of the cavity for a free atom. From equation 92 it follows that in equation 91 the term $J_j^2(k_p z_a)$ must be substituted with $\left|\langle n|e^{ikz}|n'\rangle\right|^2$ in order to obtain the cooling (heating) rate for the transition from the vibrational state $|n\rangle$ to the vibrational state $|n'\rangle$.

The cooling rate of a thermal sample

An estimate for the cooling (heating) rate at a given temperature can be found by averaging equation 91 over a thermal distribution:

$$\frac{dE}{dt} = \sum_{n,n'=0}^{\infty} p_n\left(\frac{\hbar^2 k_p^{\ 2}}{m} - \hbar(n-n')\Omega_z\right)\left|\langle n|e^{ikz}|n'\rangle\right|^2 \eta_0 \frac{\Gamma_{free}}{1+\frac{(\delta - R - (n-n')\Omega_z)^2}{\Delta\upsilon^2}} \qquad (93)$$

where p_n is the probability for the atom to be in the vibrational state $|n\rangle$ and $R = \frac{\hbar k_p^{\ 2}}{m}$. It was required to evaluate equation 93 in the limit of low temperatures. At low temperatures it is possible to assume that all the relevant eigenstates are strongly bound in the trap $\left(k_p\sqrt{\langle n|z^2|n\rangle} << 1\right)$ and with this assumption $\left|\langle n|e^{ik_p z}|n'\rangle\right|^2$ can be approximated to $\left|\langle n|1+ikz|n'\rangle\right|^2$. The matrix elements can be evaluated as: $\langle n|z|n'\rangle = \sqrt{n} z_b \delta_{1,|n-n'|}$ and $\langle n|n'\rangle = \delta_{n,n'}$, where $z_b = \sqrt{\frac{\hbar}{2m\Omega_z}}$ is the width of the ground state [59].

The detuning δ of the pump beam is chosen such that the scattered photon from the pump beam into the sideband ω+Ω is resonant with the cavity $(\delta = R + \Omega)$, and it is assumed

that: $\Omega_z >> R$ and $\Omega_z >> \Delta\nu$. From these approximations, the cooling rate at low temperatures can be estimated as:

$$\frac{dE}{dt} \approx \eta_0 \Gamma_{free} \sum_{n=0}^{\infty} p_n \left(\hbar \Omega_z z_b^2 k_p^2 (n+1) \frac{\Delta\upsilon^2}{4\Omega_z^2} + \frac{\hbar^2 k_p^2}{m} \frac{\Delta\upsilon^2}{\Omega_z^2} - \hbar \Omega_z z_b^2 k_p^2 n \right) \approx \eta_0 \Gamma_{free} \frac{\hbar^2 k_p^2}{m} \left(\frac{9\Delta\upsilon^2}{8\Omega_z^2} - \frac{1}{2} \langle n_z \rangle \right) \tag{94}$$

where $\langle n_z \rangle = \sum_{n=0}^{\infty} p_n n$. The cooling rate in equation 94 is valid for scattering from one direction of the pump beam into one direction of the cavity mode. The total cooling rate for scattering from both directions of the pump beams and into both directions of the cavity mode is 4 larger than the rate given in equation 94.

The heating rate due to scattering from the pump beams into free space is given by equation 74 and the total cooling rate is then:

$$\frac{dE}{dt} \approx \eta_0 \Gamma_{free} \frac{\hbar^2 k_p^2}{m} \left(\frac{1}{2\eta_0} + \frac{9\Delta\upsilon^2}{8\Omega_z^2} - \frac{1}{2} \langle n_z \rangle \right) \tag{95}$$

The steady temperature

The steady state is found by setting $\frac{dE}{dt} = 0$:

$$\langle n_z \rangle_{sready\ state} = \frac{1}{\eta_0} + \frac{9\Delta\upsilon^2}{8\Omega_z^2} \tag{96}$$

The temperature of the steady state is given by:

$$T = \frac{h\Omega_z \langle n_z \rangle_{sready\ state}}{k_B} = \frac{h}{k_B} \left(\frac{\Omega_z}{\eta_0} + \frac{9\Delta\upsilon^2}{8\Omega_z} \right) \tag{97}$$

Number of vibrational states that can be simultaneously cooled

In equation 63 the energy difference between the vibrational states $|n+1\rangle$ and $|n\rangle$ due to the fourth order terms in the potential was calculate. From this calculation, one can see that if the pump beam is resonant with the transition from $|1\rangle$ to $|0\rangle$, the pump beam has a detuning to the transitions from $|n+1\rangle$ to $|n\rangle$ vibrational states.

The number $n_{capture}$ where the detuning is less than the linewidth of the cavity can be estimated from equation 98:¨

$$n_{capture}\frac{\hbar^2 k^2}{2m} = \hbar\Delta\nu \Leftrightarrow n_{capture} = \frac{2m\Delta\nu}{\hbar k^2} \tag{98}$$

From equation 98 one can see that $n_{capture}$ is the number of random recoils the atom can undergo before it moves out of resonance. In cavity Doppler cooling the number of random recoils the atom can undergo, before the Doppler shift is too large for the atom to be resonant with the transition from the pump beam to the cavity mode, is the same as the one in equation 98.

Parameters relevant for cavity sideband cooling with the cavity

In Table 4 the heating rates, the cooling rate and trap parameters for the dipole trap with the power of the incoming beam at 1 μW (P) are calculated. The heating rate due to lattice is calculated at the wavelength 825 nm. The saturation of the pump beam (s_p) is set to 1000 at the position of the atomic cloud, and the detuning to D2 line is 0.2 nm red-detuned (10 GHz).

Parameter	**Value**
Ω_x , Ω_y	45 kHz
Ω_x	8.3 MHz
$n_{capture}$	2.7
Trap depth	4.7 mK
P_{heat}	0,15 nK/ms
$P_{sideband,\ cooling}$	$500\ \frac{nK}{ms}\langle n_z\rangle$
$P_{sideband,\ heating\ (z\text{-}axis)}$	30 nK/ms
$P_{sideband,\ heating\ (x\text{-}axis)}$	2 μK/ms
$\langle n_z\rangle_{sready\ state}$	0.06
$\langle n_x\rangle_{sready\ state}$	4.3
Energy of $\langle n_z\rangle_{sready\ state}$	$kb\,25\,\mu K\,\langle n_z\rangle$
Energy of $\langle n_x\rangle_{sready\ state}$	$kb\,9{,}5\,\mu K\,\langle n_z\rangle$

Table 4 Parameters for sideband cooling of a single atom. Power of the incoming beam to the in-coupling mirror is 1 μW.

$$\text{where } P_{sideband\ cooling} = 2\eta_0\Gamma_{free}\frac{\hbar^2 k_p^2}{m} \text{ and } P_{sideband\ heating} = 4\eta_0\Gamma_{free}\frac{\hbar^2 k_p^2}{m}\left(\frac{1}{\eta_0}+\frac{9\Delta\upsilon^2}{4\Omega_z^2}\right).$$

The values for the x-axis come from substituting z with x in the relevant equations.

4.5 Cavity cooling with a blue detuned cavity mode

In the previous chapters a laser beam which is red-detuned to a cavity resonance was considered. Another possibility for cooling is to have two cavity mode with a specific frequency difference. A dissipative process is created if light is scattered from the cavity mode with the least frequency of the two modes to the other cavity mode.

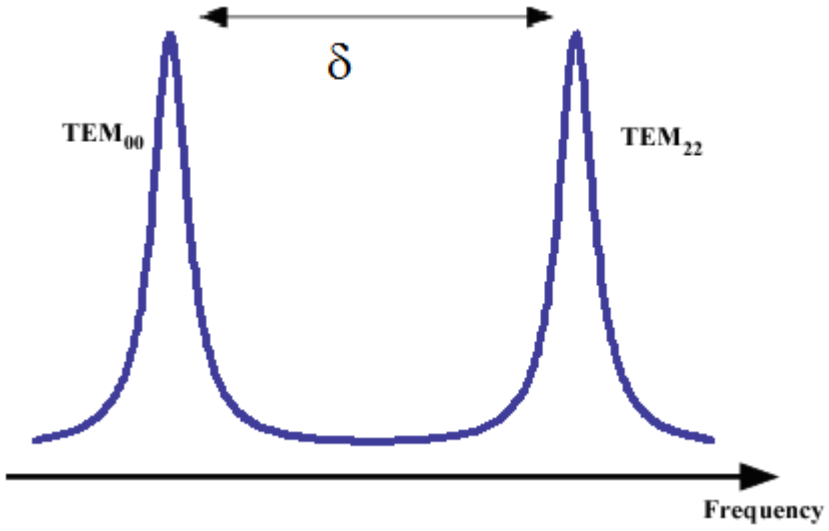

Figure 15: Cavity cooling with two cavity modes. The frequency difference between the two modes is δ. Light is coupled into the TEM_{00} mode, and when light is scattered from the TEM_{00} into the TEM_{22} mode, energy is transferred from the kinetic energy of the atom to a light field.

Cavity length for frequency degeneracy of a TEM_{00} and a TEM_{22} mode

The higher-order Gaussian mode with the highest field per photon in the centre of cavity is the TEM_{22} mode. The mode volume of the TEM_{22} is four times higher than the TEM_{00} mode, and due to this the scattering ratio into the TEM_{22} mode compared to the TEM_{00} mode is four times lower. The resonance frequency of a higher-order Gaussian mode is given by [39]:

$$f_{q,m,n} = \frac{c}{2L}\left(q + \frac{1}{\pi}(m+n)\mathrm{Cos}^{-1}\left(\sqrt{g_1 g_2}\right)\right) \tag{99}$$

According to equation 99, the condition of the g-numbers for a TEM_{00} mode and a TEM_{22} mode to have a resonance frequency at the same length is: $\mathrm{Cos}^{-1}\left(\sqrt{g_1 g_2}\right) = \frac{\pi}{4}$. From this condition, the length of the cavity can be calculated $\left(L = \left(1 \pm \sqrt{2}\right)R\right)$.

Drift of the frequency difference between the two modes due a length change of the cavity

The frequency change between TEM_{00} and TEM_{22} modes due to a small change in the length of the cavity (ΔL) to the first order in ΔL at $L = \left(1+\sqrt{2}\right)R$ is:

$$\Delta f = \sqrt{2}\frac{\Delta L}{R}\frac{c}{2L} \tag{100}$$

Frequency oscillation of the cavity

Because of the fact that the amplitude of the oscillation of the cavity length can be estimated by locking a laser to a reference cavity (transfer cavity), which one can assume to be absolutely stable compared to the cavity (experimental cavity), one wish to measure the oscillation amplitude of (for the set-up see chapter 5.10). The length of the experimental cavity can be varied by adding a voltage ramp to a piezo, which one mirror of the experimental cavity is mounted upon. A voltage scan of 33 V changes the frequency of a cavity mode with one FSR (3 GHz). On the scan of piezo it can be observed that the random swinging of the cavity mode of the experimental cavity corresponds to 0.2 V applied to piezo, and from this it follows that the cavity mode at 825 nm has an absolute variation of 20 MHz. The corresponding length change of the experimental cavity is 3 nm if it is assumed that the entire swinging of the cavity mode is due to the length change of the experimental cavity. By inserting 3 nm for ΔL in equation 100 the frequency variation between the TEM_{00} and the TEM_{22} due to the oscillation of the cavity length is 500 Hz. This frequency variation is significantly smaller than the linewidth of the experimental cavity.

An advantage of using a blue detuned cavity mode for the atoms to scatter into instead of having a red detuned laser beam is that the in-coupled light can be directly locked to the experimental cavity with the current lock. The current lock has a much greater frequency span than the AOM lock where it can follow the oscillation of the cavity mode and it has a much simpler technical realization. Another experimental advantage of using a blue-detuned cavity mode is that atoms perfectly overlap with the cooling mode when they are trapped in the TEM_{00} mode.

The disadvantage is the extra heating due to having a resonant cavity mode, and the lower mode volume of a TEM_{22} compared to a TEM_{00} mode.

4.6 Normal mode splitting of a ring cavity mode

In the previous chapter a blue detuned higher-order Gaussian mode was suggested to be used for cooling. One of the disadvantages of using a higher Gaussian order mode compared to a TEM_{00} mode for cooling is the higher mode volume. A method to avoid this problem is to use the normal mode splitting of a cavity mode in the strongly coupled regime [61].

In the strongly coupled regime between an atomic sample and a cavity mode the resonance of the cavity mode splits into two resonances. By scattering light from the normal mode with the lower frequency of the two normal modes into the other normal mode, a dissipative process can be created. The advantage compared to the method suggested in the previous chapter is that both normal modes are TEM_{00} modes. The disadvantage is that the frequency difference between the two normal modes depend on the atom number, and thus the resonance condition therefore has to be adjusted when the atom number changes.

The normal mode splitting has been investigated with near resonant probe beams [62,63]. One of the major advantages of cavity cooling is the possibility to use far off-resonant light, and the normal mode splitting has been measured with a far off-resonant probe in a ring cavity [86]. The theoretical background and the results of the measurement of the normal mode splitting of a mode in a ring cavity with a far off-resonant probe are reported in this chapter.

The dynamics of N atoms in a ring cavity

In [64] the dynamics of N two-level atoms in a weakly pumped ring cavity is investigated. The two propagation directions in the ring cavity are denoted by + and -, and the electrical fields for the two directions are given by:

$$\left\langle \dot{\alpha}_{\pm} \right\rangle = \left(-\kappa - N\Gamma_0 + i\left(\delta - NU_0\right)\right)\left\langle \alpha_{\pm} \right\rangle - \left(\Gamma_0 + iU_0\right)\left\langle \alpha_{\mp} \right\rangle \sum_{n=1}^{N} e^{\mp ikz_n} + \eta_{\pm} \tag{101}$$

where $\left\langle \alpha_{\pm} \right\rangle$ is the amplitude of the electrical field of the cavity mode propagating in the (±)-direction and $\eta_{\pm}$ is the pumping strength in the (±)-direction. The other quantities are the same as the ones in equation 79. For an even distribution along the propagation direction of the cavity modes: $\sum_{n=1}^{N} e^{\mp ikz_n} = 0$ which means that no photons are scattered by the atoms from one direction into the other. Only forward scattering by the two directions is possible.

For an inhomogeneous atomic distribution the term $\sum_{n=1}^{N} e^{\mp ikz_n}$ can be different from zero, and in that case, photons can be scattered from one direction into the other. The number of photons scattered from one direction into the other direction depend on the number of atoms and their localization along the propagation direction of the cavity modes. The localization along the propagation direction of a cavity mode is defined as:

$$\xi_{ax,\pm} \equiv \frac{1}{N} \sum_{n=1}^{N} e^{\mp ikz_n} \tag{102}$$

When the number of photons scattered from one direction to the other for a perfectly localized atomic distribution $\left(\xi_{ax,\pm} = 1\right)$ is comparable to the number of forward scattered photons, the interaction between the atoms and the cavity mode is said to be in the strongly coupled regime. It is defined as: $NU_0 \geq \kappa$.

The steady state solutions of the electrical fields in the two directions of equation 101 are:

$$\langle \alpha_{\pm} \rangle = \frac{\eta_{\pm}\left(-\kappa - N\Gamma_0 + i\left(\delta - NU_0\right)\right) + \eta_{\mp}\left(\Gamma_0 + iU_0\right)N\xi_{ax,\mp}}{\left(-\kappa - N\Gamma_0 + i\left(\delta - NU_0\right)\right)^2 - N^2\xi_{ax,\pm}\xi_{ax,\mp}\left(\Gamma_0 + iU_0\right)^2} \tag{103}$$

To simplify equation 103, it is assumed that the scattering rate of an atom into free space can be set to zero ($\Gamma_0 = 0$). The effective detuning is defined as: $\delta_{ef} = \delta - NU_0$. The atomic distribution is assumed to be periodic with half the wavelength ($\lambda/2$) of the cavity modes and with a phase difference χ to the optical lattice formed by the two counter propagating cavity modes. In that case $\xi_{ax,\pm} \equiv \frac{1}{N}\sum_{n=1}^{N} e^{\mp ikz_n} = \left|\frac{1}{N}\sum_{n=1}^{N} e^{\mp ikz_n}\right| e^{-i\chi} = \xi_{ax} e^{-i\chi}$ where $0 \le \xi_{ax} \le 1$.

ε is defined as the fraction in the intensity pumped into the (+)-direction subtracted the fraction pumped into the (-)-direction: $|\eta_{\pm}|^2 = \frac{(1 \pm \varepsilon)}{2}\left(|\eta_{+}|^2 + |\eta_{-}|^2\right)$. The effective coupling between the optical lattice and the cavity mode is defined as: $g_{ef} = N\xi_{ax}U_0$.

From the mentioned simplifications the electrical field of the two cavity modes are proportional to [86]:

$$\langle \alpha_{\pm} \rangle \sim \frac{\sqrt{1 \pm \varepsilon}\left(i\delta_{ef} - \kappa\right) + ig_{ef}e^{\pm i\chi}\sqrt{1 \mp \varepsilon}}{\left(i\left(\delta_{ef} - g_{ef}\right) - \kappa\right)\left(i\left(\delta_{ef} + g_{ef}\right) - \kappa\right)} \tag{104}$$

In the following paragraph ε is set to 1 and the intensity in the (+)-direction is considered $\left(\left|\langle \alpha_{+} \rangle\right|^2\right)$.

Normal mode splitting

When the coupling between the atoms and the optical lattice is weak $\left(g_{ef} \le \kappa\sqrt{\sqrt{5} - 2}\right)$, there is only a single maximum at $\delta_{ef} = 0$ for $\left(\left|\langle \alpha_{+}(\delta_{ef}) \rangle\right|^2\right)$. For $\left(g_{ef} > \kappa\sqrt{\sqrt{5} - 2}\right)$ the resonance splits into two and there is a local minimum at $\delta_{ef} = 0$. When $g_{ef} >> \kappa$ the frequency difference between the two normal modes ($\Delta\omega$) is:

$$\Delta\omega = 2g_{ef} = 2N\xi_{ax}U_0 \tag{105}$$

The normal mode splitting can be understood in a simple picture. In the strongly coupled regime an optical lattice is formed due to scattering between the two directions. The anti-nodes of the optical lattice can either be at the maximums of the atomic distribution or at the minimums. In the case where the anti-nodes are at the maximums of the atomic distribution, the interaction is maximized. Similarly if the anti-nodes are the minimums of the atomic distribution, the interaction is minimized.

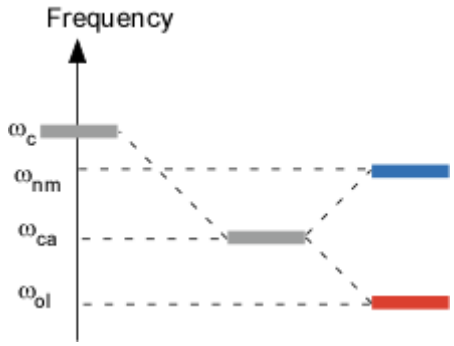

Figure 16: The relative frequency of the cavity mode is shown for different atomic distributions along the propagation direction of the cavity mode. ω_c is the frequency of the cavity mode in case of no atoms in the cavity mode. ω_{ca} is the frequency of the cavity mode for an even distribution of the atoms along the propagation direction of the cavity mode. ω_{nm} and ω_{ol} are the frequencies of the two normal modes in the strongly coupled regime, and for an atomic distribution with a periodicity of λ/2.

If the atomic distribution is perfectly localized at the nodes of the optical lattice, the frequency of corresponding normal mode is the same as the one for the cavity mode without any atoms in the cavity mode. The atoms are sitting completely in the dark.

Equation 101 does not accounted for the fact that the atoms are not perfectly localized radial on the propagation direction of the cavity modes. The radial localization can be defined as: $\xi_{rad} \equiv \frac{1}{N}\sum_{n=1}^{N} e^{\frac{-2\left(x_n^2+y_n^2\right)}{w_0^2}}$. The effective detuning and the effective coupling are respectively by including the radial localization: $\delta_{ef} = \delta - \xi_{rad} N U_0$ and $g_{ef} = N\xi_{rad}\xi_{ax} U_0$.

The ring cavity set-up

The experimental set-up used to measure the normal mode splitting is a different experimental set-up than the one described in the other chapters in this thesis. The experimental set-up is a ring cavity where a cold atomic sample of a few 10^6 atoms at 100 μK can be loaded into an optical lattice from a MOT. An optical lattice is created by two counter-propagating modes of the ring cavity, which are pumped with the same intensity. Only the (-)-direction is kept resonant with the ring cavity with a PDH lock.

A probe laser phase locked to the laser, which generated the beams for the optical lattice, was used to probe the transmission spectrum of the cavity with different number of atoms in the cavity mode. The power of the (+)-direction of the probe beam and the lattice laser is measured with a photodiode.

An outline of the experimental set-up can be seen in Figure 17, and in [65,71] a detailed discussion of the entire experimental set-up can be found.

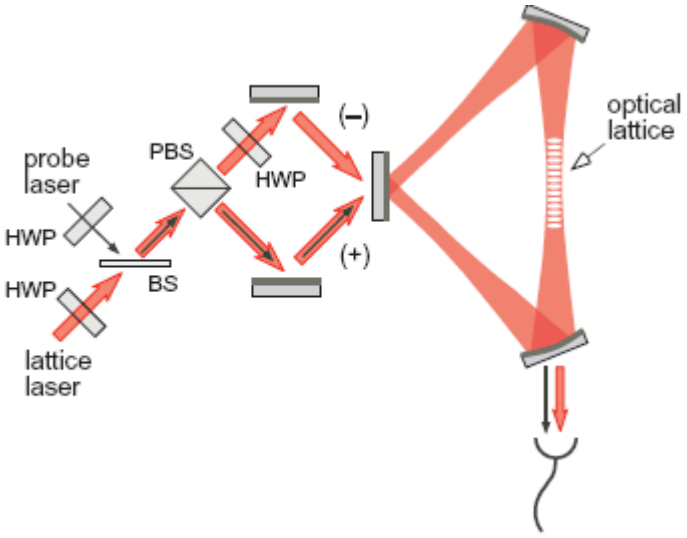

Figure 17: Outline of the experimental set-up. The ring cavity has stable cavity modes propagating in opposite direction. One direction is denoted as the (+) direction and the other direction as (-). A far detuned laser (the lattice laser) is coupled into two modes with opposite directions with equal intensity, and the two counter propagating modes forms an optical lattice. An atomic sample is held in this optical lattice. A second laser (the probe laser) is used measure the transmission spectrum of the ring cavity, and the polarization of the probe laser beam is chosen such that the maximum fraction of the light is coupled to the (+) direction (96,5%). The probe laser is phase locked to the lattice laser, and the technical details of the phase lock can be found in [87]. The direction (-) is kept with a PDH lock resonant with a ring cavity mode. PBS = Polarizing beam cube. HWP = Half Waveplate. BS = Beamsplitter.

Parameter	Value
Finesse	$1.8\ 10^5$
Waist	97 μm
Cavity linewidth	17 kHz
η_c	0.6
Lifetime of the atomic sample in the optical lattice	300 μs
Temperature of the atomic sample in the optical lattice	123 μK
Trap depth	350 μK
Axial trap frequency	331.1 kHz
Radial trap frequency	459 Hz

Table 5: Parameters for the ring cavity and the properties of the optical lattice of the lattice laser can be seen in [65,71]. The lattice of the probe laser is not included in the numbers.

Measurement results of the normal mode splitting

The wavelength of the probe and the lattice beams is: 780.9 nm. The transmission spectrum of the probe laser as a function of the frequency for various atom numbers was measured (see Figure 18). In Figure 18 the normal mode splitting can be observed at an atom number slightly above 10^6 atoms, and 10^6 atoms is the predicted atom number for strong coupling at the atomic detuning of 0.7 nm. The two normal modes do not have the same amplitude and this is due to the fact that the probe beam pumps both directions.

If $\varepsilon = 1$, the two normal modes would have identical amplitudes as the term with $e^{-i\chi}$ drops out of the equation for $\langle \alpha_+ \rangle$.

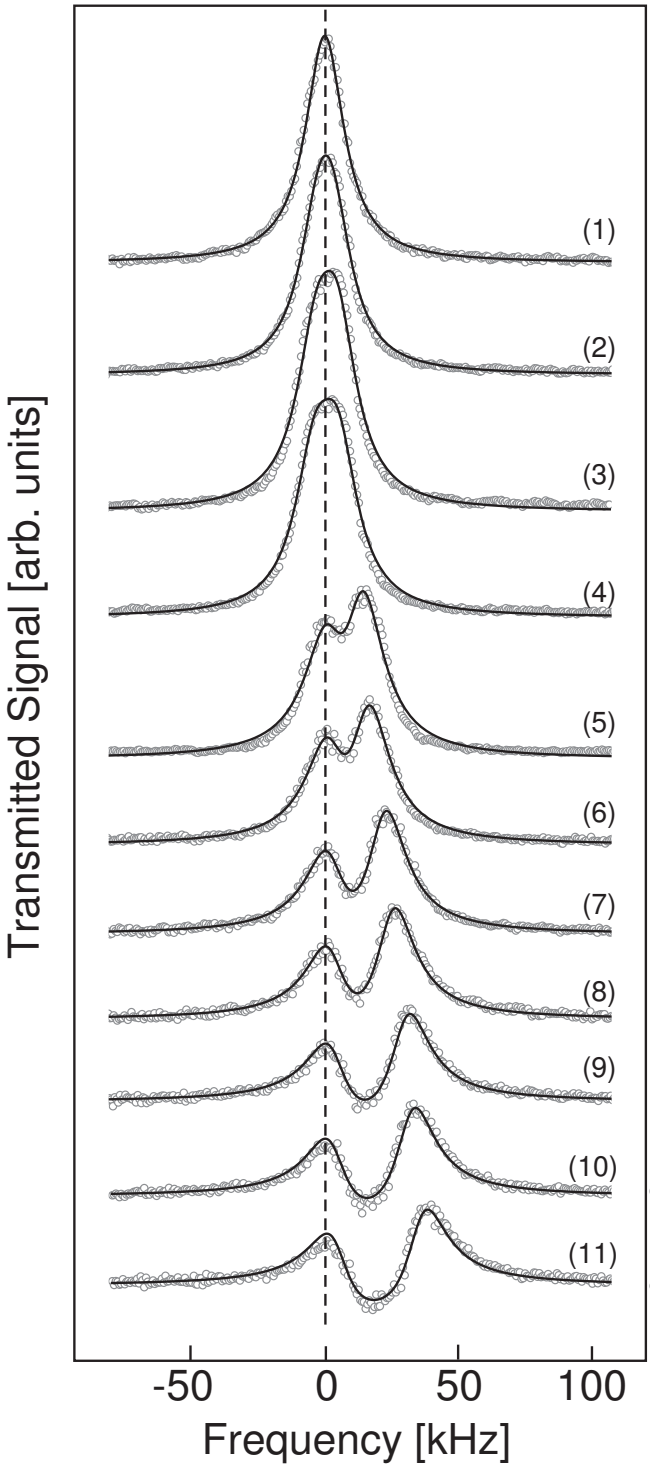

Figure 18: The transmission spectra of the probe laser as a function of the effective detuning of the probe laser beam for different atom numbers. The traces are numbered from above from 1 to 11 at the bottom. The corresponding atoms are (0, 0.28, 0.55, 0.83, 1.10, 1.38, 1.66, 1.93, 2.21, 2.48, 2.76) x 10^6 where trace 1 is for no atoms in the cavity mode. The grey circles are the measured values, and the black lines are the fitted functions to measure experimental measured values (see equation 106). At each value the transmitted field was allowed to reach its steady state value.

In Figure 18, the measured intensity at $\delta_{ef} = 0$ with the highest atom numbers is below the level when the probe beam is far off resonant with any of the two normal modes. To explain this phenomenon, the effect on the atomic distribution by the scattering of photons from the probe beam in the (+)-direction into the (-)-direction has to be included.

A scattering event by an atom of a photon from a mode into the mode of the ring cavity with opposite propagation direction creates a momentum transfer on the atom, and this creates a force on the atom. There are four laser beams exerting a force on the atoms: the lattice beams in the (+) and (-)-directions, and the same for the probe laser beams. The lattice laser is kept resonant with the (-)-direction of the ring cavity with a PDH lock, and thus it has a constant in-coupling. 96.5 percent of the power of the probe beam is coupled into the (+) direction, and in the strongly coupled regime a significant part of the light from the (+) direction is scattered into the (-) direction.

In steady state the light forces on the atoms must be balanced, and the only possibility for the forces to be balanced is for the force from the (+) direction of the lattice laser to decrease if the force on the atoms due to light being scattered from the (+) direction of the probe beam into the (-) direction increases. It is assumed that the light power scattered from the (+) direction of the probe beam into the (-) direction is proportional to the light power in steady state for the (-) direction of the probe beam, which is $\left|\langle\alpha_-\rangle\right|^2$. With this assumption, the light power measured on the photodiode shown in Figure 17 consists of the two parts: the transmission spectrum of the probe laser, and the decrease in the intensity in the (+) direction of the lattice laser due to scattering of photons from the probe laser into the (-) direction.

The light power on the photodiode can be estimated as [86]:

$$P = S\left(\left|\langle\alpha_+\rangle\right|^2 - R\left|\langle\alpha_-\rangle\right|^2\right) \tag{106}$$

where S is a scaling factor, R is the fraction between the scattering power from the probe beam and the steady state intensity in the (-) direction of the probe beam. In Figure 18, the fitting parameters for the plots are: S, R, g_{ef} and χ. The fitting parameters for different atom numbers are plotted in Figure 19, Figure 20 and Figure 21:

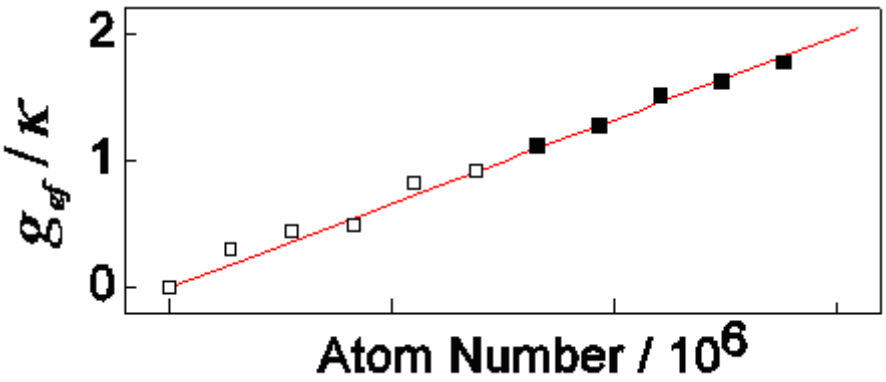

Figure 19: The coupling strength for different atoms numbers in the cavity mode. The black boxes show the strongly coupled regime.

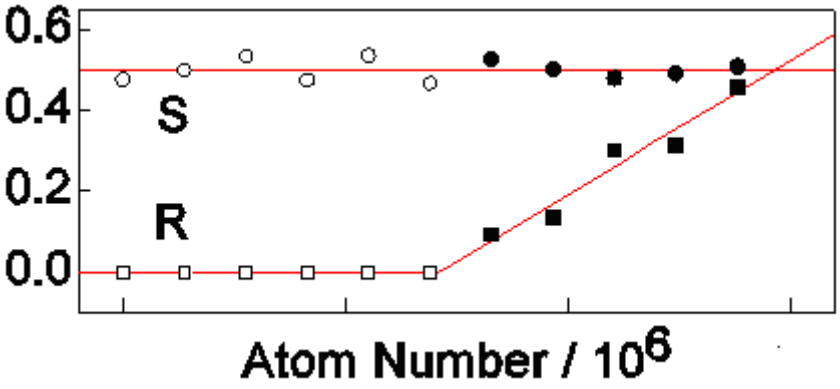

Figure 20: The scattering of photons from the (+) probe beam into the (-) direction first exerts a significant force on the atoms in the strongly coupled regime, and thus R = 0 in the weakly coupled regime.

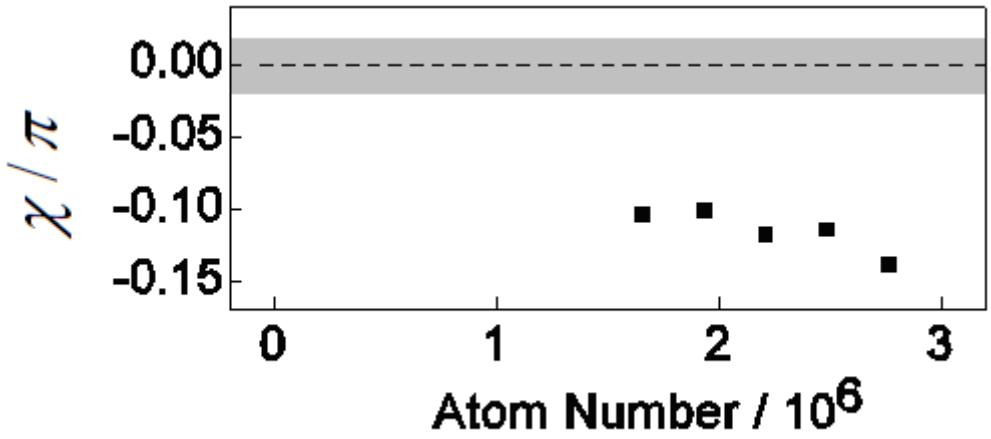

Figure 21: The relative phase between the optical lattice of the lattice laser beams and the optical lattice of the probe laser beams (χ). When the coupling between the atoms and the cavity modes is weak, the effect of χ on the transmission spectrum is small. Hence, no reliable value of χ can be found from the transmission spectrum, when the coupling is weak. The grey area in the plot shows the value of χ due to different optical path lengths from the beam cube to the in-coupling mirror of the ring cavity (see Figure 17).

In [61,65,71] the possibility to observe cooling with the normal mode splitting is discussed. The two major experimental obstacles in the ring cavity set-up in order to observe cavity cooling were a low value for η_c and the short time the resonance condition for the dissipative process is fulfilled. With a lifetime of 1.7 s and 10^6 atoms captured in the optical lattice the resonance condition is only fulfilled for a few ms. As $\eta_c = 0.6$ the cooling rate due to scattering into the cavity mode and the heating rate due the scattering rate into free space are of the same magnitude.

The major advantage of the new experimental set-up compared to the ring cavity set-up in regards to cavity cooling is the high value of η_c of the standing wave cavity described in chapter 5.8.

5 Experimental apparatus and procedures

In this chapter the experimental set-up and the procedures used for creating a BEC are described. In chapter 6 the individual experimental steps for creating a BEC are characterized.

In chapter 5.1 the stabilization on atomic and cavity resonances is discussed, in chapter 5.2 the source of cold Rb_{87} atoms is described (the first MOT) and in chapter 5.3 the second MOT is described, which is used to capture the atoms from the cold atomic beam from the first MOT. In chapter 5.4 the optical pumping set-up is described and in chapter 5.5 the magnetic traps are described, in chapter 5.6 the two imaging set-ups are explained. In chapter 5.7 the vacuum set-up is shown, in chapter 5.8 the cavity set-up is explained. Chapter 5.9 describes the radio frequency source for evaporative cooling and in chapter 5.10 a system for stabilizing a laser off-resonant to cavity resonance is described.

5.1 Laser stabilization on atomic and cavity resonances

All laser beams in this experiment are generated by diode lasers. If the laser diode is used without additional feedback, it is said to be operating in free running mode, and beam from a free running laser diode is not suitable for operating a MOT for a number of reasons. Firstly, the width of the emission spectrum is a few MHz, secondly, the emission spectrum is often far from the desired atomic transition and lastly the laser diode is often running multi mode. To overcome these problems, additional feedback is created by reflecting some of the emitted light back into the laser diode by a grating. The external cavity set-up with the grating is further discussed in the appendix A.

The emitted frequency of the laser diode in the external cavity set-up can drift due to reasons such as temperature changes or drifts in the current flowing through the diode. In order to be able to correct the frequency drifts, one must first be able to detect it. This is done through saturation spectroscopy for stabilization on an atomic resonance [66,67], and for stabilization on a cavity resonance the reflected light from cavity is used.

Saturation spectroscopy

With saturation spectroscopy it is possible to identify the hyperfine transitions in the spectrum of Rubidium atoms at room temperature. The Doppler broadening at room temperature of Rubidium is around 1 GHz, and the natural line width is 6 MHz. An absorption spectrum can be made by scanning the frequency of the laser over the relevant transitions, and by having a laser beam passing through a Rubidium cloud. At each frequency in the spectrum, there will be several velocity classes of atoms, which have a Doppler shift such that they are resonant to a hyperfine transition. Since the Doppler broadening is so much larger than the natural line width, the fraction of atoms with a Doppler shift around zero compared to the fraction of atoms with Doppler shifts of several MHz to a hyperfine transition is nearly equal.

In saturation spectroscopy, the laser beam passes two times through a Rubidium cell and the incident and the retro reflected beam coincide. Atoms with zero Doppler shift have the same detuning compared to the two laser beams, while atoms with a Doppler shift have a different detuning compared to the two laser beams.

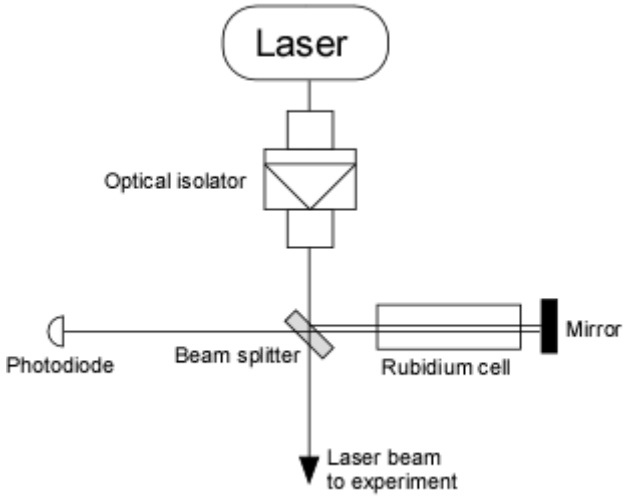

Figure 22: Saturation spectroscopy set-up.

When the laser beam is resonant with a hyperfine transition, the retro-reflected beam will have less relative absorption than when the laser beam is not resonant with a hyperfine transition. This is due to the fact that some atoms with zero Doppler shift are in an excited state due to absorption from the incident beam. If the detuning of the laser beam is between two hyperfine transitions, the group of atoms with a Doppler shift with this detuning will firstly be resonant with the incident beam on one of the transitions, and then the retro reflected beam will be resonant on the other transition. These peaks on the saturation spectrum are called the cross-over peaks. For frequencies far from a hyperfine transition or a cross over peak, the saturation effect of the incident beam is negligible, and at these frequencies the normal Doppler broadening spectrum is seen.

Stabilization on a resonance with the Pound-Drever-Hall technique

From a saturation spectrum one can get the frequency information needed, but in order to lock the laser on a specific frequency it is needed to differentiate the signal. In this experiment the signals are differentiated with the Pound-Drever-Hall technique (PDH) [68], which is similar to the frequency modulation spectroscopy [69]. The differentiated signal is called the error signal. The PDH technique is used both for stabilizing on atomic and cavity resonances.

The basic concept in the PDH technique is that the laser is modulated with a much larger frequency than the linewidth of the atomic transition or linewidth of the cavity resonance with small amplitude. For sufficiently small amplitude, the frequency spectrum emitted from the laser can be understood to consist of three parts: a carrier and two sidebands. The frequency of the carrier is the one emitted by the laser with no modulation, and the frequencies of the sidebands are the carrier frequency and respectively plus and minus the frequency of the modulation.

The modulation level for stabilization on an atomic resonance was chosen such that the saturation spectrum was not noticeably affected by the modulation. Similar the modulation level for stabilization on a cavity resonance was chosen such that the incoupling into the cavity mode was maximized.

The modulation frequency for stabilization on atomic resonances was chosen to be 40 MHz for all laser expect for the second MOT laser, which was set to 80 MHz. 40 MHz is much larger than the natural line width (6.1 MHz), while at the same time much smaller than the frequency difference from the cooling transition to the next hyperfine transition (265 MHz). The second MOT laser is detuned 20 MHz more in the compressed MOT phase compared to the standard MOT phase (see 5.3), and it is not desirable that one of the side bands become resonant during the CMOT phase. Thus, the modulation frequency of the second MOT laser was higher than the ones for the other lasers.

The error signal was generated by multiplying (demodulating) the signal from the photodiode (see Figure 22) with the modulation itself in a mixer. The phase of the modulation and the signal from the photodiode had to have the same phase in the mixer to achieve the largest error signal. By varying the cable length from the source of the modulation to the input on the laser diode the phase of the signal from the photodiode could be varied.

The circuit diagrams for the electronic components used to create the error signal can be found in [70,71]. For stabilizing on an atomic resonance it was sufficient to send the error signal to the piezo (see Figure 50) in the external grating set-up as only sub MHz linewidth of the emission spectrum of the laser was needed.

Stabilization on a cavity resonance

Stabilization on a cavity resonance instead of an atomic resonance was similar, however, the linewidths of the cavities used in this experiment were of the order 10 kHz. The technical solution to stabilize on such a narrow cavity linewidth was based on [72].

Stabilization consisted of three different branches. As in the stabilization on an atomic resonance the error signal was sent to a piezo. In addition the error signal was also sent to modulate the current output of the current controller (current feedback) and the voltage over the laser diode (direct feedback). The fastest branch was the direct feedback, and it was AC coupled (over a capacitor 1 μF) to the input pin of the laser diode. To vary the phase behaviour of the direct feedback to the laser diode a loop filter was used.

5.2 Atom source

The atomic source was used to send a cold atomic beam of Rb_{87} atoms into the second chamber where they were recaptured in a second MOT. A free atomic Rb_{87} vapour was generated by two Rb dispensers. In the dispenser Rubidium, there was a chemical composition that broke when it was heated. The dispensers were heated by a current (operating at 3.3 A) and they released a free Rb vapour into the source chamber. The dispensers were mounted on ceramic Alumina rods.

The atomic source was designed as a 2D-MOT, and the design was similar to [73].

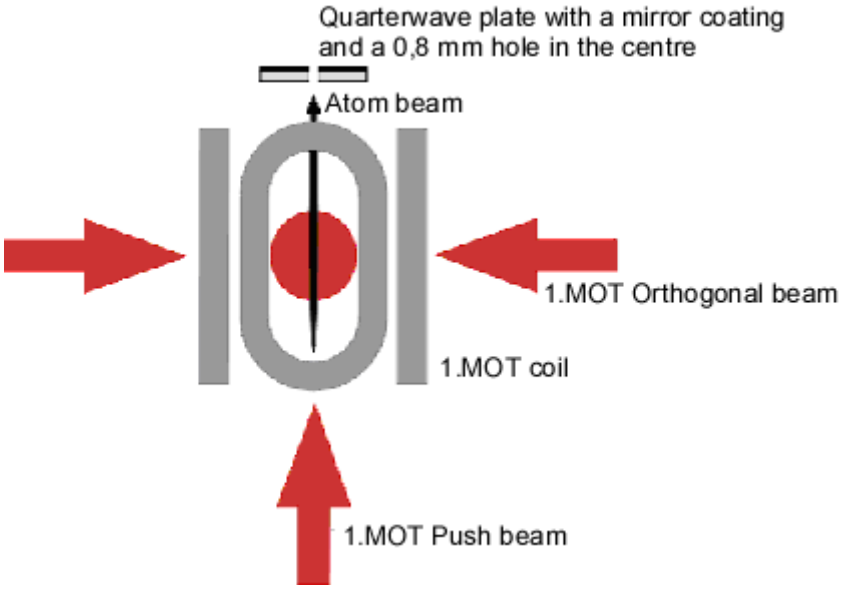

Figure 23: The set-up for the 1. MOT. Due to the hole in the quarterwave plate, which reflected the 1.MOT push beam, there was an unbalanced pressure in the centre of the 1.MOT. Thus an atomic beam was created, which pushed the atoms into the second chamber.

The magnetic field was generated by four racetrack coils. This gave a strong magnetic gradient along the two orthogonal directions to the atomic beam compared to the gradient along the atomic beam. The advantage of having only strong gradients along the orthogonal directions was that the atomic density was lower than if there were strong gradients in all three dimensions. As explained in chapter 2.2 at a certain density the internal light pressure in the MOT limits the density.

For the first MOT 3 pairs of two counter propagating beams perpendicular to each other were used. The first MOT push beam was a beam along the vertical axis and it pushed the atoms into the second MOT. This beam was retro reflected by a quarter-wave plate (diameter 38 mm) with a mirror coating on the backside inside the vacuum chamber. The quarter-wave plate had a small hole (0.8 mm) in the centre. This created a vertical column, where there was no counter propagating beam. In this region the atoms were pushed out of the chamber and into the next chamber.

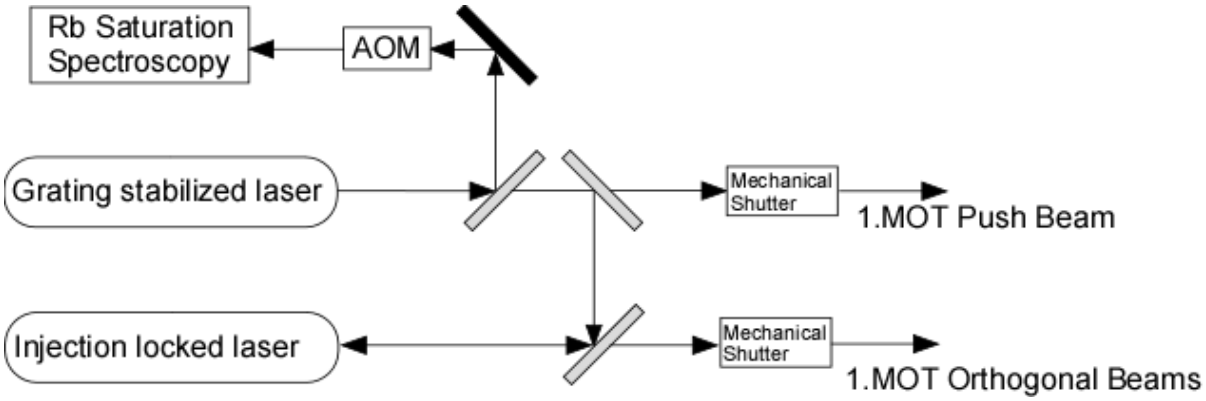

Figure 24: Laser set-up for 1.MOT. The AOM decreased the frequency of the laser light by 114 MHz and when the beam after the AOM was locked in the centre of the crossover peak, the beam before the AOM had a detuning of 3 γ to the cooling transition.

The loading time of the second MOT was typically 20 s, and thus the switching time of the mechanical shutters (around 20 – 30 μs) was sufficiently short to not affect the final atom number in the second MOT. The advantage of having the AOM in the stabilization branch instead of in the part of the beam going to the experiment was slightly higher power in the push beam and it was also much easier to make a large change in the detuning of the first MOT with the AOM in the stabilization branch. The stabilization branch was not so sensitive to a small dis-alignment from a frequency change for the AOM, and it was also much faster to adjust it than the whole path of the beams to the first MOT.

The repump laser was only overlapped with the two orthogonal beams.

Laser beam	**Transition (all d2 line)**	**Power (mW)**	**Diameter (mm)**	**Detuning (MHz)**
1. MOT Push beam	F = 2 to F =3	7	25	20
1. MOT Orthogonal beam	F = 2 to F =3	25	30	20
Repump beam	F = 1 to F = 2	3	30	resonant

Table 6: Laser powers for the first MOT laser beams.

5.3 The second MOT

In the second chamber the atoms, which were transferred into it from the first MOT, were captured in a second MOT. The distance from the centre of the first MOT to the second MOT is 36 cm, and in order for the atoms to reach the second MOT, the atoms must have a velocity above 3 m/s. In [73] the velocity along the push direction was around 8 m/s.

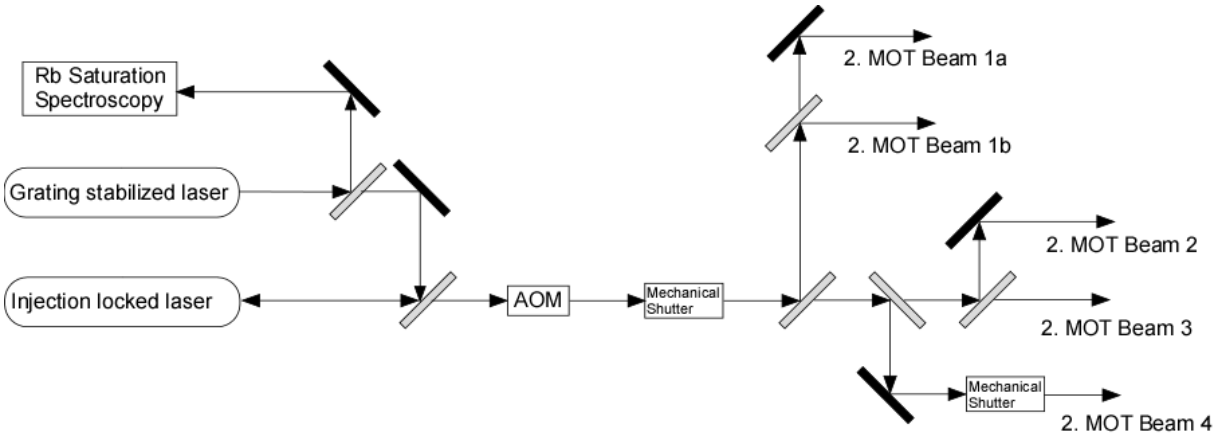

Figure 25: The laser set-up for the second MOT.

For the second MOT, a single injection locked laser diode generated all the laser beams except for the re-pumping transition. For the second MOT it was necessary to quickly switch the laser power off, when the atoms were transferred from the MOT into the magnetic trap. Therefore an AOM was placed in the beam going to the experiment. The AOM could switch the laser beam to zero intensity in a time below 1 μs. To ensure that no light power was going to the experiment, a mechanical shutter was shut after the AOM.

The magnetic field for the second MOT was built as a standard anti-Helmholtz configuration. The gradient along the strong direction is 9.3 Gauss/cm and along the weak direction 4.6 Gauss/cm. The laser beams along the weak propagation direction were retro-reflected by mirrors inside the chamber (2. MOT beam 2 and 3 in
Figure 25), and the lasers beams along the strong direction were two independent laser beams (2. MOT beam 1a and 1b in
Figure 25). The two retro-reflected beams were due to design reasons of the chamber.

Displacement of the second MOT due to absorption of the MOT beams

When the atom number in the second MOT had reached its steady state value, the relative absorption of the two retro-reflected beams that had been one time through the MOT was of the order 5%. This imbalance in the beam intensity of two retro reflected beams created a displacement of the MOT from the zero point of the magnetic field. The centre of the MOT had to be positioned at the magnetic zero point of the magnetic field when the atomic sample was transferred into the magnetic trap to achieve the least amount of heating in the transfer process. To push the MOT to the desired location, a 7th laser beam was added (2.MOT beam 4 in figure 26). The repump laser beams were overlapped with the two retro-reflected beams.

The compressed MOT phase (CMOT) and the optical molasse

To increase the phase space density of the atomic cloud, a compressed MOT phase [74],[75],[76] was used followed by an optical molasse. In the compressed MOT phase (CMOT) the detuning and the magnetic gradients were increased. The characteristics of the CMOT and the optical molasses (temperature, radius) did not strongly depend on the detuning on the scale of one linewidth [76], and due to this, a sample and hold technique was chosen to detune the cooling beams during the CMOT and the optical molasse.

The 2. MOT laser was unlocked, and a voltage to the piezo in the grating stabilized set-up was ramped over 20 ms to its end value.

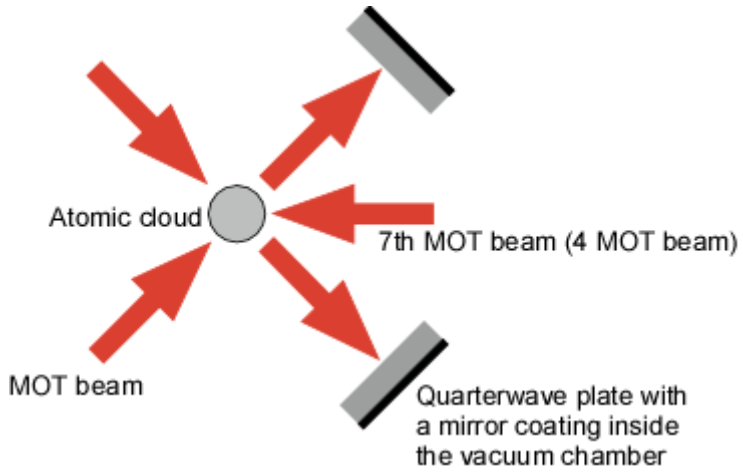

Figure 26: The 7th MOT beam was used to counteract the absorption of the retro-reflected MOT beams in the second MOT.

Laser beam	Transition (all d2 line)	Power (mW)	Diameter (mm)	Detuning (MHz)
2. MOT beam 1a	F = 2 to F =3	1.1	10	8
2. MOT beam 1b	F = 2 to F =3	2	10	8
2. MOT beam 2	F = 2 to F =3	6	20	8
2. MOT beam 3	F = 2 to F =3	3	20	8
2. MOT beam 4	F = 2 to F =3	0.25	10	8
2. MOT repump power	F = 1 to F = 2	0.4	20	resonant

Table 7: The powers of the laser beams for the second MOT. The laser powers are given for the MOT phase. In the optical molasses and the CMOT the laser powers of the beams are three times higher than in the MOT phase.

In an optical molasse the magnetic field was switched off. The magnetic field gradient limits the sub-Doppler cooling (see chapter 2.2) and much lower temperatures can be reached by switching the magnetic field off. The detuning during the optical molasse was increased to 50 MHz for 5 ms and followed by period of 3 ms with 90 MHz detuning with the same

method as the one used for the compressed MOT phase. During the optical molasse, the atomic sample could expand, and the time of the optical molasse was a compromise between a low temperature and a small expansion.

Overlap of the optical molasse and the magnetic trap

The position of the optical molasse was overlapped with the centre of the magnetic trap. This was done by comparing the position of the optical molasse at high current (~5A) in the MOT coils during the CMOT and a low current (~1A) during the CMOT. The position of the centre of the atomic sample at a low current in the MOT coils during the CMOT was adjusted by varying the current in tree compensation coils. Due to the large radius of compensation coils compared to the radius of the atomic sample, the magnetic field from the 3 compensation coils was nearly constant over the atomic sample. The ratios between the intensities in the MOT beams were adjusted such that the atomic sample would fall down straight when the magnetic field was ramped to zero.

5.4 Optical pumping

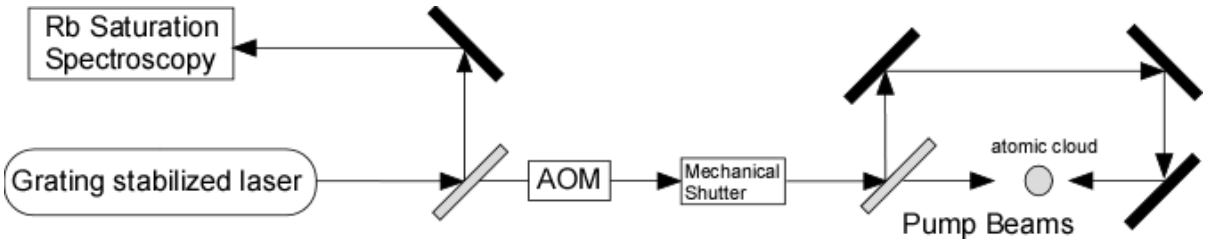

Figure 27: The atomic cloud was pumped by two counter propagating laser beams with the same polarization.

The population among the Zeeman levels in ground states $\left|5S_{1/2}, F = 2, m\right\rangle$ is not well defined after a optical molasse, and in the case of a random distribution, one can at most capture 2/5 in a magnetic trap. By spin polarizing the atomic sample before it is transferred into the magnetic trap, the transfer efficiency can be significantly increased. If an atom in the state $\left|5S_{1/2}, F = 2, m \le 1\right\rangle$ absorbs a photon with σ^+ polarization relative to the quantification axis for the magnetic field, it will then be excited to the state $\left|5P_{3/2}, F = 3, m+1\right\rangle$. Then the atom can spontaneously decay to the states: $\left|5S_{1/2}, F = 2, m+1+n\right\rangle$, where n = -1,0,1 (only for m ≠ 1,2). On average, an atom will by absorbing a photon with σ^+ polarization and spontaneously emitting a photon end up in a Zeeman state with m number one higher than the original state, unless it is already in the state $\left|5S_{1/2}, F = 2, m = 2\right\rangle$.

To ensure that all atoms had approximately the same quantification axis, the current in one of the coils for the second MOT was quickly switched off, and this created a nearly uniform magnetic field of a few Gauss for the atoms in the atomic sample. The atoms were illuminated for 10 μs with two counter-propagating laser beams with σ^+ polarization resonant

on the cooling transition. The total pump intensity had a saturation parameter of 4 and the pump period was 10 μs, which was the minimum time in the computer control system. No measurable increase in the atom number in the magnetic trap was observed for longer pump periods, and no increase in the temperature could be measured due to the optical pumping. Furthermore, no increase in atom number in the magnetic trap was measured by adding the repump laser beams during the pumping.

The pump period can be estimated by the following consideration. The diameter of the atomic sample after the optical molasses is roughly 5 mm, and the scattering rate of a single atom with the saturation 4 is close to $\gamma/2$.

The atomic sample after the optical molasse is optical dense for resonant light and the penetration depth of the light at the density $n = 10^{10}$ atoms/cm^3 is: $\frac{1}{n\sigma_{ge}} = 340$ μm where σ_{ge} is the absorption cross section $\left(\frac{3\lambda^2}{2\pi}\right)$. Atoms, which are initially in the ground state m = 2, can only spontaneously emit photons with the polarization σ^+ after having been excited. The spontaneous photons are in a random direction, and one can assume that an optical thick layer of atoms in the state m = 2 lowers the number of σ^+ photons passing through with a factor ½.

The time to pump all atoms in the atomic sample into the state $|F = 2, m = 2\rangle$ is estimated to be 30 times longer than the pump time for a single atom. An atom in the state $|5S_{1/2}, F = 2, m = -2\rangle$ needs on average 4 scattering events to be pumped into the state $|5S_{1/2}, F = 2, m = 2\rangle$. With these considerations, the pump time is estimated to be 7 μs.

The pumping efficiency was limited by imperfect σ^+ polarization of the light as it led to pumping of atoms from the m = 2 state to lower m states. The optical pumping stage increases the number of atoms into the magnetic trap by a factor 2.

5.5 Magnetic trapping

The initial magnetic trap after the atoms had been loaded from the MOT into the first magnetic trap was made by increasing the current in the MOT coils to 16A in 500 μs. The fast switch on-time was made possible by drawing the needed current from a charged capacitor in the first 10 ms. After the 10 ms the power supply could deliver the 16A. A second pair of coils (transfer coils) were used to move the trapped sample from the position of the MOT to the position of the quadrupole-Ioffe trap (QUIC).

The transport was done by increasing the current in the transfer coils and then lowering the current in the MOT coils. This method was the same as the first method described in [77].

The QUIC trap

The QUIC trap consisted of three coils. The design of our trap was similar to [78]. The two coils (quickcoils on Figure 28) were placed in an anti-Helmholtz configuration, and the two coils are connected in series to a power supply. The current supplies had a low waviness of the current 10^{-3} (characteristic multiplication factor).

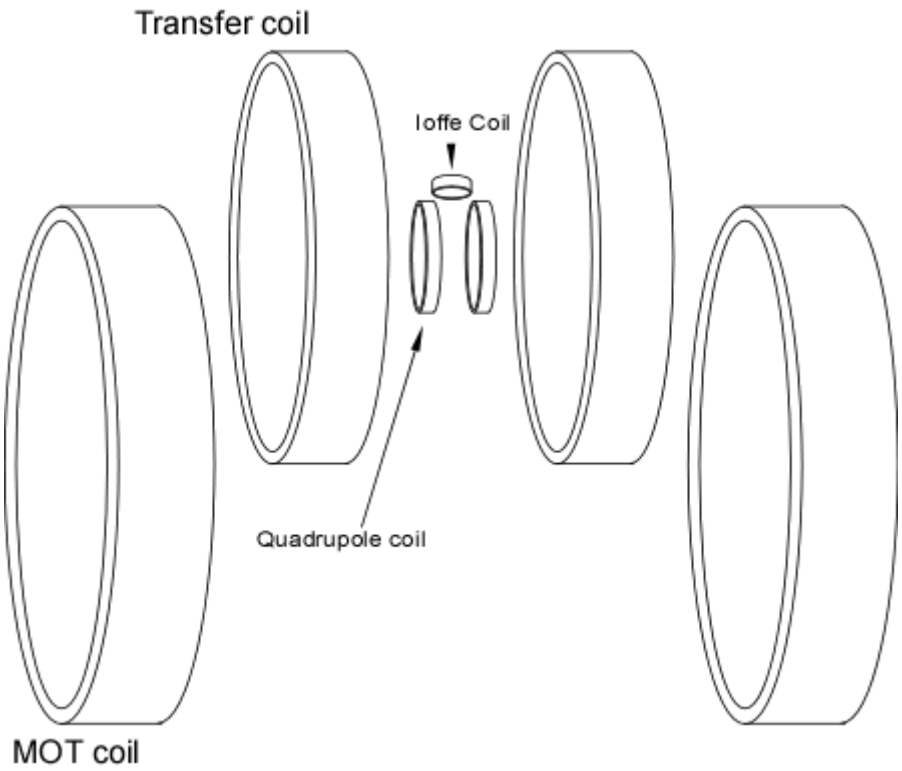

Figure 28: The relative position of the coils is shown in the figure. The coils are not drawn to scale.

Heating rate of the atoms in the magnetic trap due to current fluctuations

The heating rate from the current fluctuations can be estimated from [79]:

$$\frac{1}{\tau_{trap}} = \pi^2 \nu_{trap}{}^2 S(2\nu_{trap}) \tag{107}$$

where ν_{trap} is the trapping frequency, $S(2\nu_{trap})$ is the one sided power spectrum of the fractional intensity noise and τ_{trap} is the e-folding time for the energy.

The $S(2\nu_{trap})$ can be estimated as $\epsilon^2/\Delta\nu$ [80] where ϵ is the root mean square average of the noise in the bandwidth $\Delta\nu$. The trapping frequency in the radial direction is the largest and it is measured in chapter 6.2 ($\omega_{radial} = 2\pi$ x 255 Hz). With a relative current variation of 10^{-3} the time for the energy of the atoms to be increased by a factor e is estimated to be approximately 3000s. No heating was observed for the atomic cloud captured in the QUIC trap before evaporation.

To be able to control the magnetic offset the Ioffe coil was controlled by a separate current supply. If a current was flowing through the Ioffe coil such that there was a magnetic minimum different from zero, it will be referred to as the QUIC trap. If no current was flowing in the Ioffe coil, it is referred to as a QUAD trap.

Cooling of the magnetic coils

Several copper rods were used to transport the heat dissipated in the coils away when current were flowing through them. One end of the copper rods was in thermal contact with the mounting of the coils inside the vacuum chamber, and the other end was outside the vacuum chamber. The end outside the vacuum chamber was in thermal contact with a Peltier element and it was cooled to around –40 °C, and the Peltier elements were water cooled.

In one experimental cycle the cooling time was set in such a way that there were no spikes in the pressure during one cycle, and this criterion gave a total cooling off time of 1 min including the 20 seconds loading of the second MOT.

Magnetic field configuration

The magnetic field configuration can be calculated by assuming the wire windings in the coils can be treated as separate closed loops. The formula for the magnetic field from a closed loop with a current I can be found in [81],[82].

B field gradient along the x-axis	190 gauss/cm
B field gradient along the z-axis	56 gauss/cm
Trap depth	70 Gauss (5 mK)

Table 8: MOT magnetic trap (current in the MOT coils: 16 A).

B field gradient along the y-axis	250 gauss/cm
B field gradient along the z-axis and x-axis	125 gauss/cm
Trap depth	60 Gauss (4 mK)

Table 9: QUAD trap (current in the QUAD coils: 23 A).

B_0	1.8 Gauss
B'	180 Gauss/cm
B''_{radial}	12800 Gauss/cm^2
B''	640 Gauss/cm^2
Trap depth	13 gauss (900 μK)

Table 10: Ioffe-quadrupole trap (current in the QUAD coils: 2.3 A, Ioffe coil: 2.85 A).

There were three local minimums in the field configuration in the Ioffe-quadrupole trap. One of the minimums was on the symmetry axis of the Ioffe coil (z-axis), and it was in this minimum the atoms were captured in. A contour plot of the field configuration can be seen in
Figure 29. The trap depth was limited by the barrier between the centre minimum and the two other local minimums. The amplitude of the magnetic field along the z and x axes is shown in Figure 30.

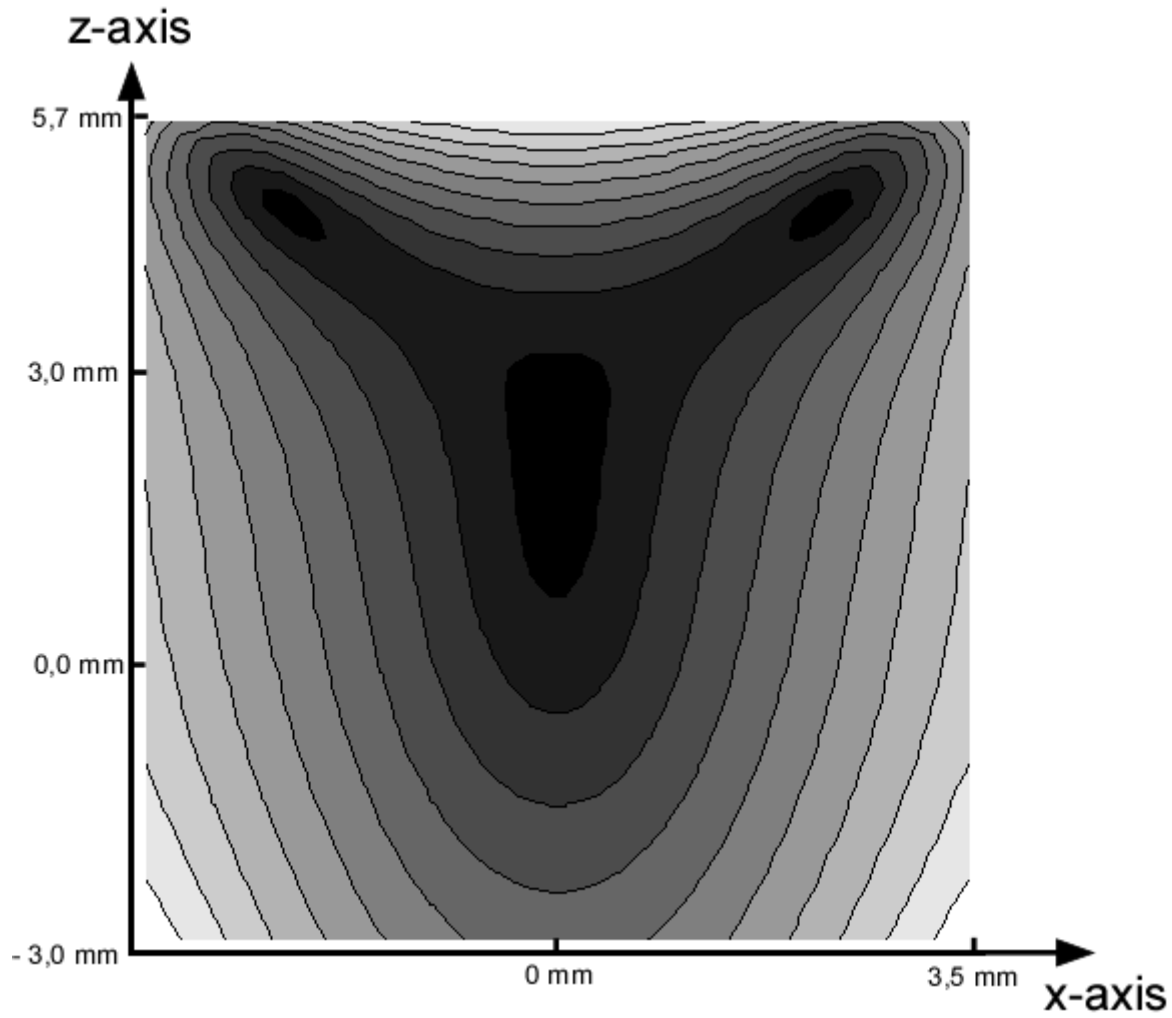

Figure 29: The z-axis is the rotational symmetry axis of the Ioffe coil.

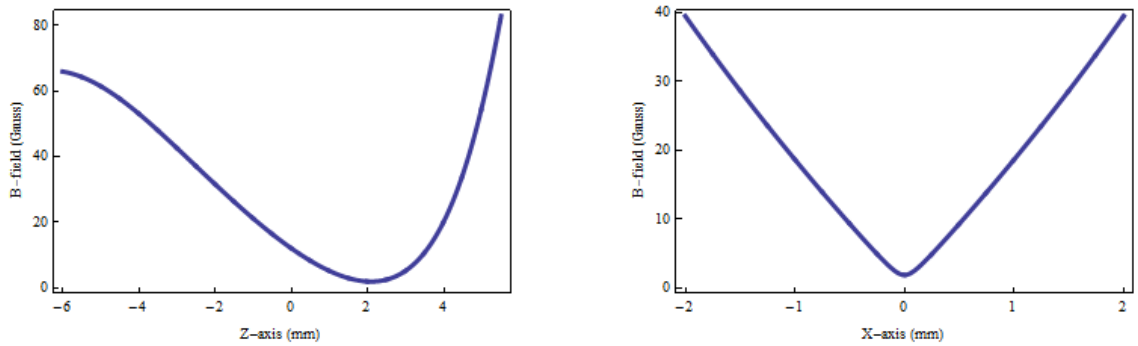

Figure 30: The magnetic field along the rotational symmetry axis of the Ioffe coil on the left image (x=y=0). The centre of the Ioffe coil is at z = 7.8 mm and the minimum value of the magnetic field is at z = 2.1 mm. The magnetic field along the x-axis at z = 2.1 mm is shown on the right image.

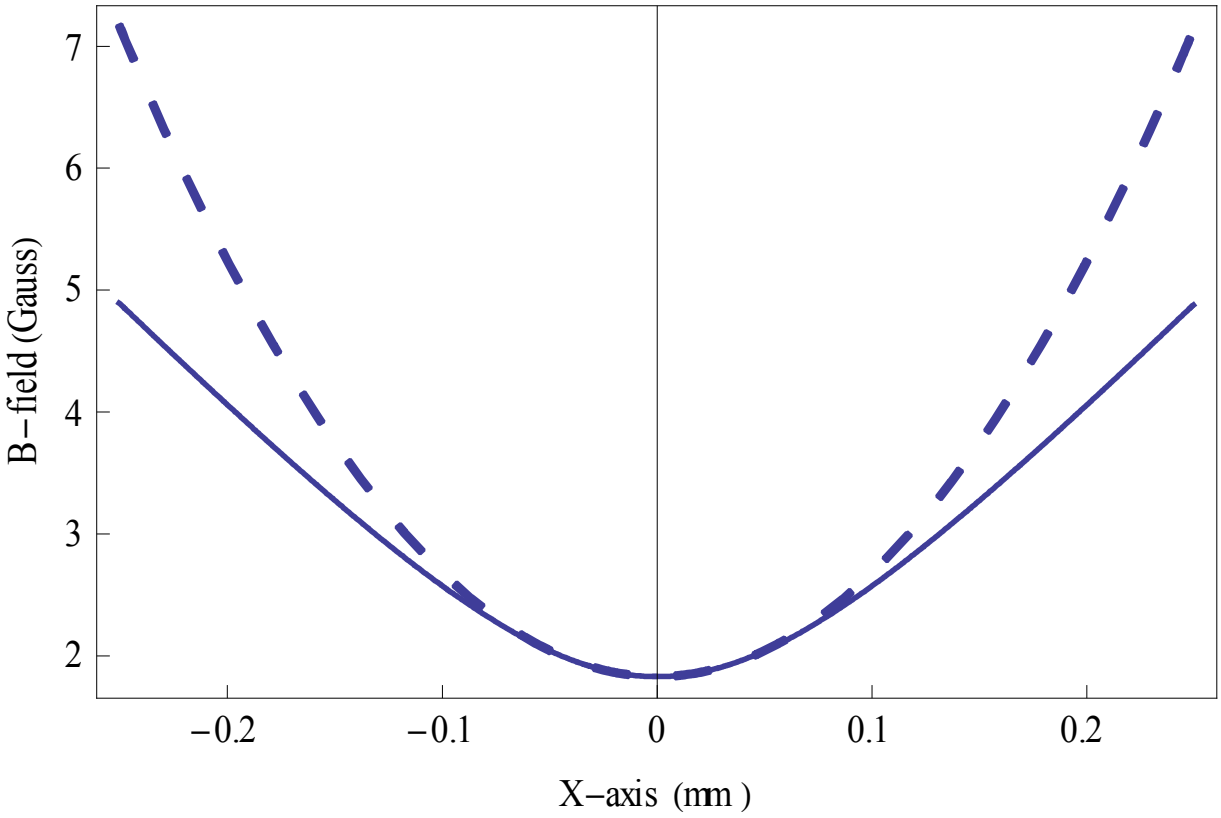

Figure 31: The magnetic field along the x-axis at z =2.1 mm around zero and a fitted parabola to the magnetic field near the minimum (the dashed line). From a comparison of the fitted parabola and the calculated values of the magnetic field it can be seen that for $|x|$ less than 0.1 mm the magnetic field configuration is approximately harmonic.

Displacement of the magnetic trap due to gravity

The direction of the gravitational force was along the z-axis, and the displacement (Δz) due to gravity in the Ioffe-quadrupole trap is given by:

$$\Delta z = \frac{mg_{earth}}{\mu_B B''/2} \approx 0.5 \ \ mm \tag{108}$$

where g_{earth} is the gravitational acceleration of the Earth (9.8 m/s^2), and ω_z is the trap frequency on the z-axis of the Ioffe-quadrupole trap.

The trap frequencies in the harmonic regime can be calculated from: $\omega_{axial} = \sqrt{\frac{\mu_B B''}{m}}$ and $\omega_{radial} = \sqrt{\frac{\mu_B B''_{radial}}{m}}$. The trap frequencies are slightly changed due to the gravitational field, and by taking this into account the trapping frequencies in the harmonic regime were estimated to be: $\omega_{axial} = 2\pi$ x 31.3 Hz and $\omega_{radial} = 2\pi$ x 221 Hz.

5.6 Imaging system

To image the atomic cloud at various stages in the experiment, two different imaging set-ups with different magnification were set up. Set-up 1 was used to image the atomic sample close to the transition to BEC, and it had a magnification of 2 (one pixel on the CCD camera corresponded to 3.6 μm). The other imaging set-up, set-up 2, was used to image the atomic sample at the MOT position and the magnification was 1/3 (one pixel corresponded to 25 μm).

A single grating stabilized laser was used to generate the two laser beams for both imaging set-ups and the placement of the AOM, and the mechanical shutter was the same as for the pumping laser. The exposure time was 10 μs and the typically expansions' times were between 3 ms for the atomic cloud in the QUAD trap before evaporation to 25 ms for observing the bimodal distribution of the BEC. The saturation of the cooling transition of the imaging beams was 0.25 and this corresponds to 6 scattering events for the imagining beam being resonant on the cooling transition during the image.

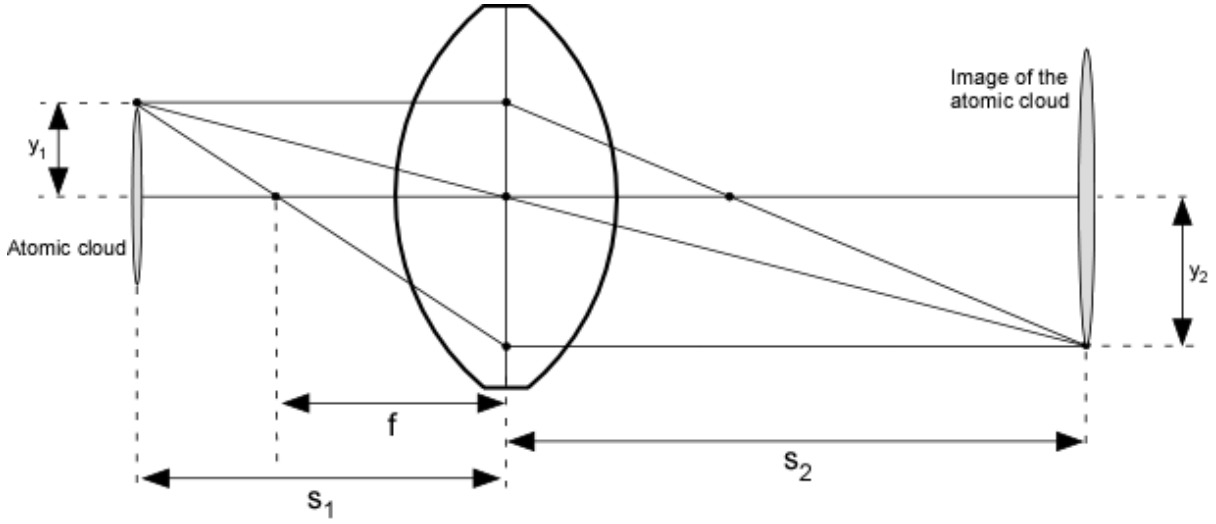

Figure 32: The imaging set-up with a single lens.

Magnification

For both imaging set-ups a single lens was used to image the atomic cloud on the CCD chip. The magnification (M) is given by equation 109 [83]. A negative value means that the image is inverted.

$$M = \frac{y_2}{y_1} = -\frac{s_2}{s_1} \tag{109}$$

Resolution limit

The resolution limits for the imaging set-ups are given by equation 110, where f is the focal length of the lens, D is the diameter of the lens and λ is the wavelength of the light [84].

$$d = 2.44\frac{f\lambda}{D} \tag{110}$$

The resolution limit of imaging set-up 1 was: 7.5 μm and for imaging set-up 2 the resolution limit was: 37 μm. Due to the fact that the imaging lens being outside the vacuum chamber and that the imaging beam had to move through a tunnel inside the vacuum chamber, it was not possible to significantly decrease the resolution limit for imaging set-up 1.

Maximum measurable optical density

The resolution of the digital readout of the camera was 12 bit, and this gave a theoretical upper limit for the measurable optical density of 8.3. If the imaging light is completely absorbed by the atomic cloud and then spontaneously reemitted evenly in space, the maximum measurable optical density is given by:

$$D_{\max} = Ln(\Omega) = Ln\left(\frac{\pi D^2}{4\pi R^2}\right) \tag{111}$$

where D is the diameter of the imaging lens and R is the distance between the imaging lens and the atomic cloud. The maximum measurable optical density for imaging set-up 1 was approximately 4.3. The maximum measured optical density was 5. That the measured maximum optical density is higher can be explained by absorption on the optical elements from the atomic cloud to the camera and that random scattered light is not isotropically emitted from the atomic cloud.

Blurring of the image due to random recoils during the image

When an atom, that has absorbed a photon from the imagining beam, spontaneously emits a photon, it gets a kick in a random direction. While it is equally likely that the atoms gets a velocity in any direction due to a spontaneous emission, the amplitude of the velocity of an atom will not be zero after many spontaneous emissions. The average distance travelled by an atom due to a random walk during the exposure can be estimated from [80,85] :

$$\mathrm{r} = \sqrt{\mathrm{N}/3}\,\mathrm{v}_{\mathrm{rec}}\,\tau \approx 80 \ \mathrm{nm} \tag{112}$$

where N is the average number of spontaneous scatterings during the exposure, $\mathrm{v}_{\mathrm{rec}} = \frac{\mathrm{k}\hbar}{\mathrm{m}}$ is the recoil velocity, and τ is the exposure time.

5.7 The Vacuum Chamber

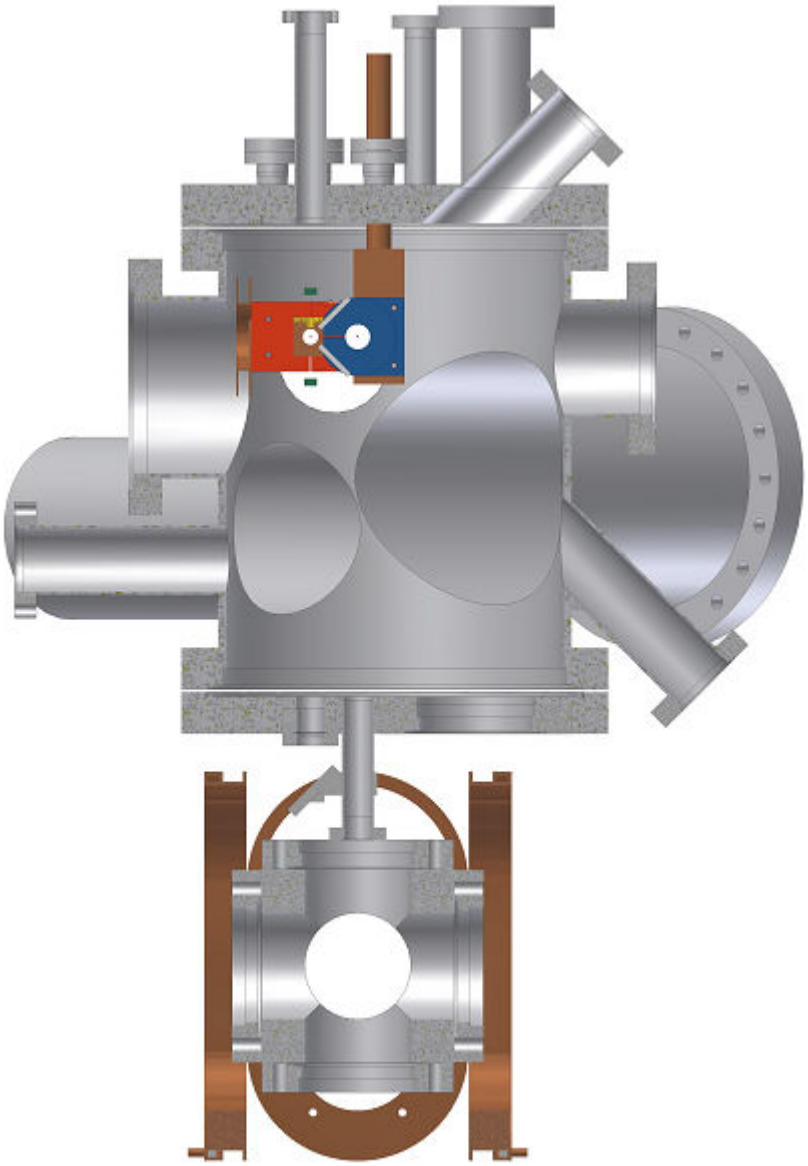

Figure 33: Outline of the vacuum chamber. The science chamber is the above while the first MOT chamber is the one below. The coil and cavity set-up are mounted to the upper flange.

The source chamber was pumped by a 40 l/s ion pump. The pressure in the source chamber can be estimated from the current in the ion pump, and it was found to be at 5 10^{-8} mbar, when the dispensers had reached their steady state temperature with 3.4 A running through them.

The second chamber was pumped with 500 l/s ion pump and a Titanium sublimation pump. To improve the pumping of the sublimation pump a cylinder sheet of copper was placed around the filaments, and this sheet could be cooled to around –30-40 °C to further improve the pumping. The Titanium sublimation pump was mounted inside a CF100 tube,

and it was possible to separate this chamber with a valve from the second chamber. This was done to protect the cavity mirrors, when Titanium was being sublimated.

The pressure in the second chamber was measured by a pressure gauge, and it was found to limit the lifetime of the atoms with temperatures close to the BEC transition significantly. It was only possible to reach the transition to a BEC, if the pressure gauge was switched off.

The vacuum chamber was first baked out at around 200 °C without the coil and resonator set-up inside the vacuum chamber. 200 °C was chosen because it was the maximum allowed value for the view-ports. After this bake-out, the pressure was below 10^{-11} mbar at room temperature. After the set-up of the resonator and the coils had been installed inside the chamber, it was baked out a second time at 110 °C because the resonator mirrors and the piezo motor limits the temperature allowed.

If the coils and the dispensers were allowed to cool off for a few hours after use, the pressure in the chamber was around 1.8-1.9 10^{-11} mbar. After a full day of experimenting with the apparatus the pressure would typically be from 2 to 2.4 10^{-11} mbar.

5.8 Cavity set-up

In chapter 3 the parameters characterizing a cavity were discussed and in chapter 4 discussed cavity cooling. For efficient cavity cooling it is desirable to have a high cavity to free space scattering ratio η_c, and for a low steady state temperature a small linewidth $\Delta\nu$ is needed. The criteria for the cavity design were to have a high η_c and a small linewidth $\Delta\nu$. η_c depends on the cavity enhancement A and the waist w_0 (see equation 42).

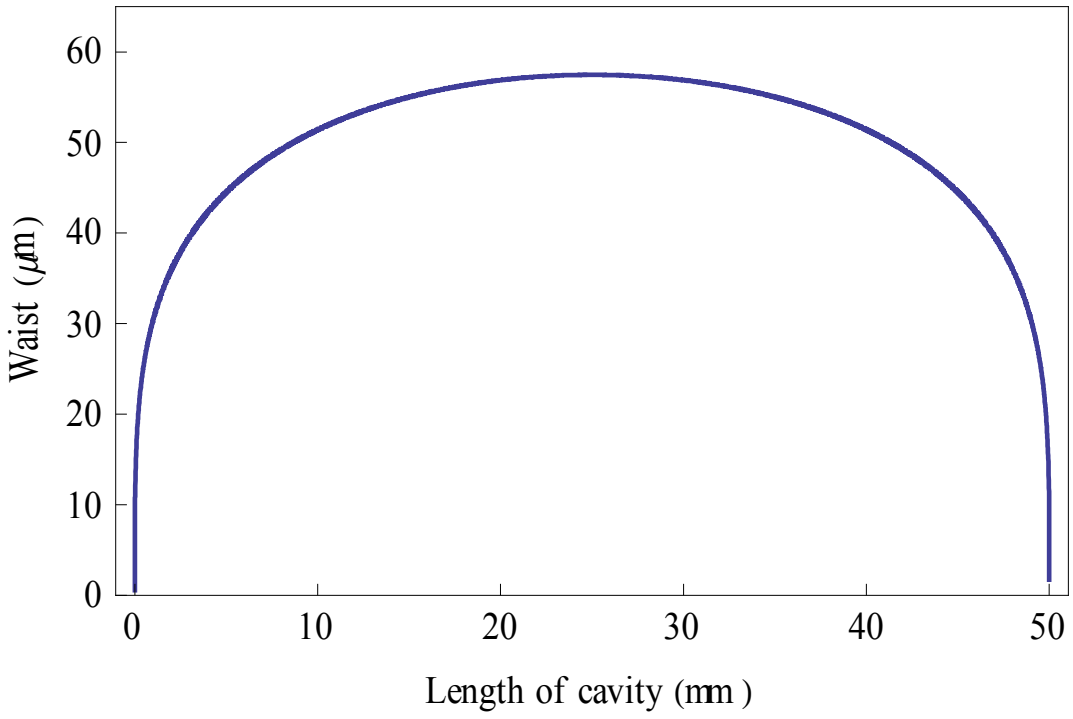

Figure 34: Waist in the centre as a function of the cavity length (R = 25mm).

From Figure 34 one can see that a length near zero or near twice the radius of the curvature gives a small waist. The linewidth for a given finesse is inverse proportional to the length of the cavity. Because the second design criterion was to have a small linewidth, the length of the cavity was chosen to be slightly less than twice the cavity length. If the cavity length is twice the radius of the curvature, the cavity is called a spherical resonator. The cavity length can be changed by up to 7 mm by a piezo motor. The maximum length was set slightly above 50 mm. By changing the cavity length with the piezo moter, the waist of the TEM_{00} mode could be varied from close to zero to around 40 μm. One mirror was mounted on a piezo tube that can vary its length by up to 6 μm over a voltage span of 500 V. This adjustment of the cavity length was used to lock the cavity to a frequency stabilized laser.

According to equation 48, the finesse is high, if the internal losses in the cavity are low. The diffuse scattering losses on the mirror have a certain minimum value given by the manufacture, which does not depend on the transmission of the mirrors. In our case the scattering loss was of the order 3 ppm. To achieve the highest incoupling, the transmission of the incoupling mirror should be equal to all other losses in the cavity (impedance match). A high incoupling is desirable as it gives a better signal to noise ratio for the error signal in the stabilization set-up.

Cavity parameter	**Value**
Cavity Length	49 mm
Radius of curvature of the mirrors	25 mm
Scattering losses on the mirrors	3 ppm
Transmission of incoupling mirror	7 ppm
Transmission of outcoupling mirror	0.5 ppm
χ	14 ppm
Finesse	$4\ 10^5$
Power enhancement (A)	$1.3\ 10^5$
1/e decay time for cavity (t_0)	24 μs
w_0	30 μm
z_0	3 mm
η_c	20
Free spectral range (FSR)	3 GHz
Linewidth	8 kHz

Table 11: The parameters for the experimental cavity at 780 nm.

5.9 Radio frequency source

The frequency generator (VFG-150, Toptica) was the radio frequency source used for evaporative cooling. The VFG had a maximum frequency output of 150 MHz and an output power from – 4 dBm to –64 dBm. The VFG could be programmed to run a sequence where the frequency and the power were varied in a series of discrete time steps. The minimum time step was 5 ns.

The signal from the VFG-150 was sent through an amplifier, which had a gain of 43 db and a maximum output power of 30W (~ 44 dBm). A 3 db attenuator was used to give a 50 ohm outout impedance of the amplifier. The output of the amplifier was connected to a rf-antenne that consisted of 1 loop with a radius of 3 cm.

5.10 Laser system for stabilizing off resonant on a cavity

In laser cooling a dissipative process is created by having a laser beam red detuned to an atomic resonance. A similar process was discussed in chapter 4, where a laser beam was red detuned to a cavity resonance to create a dissipative process. In this chapter is presented a method to have a laser beam detuned to cavity resonance with a fixed detuning and this method will in this chapter be referred to as the AOM-lock.

With the PDH technique presented in 5.2, it is only possible to lock a laser on resonance with a cavity mode. In [86] a phase lock is used to lock a laser with a specific detuning to a cavity mode. The technical details of the phase lock can be found in [87]. One laser was locked with the PDH technique on a resonance on a cavity mode and a second laser was phase locked with a specific frequency difference to the first laser.

The primary problem with using this method of having a detuned laser from a cavity resonance is the high finesse of the cavity presented in this thesis. The laser, which is locked to the cavity, has some in-coupling and the in-coupled light creates a standing wave inside the cavity. When an atom held in a magnetic trap scatters a photon, it can change its Zeeman level, which results in a shorter lifetime in a magnetic trap.

To avoid scattered light from the cavity mode to significantly affect the lifetime of the atomic sample in the magnetic trap, the laser which is locked to a cavity mode, must be far detuned from the nearest atomic resonance. The frequency difference, which can be set in the phase lock, is limited by the response time of the photodiode, which is used to detect the beat signal between the two lasers. Typically, this sets an upper limit of several GHz for the maximum frequency difference with which two lasers can be phase-locked with. As we wish the laser beam, which is coupled into the cavity mode, to be many nm away from the atomic resonance and the cooling beam to be a few GHz away from an atomic resonance, it is not possible to use a phase lock for this.

The AOM lock

In the AOM lock, frequency information of the experiment cavity was obtained by a far detuned laser (probing laser), and this information was then transferred to a laser much closer to an atomic resonance (cooling laser). The stability of the detuning of the cooling beam depended on the length stability of a transfer cavity.

The wavelength of the probing laser was 825 nm, and the wavelength of the cooling laser was 795 nm (of the order 10 GHz detuning to the D1 transition of Rb). Both lasers were locked to a cavity (transfer cavity in Figure 35) with the PDH technique. The design criterion for the transfer cavity was the absolute length stability. In [88] can be found a detailed description of the design and the properties of the transfer cavity.

Transfer cavity parameter	Value
Finesse at 825 nm	$1.8\ 10^5$
Linewidth at 825 nm	4.8 kHz
Finesse at 795 nm	$2.4\ 10^5$
Linewidth at 795 nm	3.4 kHz
Free Spectral Range	850 MHz

Table 12: Transfer cavity parameters [88].

The probe and the cooling beams were split on a bichromatic filter (reflecting for 795 nm and transmitting for 825 nm). Each laser beam went double pass through an AOM with a set-up similar to [89]. By going double pass through the AOM, the path of the beam after the double pass did not depend on the frequency of AOM. At 280 MHz, the power in the first diffraction order from the AOM was the highest.

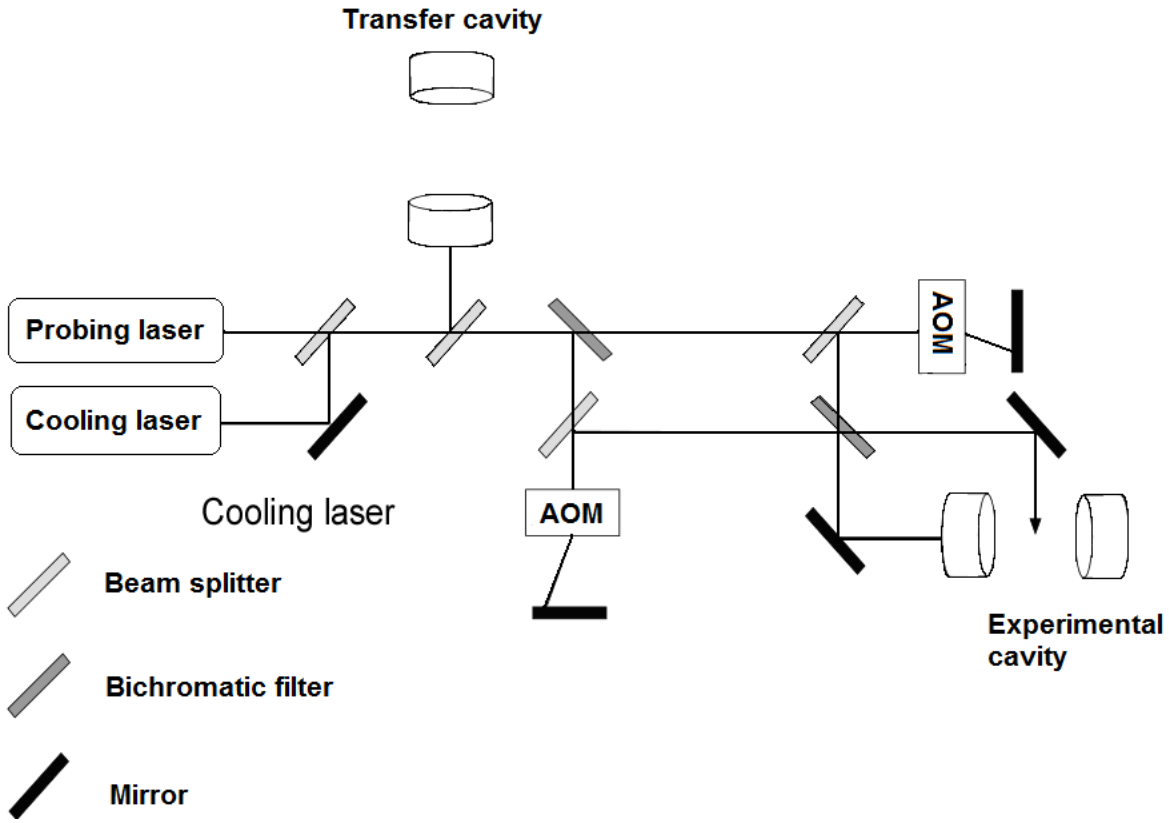

Figure 35: Outline of the optical set-up for the AOM lock. The probing and the cooling laser beams were split on a bichromatic filter and the two beams went double pass through two different AOMs. The probing laser beam goes to the in-coupling mirror of the experimental cavity and with the AOM it was locked to a cavity mode. A second removable bichromatic filter could be used to send the cooling beam to in-coupling mirror or illuminating the atoms in the cavity from the side. The error signal was sent to the AOM for the probing laser to keep it resonant with the experimental cavity. It was also sent to the AOM for the cooling laser to ensure the cooling laser had a constant detuning to the a cavity mode.

One of the mirrors of the experiment cavity was mounted on a piezo tupe (6 μm displacement over 500 V). By changing the length of the cavity by half a wavelength (λ/2), the frequency of a given longitudinal mode was changed by one free spectral range at the wavelength λ. At λ = 830 nm a scan of one free spectral range corresponded to a change of the voltage over the piezo of 33 V.

The desired detuning from the cooling beam from a longitudinal mode of the experimental cavity in the cooling schemes presented in chapter 4 was from a few kHz to a few hundred kHz. By the detuning of the cooling beam is in the following discussion meant the detuning to the longitudinal mode of the experimental cavity, which gave the least detuning.

Setting the detuning of the cooling beam

The detuning of the cooling beam could be set by three different methods. In the first method, the detuning was set by the choice of the longitudinal mode of the transfer cavity, which the cooling beam was locked on. By choosing the longitudinal mode of the transfer cavity with the least frequency difference to a longitudinal mode of the experimental cavity, the detuning of the cooling beam was less than 212 MHz (see Figure 36).

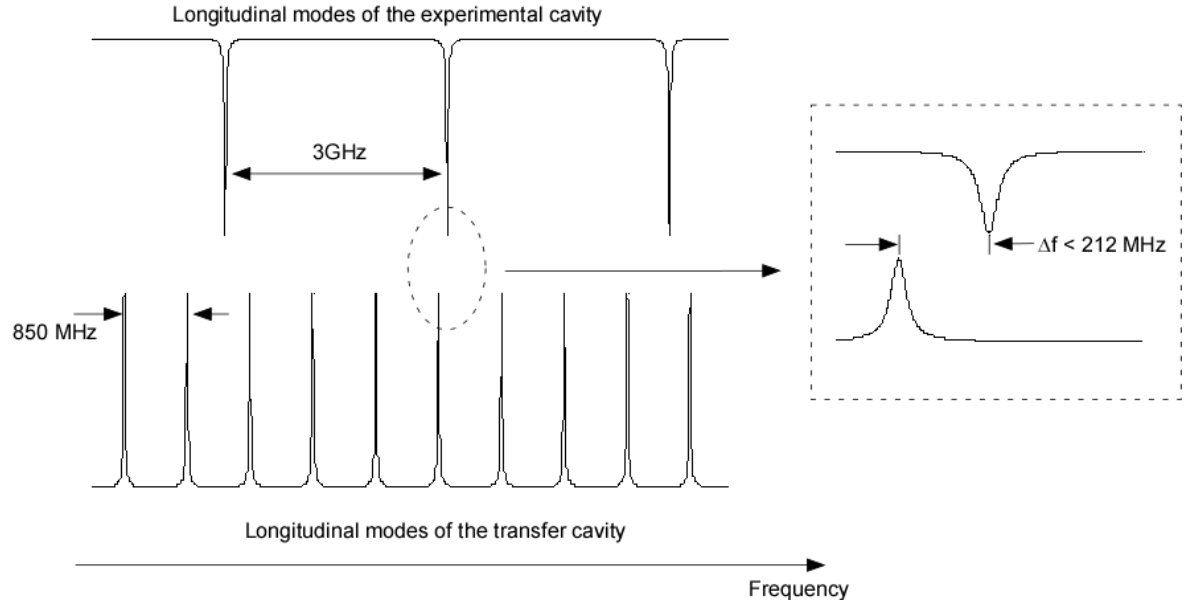

Figure 36: There were roughly 3.5 longitudinal modes of the transfer cavity between two longitudinal modes of the experimental cavity. The maximum frequency difference between a longitudinal mode of the experimental cavity and the longitudinal mode of the transfer cavity with the least frequency difference was 212 MHz.

The detuning of the cooling beam could be changed by two additional methods: either by changing the frequency of the AOMs in the paths of the cooling beam or the probe beam, or by changing the voltage over the piezo.

The first and the simplest additional method was to change the frequency of AOM in the path of the cooling beam. Without a major power loss in the first diffraction order, the frequency of the AOM could be changed with ± 25%. As the cooling beam passed through the AOM twice the maximum frequency change possible by changing the frequency of the AOM was of the order 140 MHz. Similar the frequency of the AOM in the path of the probe beam could be changed, although the piezo length had to be adjust such that the probe laser stayed resonant with the experimental cavity.

While it was possible to adjust the frequency of the two AOMs such that the cooling beam was simultaneously resonant with a longitudinal mode of the transfer cavity and a longitudinal mode of the experimental cavity, it could be difficult to do this in practice. The frequency span, in which it was possible to scan the laser in the grating stabilized set-up without mode jumps was typically at its best a few GHz. Secondly, the stabilization on the transfer cavity depended on the current and stabilization might not work well at the longitudinal mode of transfer cavity with the least detuning.

The second additional method to change the detuning of the cooling beam compared to the closest longitudinal mode was to change the voltage over the piezo in steps of 33 V. The step size had to be 33 V to keep the probe laser simultaneously resonant with both cavities. The difference in the number of wavelengths at 825 nm and 795 nm, which corresponded to one round trip in the experimental cavity, was around 4500.

Frequency stability of the cooling beam

$$\Delta F \approx 4500\Delta_{FSR} = 4500\frac{c}{2L^2}\Delta L = 4500\frac{c}{2L^2}\frac{\Delta V}{500V}6\mu m \tag{113}$$

where ΔF is the frequency change between the longitudinal modes of the experimental cavity and the longitudinal modes of the transfer cavity due to a voltage change over the piezo of ΔV. L is the length of the cavity and Δ_{FSR} is the change in the free spectral range of the experimental cavity with a voltage change over the piezo of ΔV. A change of 33 V over the piezo gives a frequency change (ΔF) of 110 MHz. The change in the cavity length is used to find a longitudinal mode of the transfer cavity that is ± 50 MHz from a longitudinal mode of the experimental cavity, has a good lock on the transfer cavity and at a current through the laser diode that gives the desired power output of the laser diode.

The drift of the detuning of the cooling beam has to be small compared to the linewidth of the experiment cavity.

$$f_c = q_{t,c}FSR_t = q_{e,c}FSR_e + f_{AOM,c} + \delta \tag{114}$$

$$f_p = q_{t,p}FSR_t = q_{e,p}FSR_e + f_{AOM,p} \tag{115}$$

where f_c is the frequency of the cooling beam, f_p is the frequency of the probe beam, FSR_t is the free spectral range of the transfer cavity, FSR_e is the free spectral range of the experiment cavity, $f_{AOM.,c}$ is the frequency change through the double pass of the AOM for the cooling beam, $f_{AOM,p}$ is the frequency change through the double pass of the AOM for the probe beam and the q number are fixed natural numbers that give the longitudinal modes, which the probe and cooling beam are locked to or detuned from on the two cavities.

When the length of the transfer cavity is changed, it is assumed the length of the experimental cavity is changed such that the probe beam stays resonant with both cavities. From this condition, the detuning of the cooling laser ($\Delta\delta$) can be calculated from equation 114 and equation 115 in terms of the AOM frequencies, the q numbers and the free spectral range of the transfer cavity:

$$\delta = q_{e,c}\left(\frac{q_{t,c}}{q_{e,c}} - \frac{q_{t,p}}{q_{e,p}}\right)FSR_t + \frac{q_{e,c}}{q_{e,p}} f_{AOM,p} - f_{AOM,c} \tag{116}$$

The change in the detuning of the cooling laser for a small length change of the transfer cavity is then:

$$\Delta\delta < \Delta\frac{\Delta FSR_t}{FSR_t} = \Delta\frac{\Delta L_{transfer}}{L_{transfer}} = \Delta\, a \tag{117}$$

where a is the relative length stability. For having a stability of the detuning of 1 kHz of the cooling beam the relative length stability of the transfer cavity must be $3.3\ 10^{-7}$.

The stabilization on a test cavity

The stabilization of the probe on a test cavity with a linewidth of 70 kHz by with the AOM lock had successfully been done. As the experimental cavity one mirror of the test cavity was mounted on a piezo tube and by varying the voltage over the piezo, the length of the test cavity can be varied. The probe laser was locked to the transfer cavity and a periodic oscillation was sent to the piezo. The oscillation was chosen such that probe laser would at one or more times during the scan be resonant with a longitudinal mode of test cavity. When the probe laser beam becomes resonant with the longitudinal mode of test cavity, an error signal is generated for the AOM lock, and this can be used for stabilizing the probe laser to the mode. The AOM lock can for certain frequency span follow the longitudinal mode and keep the probe laser resonant, while the length of the test cavity is changed. But at a certain point in the scan the frequency the AOM lock has to add for keeping the probe laser resonant with the longitudinal mode is too large, and AOM lock cannot any longer follow the frequency of the longitudinal mode (see Figure 37).

Test cavity parameter	Value
Finesse	$1.1\ 10^5$
Free spectral range	8 GHz
Linewidth	70 kHz

Table 13: Test cavity parameters [90].

The same error signal sent to the probe laser to keep it resonant with the probe beam, was sent to the AOM for the cooling beam for it to keep it at the same detuning. By using the method earlier explained in this chapter the cooling laser and the probe laser beams were both at the same length of the test cavity made resonant with a longitudinal mode of the test cavity.

Part of the error signal was sent to the piezo to keep the test cavity resonant with the probe beam. With this set-up the transmitted light power of the cooling laser did not change over a time period of an hour.

The uncertainty of the transmitted light level for the cooling laser was of the order 10%, and for the frequency drift of the cooling laser to be observable the cooling laser had to drift a 1/3 of a linewidth of the test cavity. The linewidth of test cavity was 70 kHz, and therefore the drift of the cooling laser due a length of the transfer cavity was below 20 kHz in an hour.

To stabilize the probe laser beam on the experimental cavity is significantly harder than on the test cavity. One issue is the smaller linewidth, but the most significant problem was that that the experimental cavity was much more sensitive to mechanical vibrations. The frequency variation of a mode of the experimental cavity due to mechanical vibrations was of the order 20 MHz (see chapter 4.5), and this was much larger than the bandwidths of the AOMs in the current set-up are. Two possibilities for increasing the bandwidth were to strongly focus the beams in the AOM or use a frequency shifter.

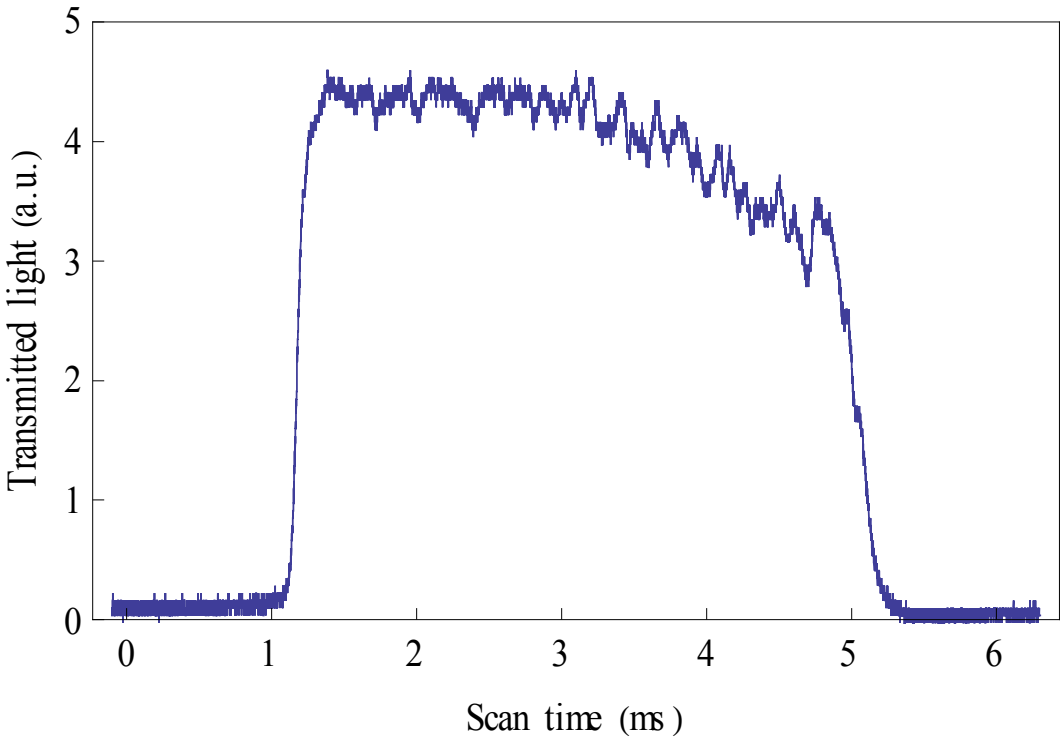

Figure 37: The transmitted light of the probe laser was measured for different times during a scan of the length of the test cavity. At a time slightly above 1 ms the probe laser beam became resonant with a longitudinal mode of the test cavity, and the AOM lock could stabilize the probe beam to that mode. At certain point (around 6.5 ms on the graph) the AOM lock could not any longer follow the mode and the probe beam went out of lock with that mode.

6 Bose-Einstein Condensation

In this chapter the experimental steps in the sequence for creating a Bose-Einstein condensate (BEC) are characterized. The experimental set-up and methods for the various steps were explained in chapter 5.

To create a BEC from a thermal gas with a temperature of several hundred Kelvin requires several experimental steps. In the first MOT Rb_{87} atoms were captured from a thermal gas released by a pair of dispensers. An atomic beam was created by an imbalanced beam pressure in the first MOT along the direction of gravity, and this beam loaded a second MOT. After a sufficient number of atoms had been collected in the second MOT, the atomic sample was compressed and cooled in a compressed MOT phase (CMOT) followed by an optical molasse, which further cooled the atomic sample.

The atomic sample is then transferred into a magnetic trap by first switching the laser beams off for the MOTs, and then ramping the current in the MOT coils to 16 A. The atomic sample was transported to a second magnetic trap (the QUAD) trap. The QUAD trap was a linear magnetic trap with a high gradient. This made it well suited for evaporative cooling until the temperature where the loss rate due to Majorana spin flips became comparable to the rate with which hot atoms were removed from the trap by the radio frequency. The atoms were then transferred into a third magnetic trap (The QUIC trap). The advantage of the QUIC trap over the QUAD trap was that it has a local magnetic minimum different from zero, however, the compression was smaller in the QUIC trap than in the QUAD trap. The atoms were in the QUIC trap cooled evaporatively to the transition to BEC.

The second MOT, the CMOT and the optical molasses are characterized in chapter 6.1. In chapter 6.2 the transfer into the MOT magnetic trap, the transport and transfer into the QUAD trap are characterized. In chapter 6.3 the forced evaporation by an applied radio frequency field is characterized and lastly in chapter 6.4 the BEC is characterized by the bimodal atomic distribution and the non-isotropic expansion of the BEC.

6.1 Preparation of the atomic sample for the magnetic trap

Loading into the second MOT

The loading of the atoms into the second MOT as a function of time from the source can be approximated as:

$$N(t) = N_0\left(1 - e^{-\frac{t}{\tau_{load}}}\right) \tag{118}$$

where N_0 is the number of atoms in the second MOT in steady state between the number of atoms loaded into the trap and the ones lost from it. τ_{load} is the 1/e loading time. The loading time may be found by measuring the number of atoms during the loading at various loading times (see Figure 38). By fitting the function from equation 118 to the data in Figure 38 the loading time was found to be: $\tau_{load} = 11.1 \pm 1.5$ s.

Due to the long cooling period (35 s) in the end of the experimental sequence, the sequence time cannot be decreased by lowering the loading time.

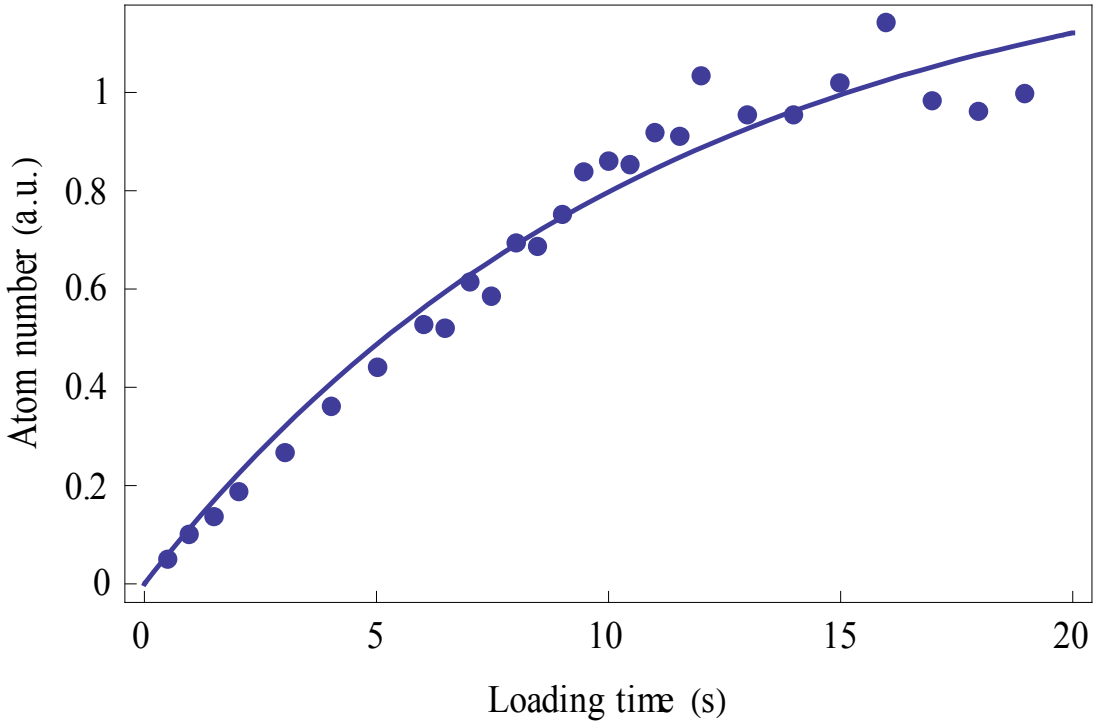

Figure 38: A loading curve of atoms into the second MOT.

Measurement of the temperatures in the second MOT

The efficiency of the evaporative cooling depends on the ratio of the collision time between the atoms and the lifetime of the atoms in the trap (see Figure 3). For the highest possible collision rate, the temperature in the magnetic trap should be as low as possible. To achieve the lowest temperature in the magnetic trap before the atomic sample was loaded into the magnetic trap it should be as cold and dense as possible, and that was the purpose of the CMOT and the optical molasse. The CMOT was used for both cooling and compressing the atomic sample, and it was optimised such that the atomic sample after the optical molasse was as dense as possible. The optical molasses was optimised for the lowest possible temperature and for the no measurable increase in the size of the atomic sample.

In chapter 2.5 it was shown that the atomic distribution of a thermal sample held in a harmonic potential in the classical limit will expand as a Gaussian distribution:

$$\sigma(t) = \sqrt{\sigma_0^2 + v^2 t^2} \tag{119}$$

where σ_0 is the 1/e radius before expansion and v is the average velocity of the atomic distribution. The atomic distributions after the optical molasse or the CMOT are not Gaussian as they are both in the density limited regime, however if the samples are allowed to freely expand for about 6 ms, the approximation of a Gaussian distribution becomes valid.

In Figure 40 a time of flight measurement for the optical molasse is shown and the function given by equation 119 is seen as a good fit.

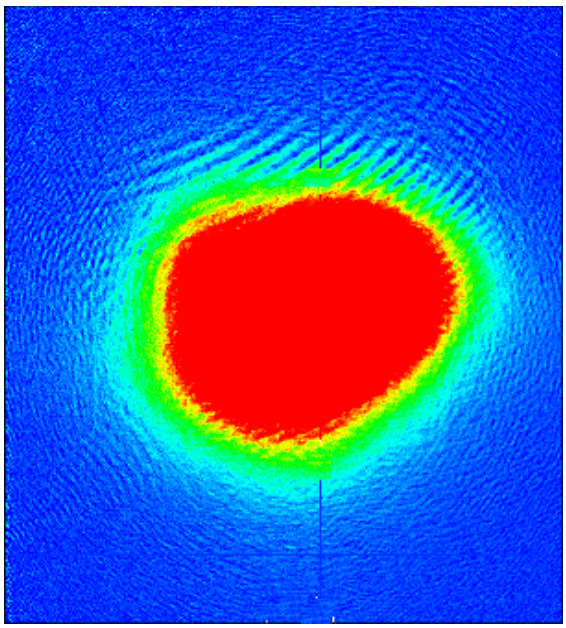

Figure 39: The shape of the atomic sample after the optical molasse.

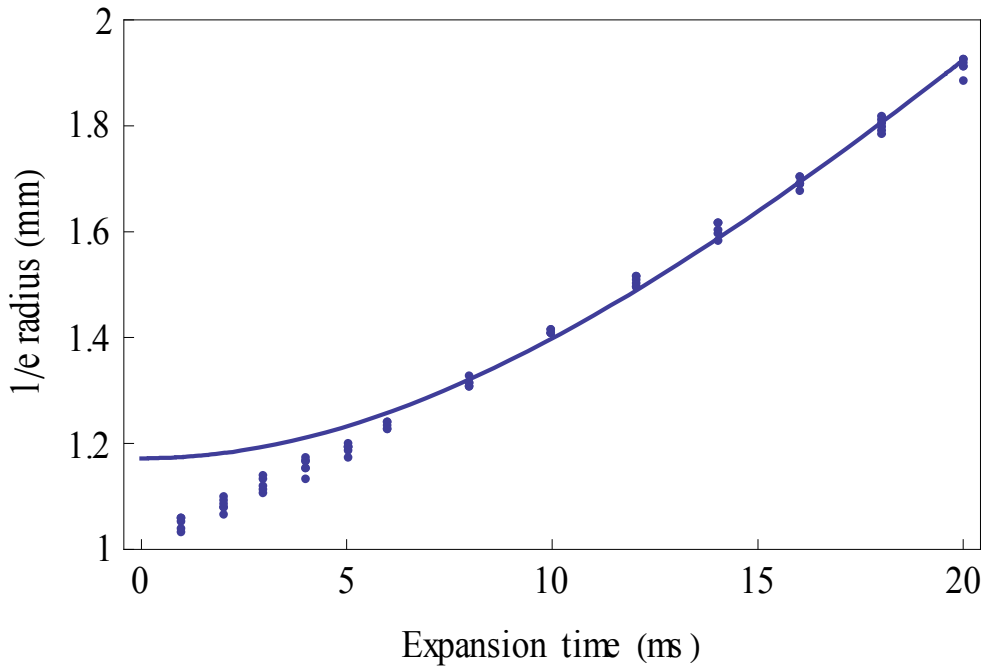

Figure 40: Expansion of the atomic sample after the optical molasse. Only the points with times greater 6 ms had been used for the fit.

In [50] it is predicated that the temperature of the atomic sample scales as I/δ, where I is the intensity of the MOT beams and δ is the detuning from the cooling transition in the optical molasse. By increasing the detuning it was found that the temperature of the atomic sample could be decreased, but lower intensity only resulted in a lower atom number. This is similar to the result reported in [91].

After the optical molasse, the atomic sample was spin polarized in an optical pumping stage. This increased the number of atoms in the magnetic trap by a factor 2 without any measurable temperature increase.

	Atom number (10^8)	Temperature (μK)	1/e radius (mm)
MOT	8-10	---	2-3
CMOT	8-10	100	1.0
Optical molasse	8-10	20	1.0

Table 14: The parameters for the MOT, the CMOT and the optical molasse. The MOT temperature could not be reliable measured due to the irregular shape.

6.2 The magnetic traps

The first magnetic trap is made by ramping the current in the MOT coils up to 16 A. It was found that capturing the atomic sample after the optical pumping stage with the highest possible magnetic field gradient gave the highest phase space density for the sample in the magnetic trap. Capturing the atomic sample after the optical pumping stage at an initially lower magnetic field gradient gave a lower atom number in the magnetic trap. The temperature difference between the sample captured with the highest magnetic field gradient, and a sample captured at a lower magnetic field gradient could be explained by the higher compression at the maximum field gradient. The temperature of the atomic sample in the MOT magnetic trap was 150 μK, and the atom number was typically 4 10^8.

The transport from the first magnetic trap to the position of the quadrupole trap was made in 1.25 s with a transfer efficiency around 80%. The number of atoms in the quadrupole trap was 3-4 10^8 at a temperature of 400 μK. The compression in the QUAD trap compared to the MOT magnetic trap was a factor 6.6, and the expected temperature increase due to adiabatic compression was a factor of 3.5.

When the radial radius (ρ) of the atomic sample was below 0.1 mm, the potential in the Ioffe-quadrupole trap is close to be harmonic in the radial direction (see Figure 31). The trap frequencies for the harmonic trap could be measured by giving an atomic sample with a radius much smaller than 0,1 mm a small kick. The atomic sample would then oscillate in the trap with the frequency of trap in the direction of the kick. The velocity of the atomic sample depends on where the atomic sample is in the oscillation cycle. The velocity of the atomic sample at a time t after the kick was measured by quickly switching the trap off (non-adiabatic) and then having the atomic sample fell freely for 25 ms. Thereafter measuring the centre position of the atomic sample as a function of the holding time after the kick.

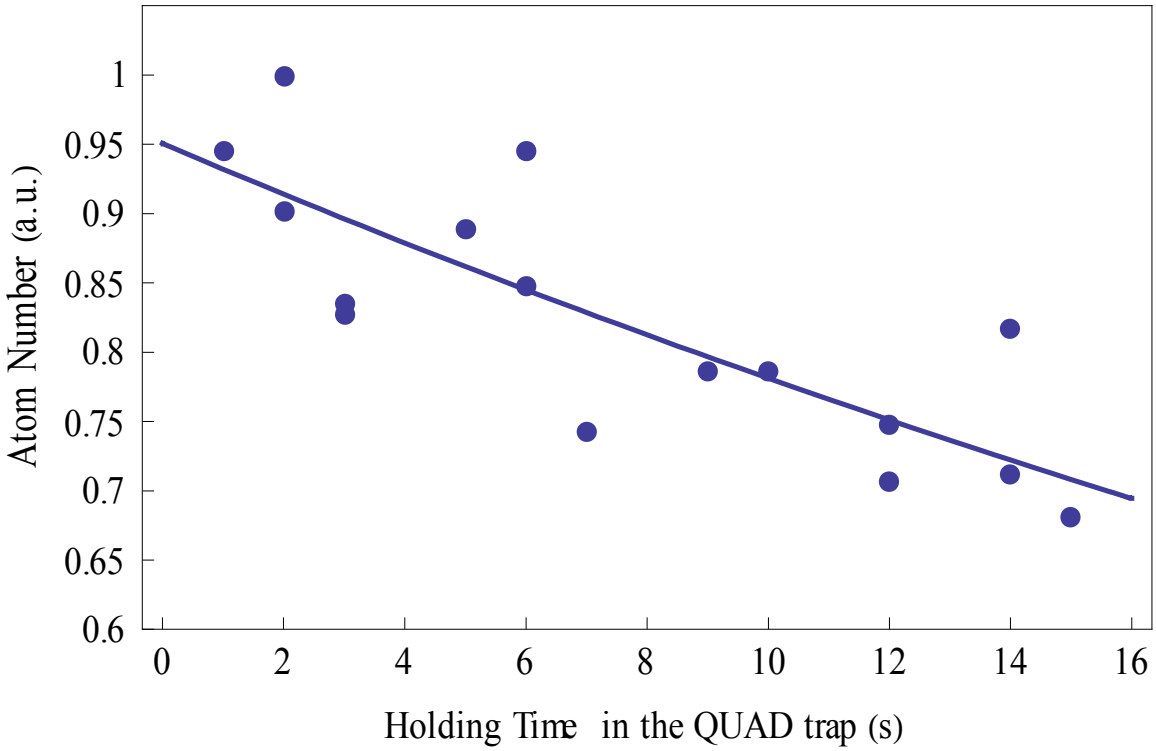

Figure 41: Life time measurement of the atomic sample in the QUAD trap. 1/e lifetime was 50 ± 10 s.

A displacement in the radial direction (perpendicular to gravity) was created by ramping a current up in an offset coil, and switching the current off in the coil so the atomic sample could not be adiabatically adjusted. An axial oscillation was created with a similar method, and the displacement was created by ramping the current in the Ioffe coil.

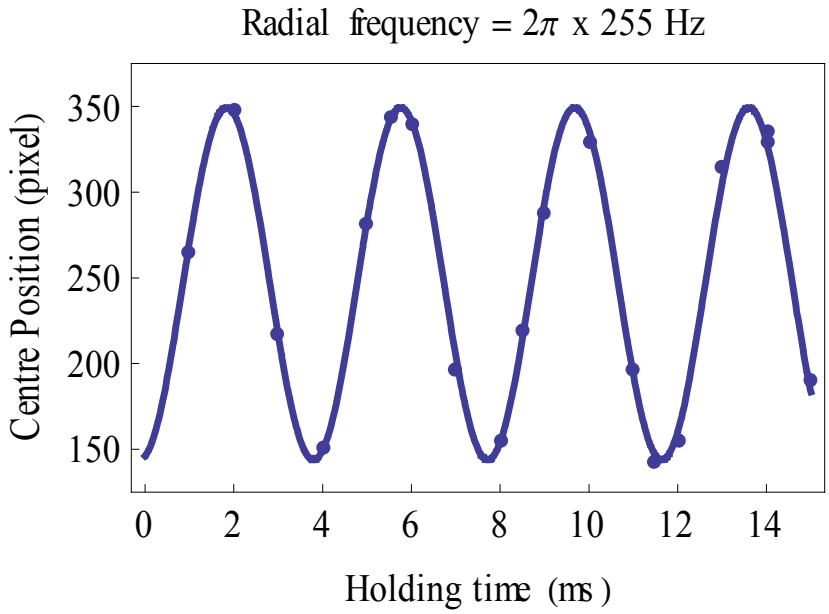

Figure 42a: Measurement of the radial trap frequency in the QUIC trap.

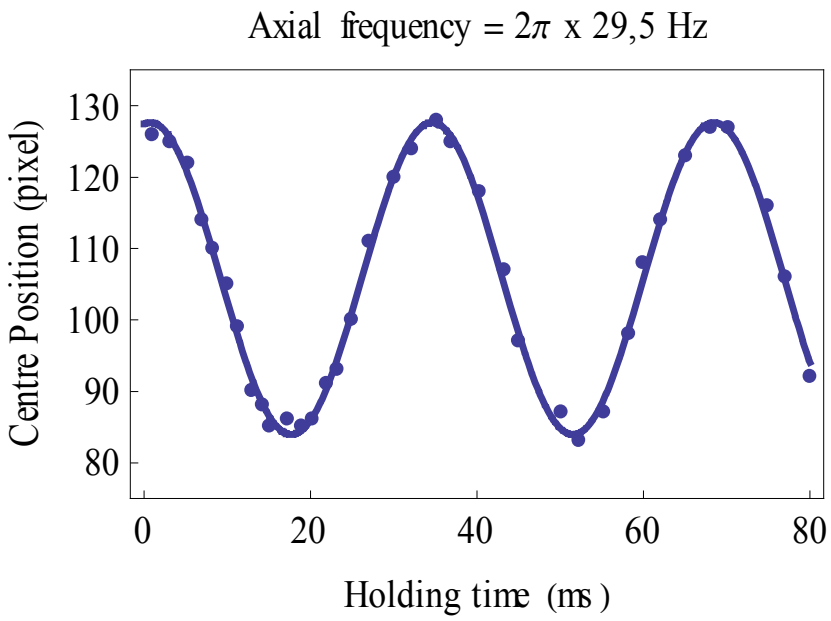

Figur 42b: Measurement of the axial trap frequency in the QUIC trap.

The measured value of the trapping frequency and the calculated one from the trapping potential were 6% off in the axial direction and 14% off in the radial direction. Thus the aspect ratio between the two trapping direction is then: $(\omega_z/\omega_\rho) = 0.11$.

6.3 Evaporative cooling

The evaporative cooling was optimised in such a way that the atomic sample had the maximum cooling per atom removed from the trap. In terms of the parameter α introduced in chapter 2.3, which means that α should be as high as possible. The temperature (T) and the atom number (N) can be measured at different times in the evaporation run and from these numbers a value of α can be estimated. The temperatures were measured with time of flight measurements. The optimal time to change the radio frequency from one fixed value to another fixed value can be found by finding the times, which give the maximal value of α. For a quick optimisation the two dimensional peak density after a small expansion that allows the magnetic field to be switched off can be measured instead of α.

To avoid a hot cloud of atoms to remain in the trap after the evaporation, a ramp from 100 MHz to 30MHz in one second at maximum power was used. Evaporating at frequencies above 30 MHz was measured to have no significant atom loss due to evaporation and because of this, 30 MHz was used as the starting frequency for optimising the evaporation run.

Initially the atomic sample was evaporated in the QUAD trap. The lowest applied frequency in the quad trap was 17 MHz, and the atomic sample was then transferred into the QUIC trap. At 17 MHz, the FWHM of the atomic sample was of the order 1 mm in the strongly confined direction. From Figure 2 in 2.4 the lifetime associated with Majorana spin flips is of the order 1 minute, which is comparable to the lifetime in the magnetic trap.

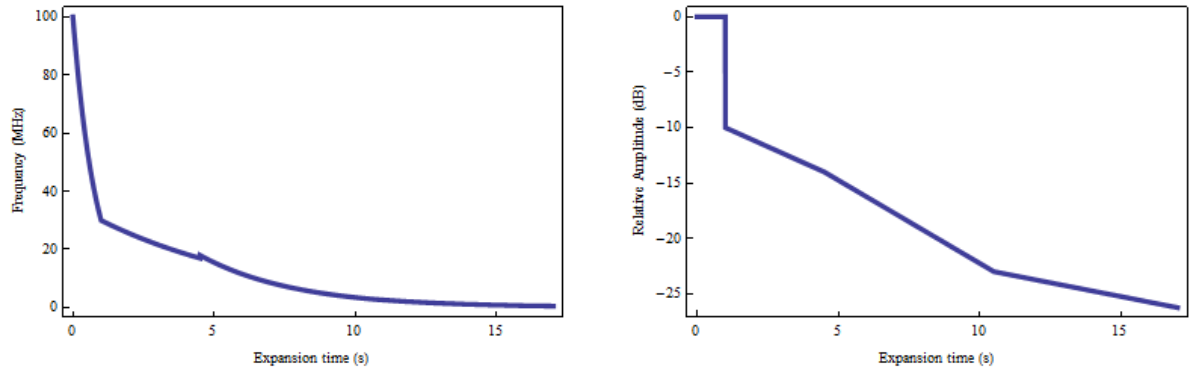

Figure 43: The frequency variation during the evaporation ramp is shown on the left graph, and the amplitude variation during the evaporation run is shown on the right graph.

Due to the displacement of the trap minimum due to gravity, atoms with the same potential energy do not experience the same magnetic field. Atoms closer towards the Earth experience a higher magnetic field than the ones further away. As the radio frequency removes atoms at a certain magnetic field, the radio frequency will more likely remove atoms close to the Earth than the ones further away. This effect becomes important, when the width of the atomic sample becomes comparable to the displacement. The displacement was 0.5 mm and the change in the magnetic field seen by the atoms at the minimum is 1.6 Gauss. To remove atoms at a magnetic field of 1.6 Gauss a radio frequency field of 4.5 MHz is needed.Hence the displacement of the trap minimum lowered the effectiveness of the evaporation below 4.5 MHz.

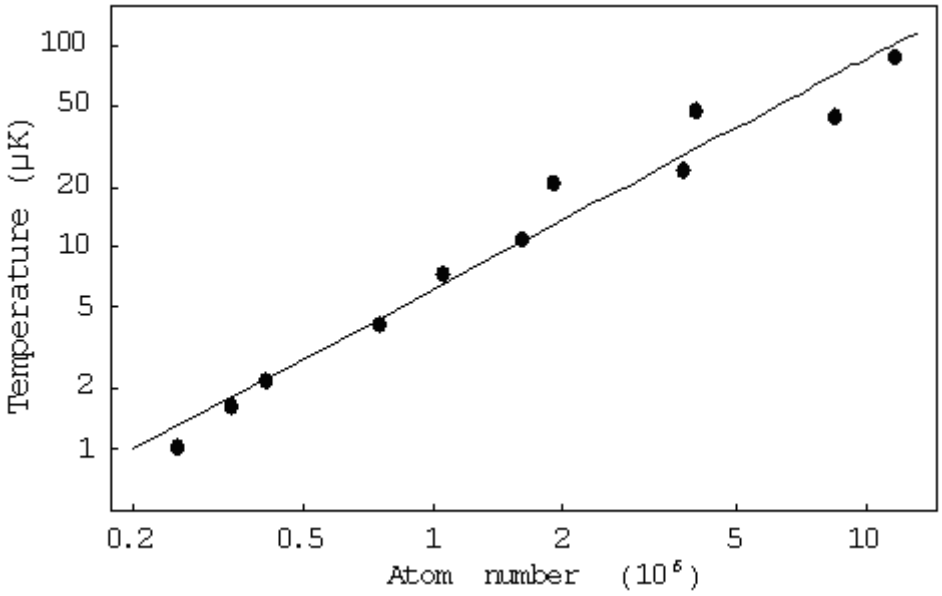

Figure 44: α measurement. The temperature (T) and the atom number (N) were measured at different times in the evaporation cycle. From the measured values of T and N α was estimated to be 1.13 ± 0.07. The atom number at 2.5 10^7 corresponds to an evaporation time of 7 seconds (see Figure 43), and at higher atom numbers the temperature and atom number could not be reliable measured due the high magnification of the imaging set-up.

The measured value of α was 1.13 (see Figure 44), and the limit for run-away evaporation in a harmonic trap is 1. The value of α for the four measurement with the lowest atom number was 1.6, and the higher value of α in the end of the evaporation ramp can be taken as an indication that 3-body recombinations were not significantly lowering the effectiveness of the evaporation close to the transition to the BEC.

The phase transition was observed when the end frequency of the evaporation was 590 kHz. The number of atoms before evaporation was around $2\ 10^8$ at 400 μK and the number of atoms in the BEC was $3\ 10^5$ at 300 nK.

6.4 Observation of a Bose-Einstein Condensation

The phase transition to a Bose-Einstein condensation can be observed with two different methods. The combined two dimensional density distribution of a partly condensed atomic sample is bimodal. The density profile of the fraction of the atomic sample in the BEC is given by the Thomas-Fermi distribution, and the density profile of the thermal cloud can be approximated as Gaussian for large atom numbers.

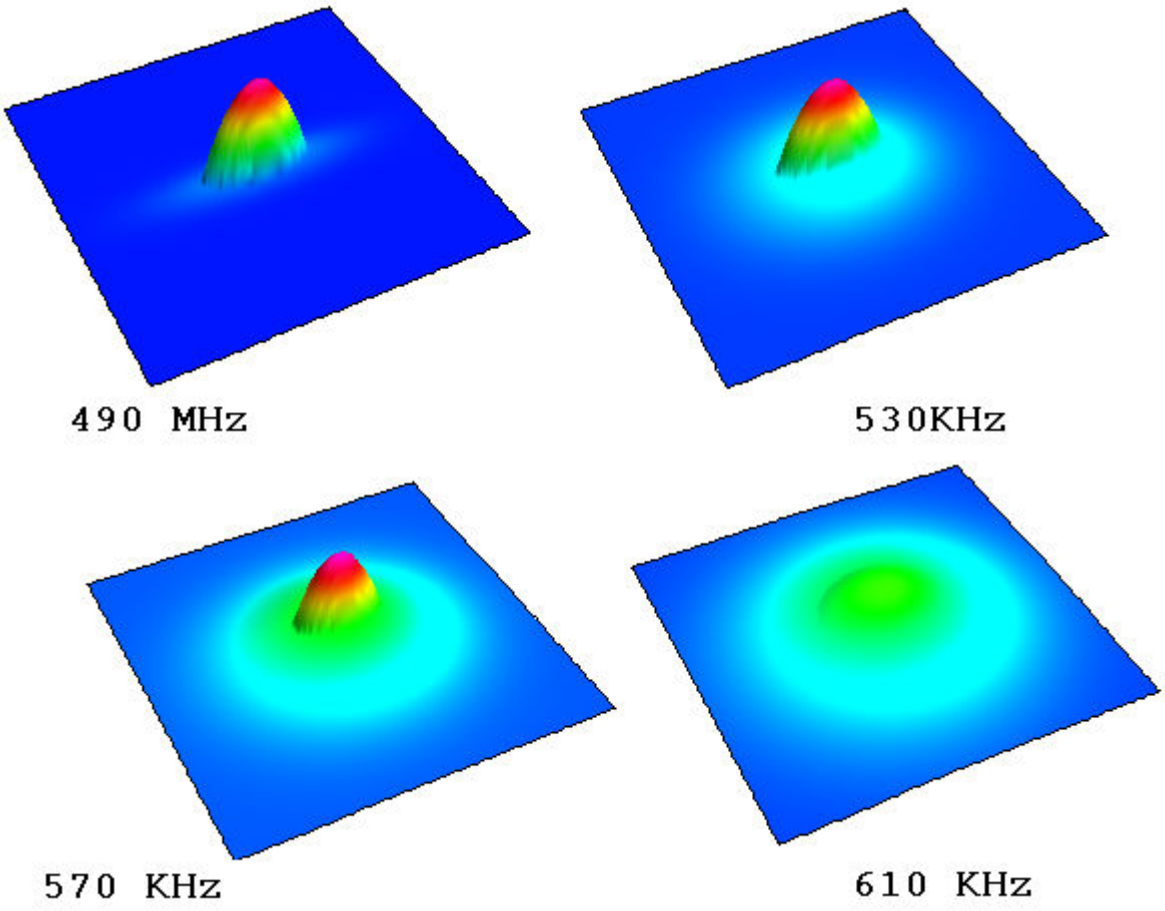

Figure 45: The atomic sample has been allowed to fall freely for 25 ms. The frequency below the pictures is the end frequency of the evaporation ramp. A nearly pure BEC can be observed at 490 kHz.

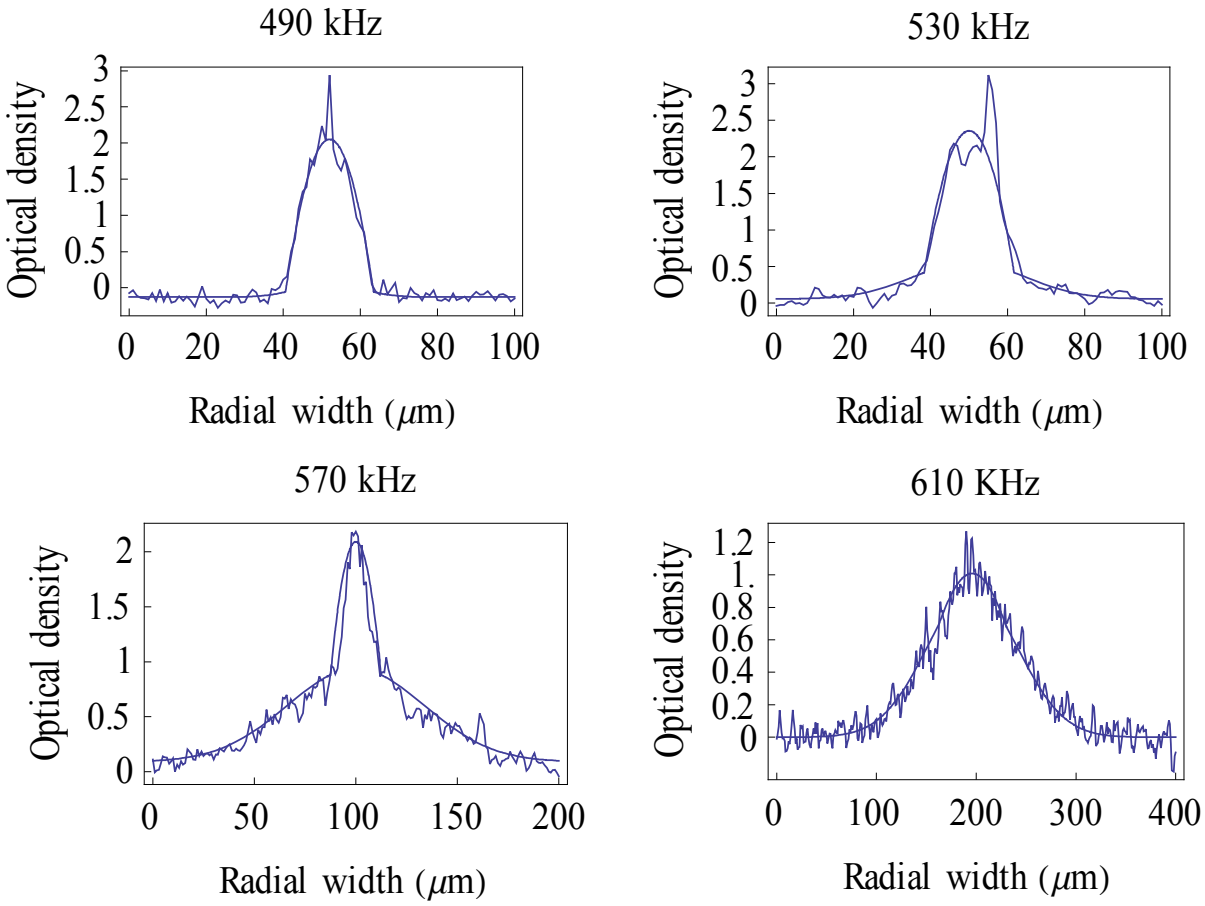

Figure 46: The radial density profile (ρ) for different end frequencies of the evaporation ramp. The source data is the same as for the pictures shown on Figure 45. Both the measured density and the fitted bimodal distribution are shown. From the bimodal fit, the fraction of the atoms in the BEC can be estimated.

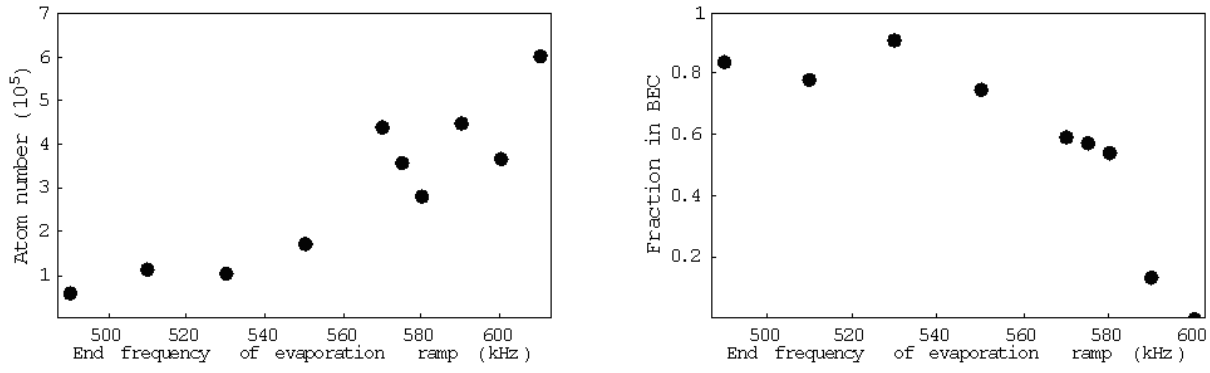

Figure 47: Condensate fraction and the atom number as a function of the end frequency of the evaporation run.

The expansion of a thermal cloud is isotropic after it has expanded to a size much larger than the original size, while this is not the case for the expansion of a BEC. Observing the non-isotropic expansion given by equation 27 and equation 28 in chapter 2.5 is a second method to identify a BEC. A pure BEC, which has been released from a confining potential, expands because the interaction energy between the atoms in the atomic sample is converted into kinetic energy when the atomic sample is allowed to freely expand. From equation 27 it can be seen that the characteristic time for the mentioned conversion in the radial direction is $\omega_\rho t = 0.6$ ms. Similar the characteristic time in the axial direction is $(\omega z^2/\omega_\rho \ t) = 44$ ms. After 27 ms expansion the atomic sample is outside of the region, which can be imagined.Thus it was not possible to detect any expansion along the axial direction (see Figure 49).

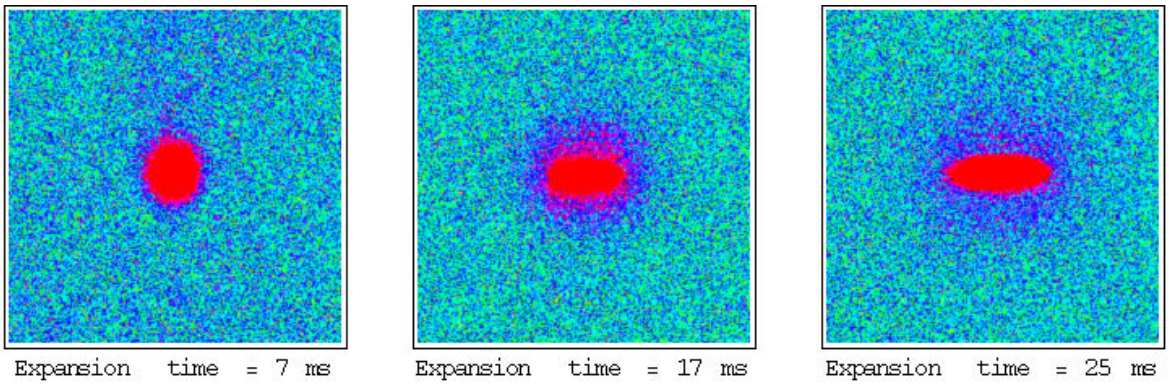

Figure 48: The end frequency of the evaporation ramp is 500 kHz.

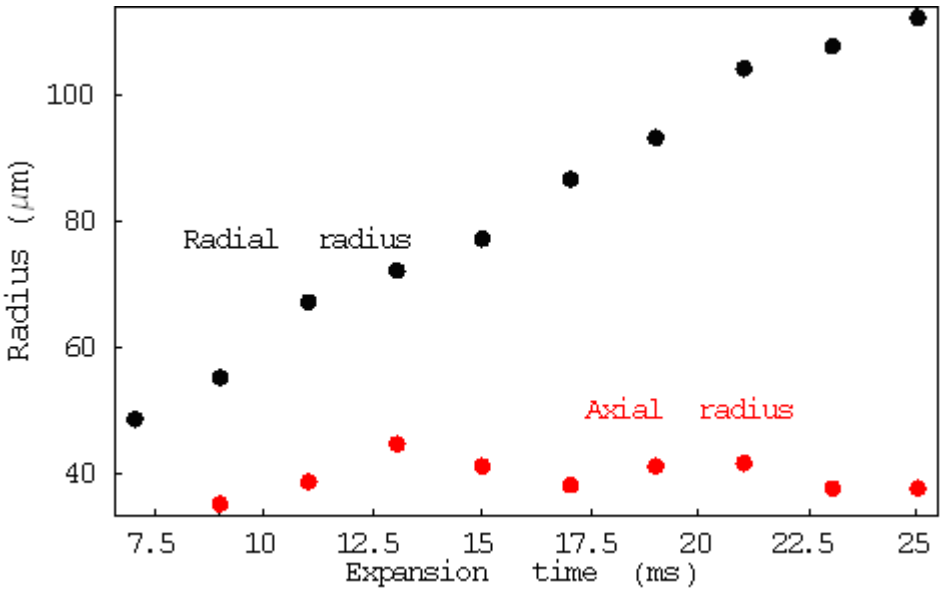

Figure 49: The radial and axial radiuses of the a pure BEC during a free expansion. The source data is the same as for Figure .

7 Perspectives

A BEC of a few hundred thousand atoms can be transferred into a cavity mode with the present experimental apparatus. To explore the atom/cavity interaction three different scenarios were considered in chapter 4: self-organization, cavity Doppler cooling and cavity sideband cooling.

The self-organization process was considered in chapter 4.3. The expected threshold intensity of the pump beam is low, even at a large atomic detuning for the pump beam (10 $\mu W/cm^2$ at 30 nm atomic detuning). The transmitted power through the transmission mirror is 1 nW at a pump intensity of 10^5 mW/cm^2. By focusing a laser beam of 10 mW to a waist of 100 μm the desired intensity at the position of the atomic sample can be achieved. The Rayleigh length of a Gaussian beam with a waist of 100 μm is about 4 cm, and this sets the accuracy of the how well the waist of the pump beam has to overlap with the atomic sample in order to obtain the desired intensity at the position of the atoms.

The detuning of the pump beam to the cavity mode with atoms in the cavity mode must be negative (the potential U_1 in equation 81 has be smaller than zero). The potential U_1 is larger for large cavity detunings, however, the number of photons scattered per atom in the cavity mode is lower (see I_0 in equation 81), and this will increase the threshold power for self-organization.

An advantage of using a high-finesse cavity with a large mode volume to investigate the self-organization is the fact that the atom number N_0 is higher for a cavity with a large mode volume for a given atomic detuning. N_0 is the atom number where the atom/cavity interaction changes from the weakly coupled regime (superradiant) to the strongly coupled regime (suppression of fluorescence). The cavity decay rate (κ) and coupling strength (g) are inverse proportional to the length of the cavity (L). Thus N_0 scales as L, and in the limit of a large atomic detuning it is proportional with the atomic detuning. In a small mode volume cavity, a single atom has a much greater relative effect on the optical path length than in a large open cavity, and thus the atomic detuning has to be much greater than in large mode volume cavity to get the same relative optical path length change. Another experimental advantage of a large mode cavity over a small mode volume cavity is the higher power in the cavity mode in the limit of $N >> N_0$, where the power in the cavity mode scales as L^2 (see equation 85).

The advantage of using a large mode volume cavity for observing self-organization is a lower threshold power. It is easier to observe the transition from the superradiant regime to the suppression of the fluorescence regime and a large power emitted through the transmission mirror.

Two different scenarios for cavity cooling were considered. Doppler cavity cooling in chapter 4.2 and cavity sideband cooling in chapter 4.4. For both scenarios, only an atomic sample close to the transition to a BEC has a small enough waist to efficiently be loaded into the cavity mode (waist of 20 μm). Furthermore, due to the small linewidth of the cavity only a few scattering events are allowed before the atom is out of resonance with the cooling transition. Hence in both scenarios only an atomic sample close to the BEC transition can be loaded efficiently into a dipole trap by a cavity mode, and only for an atomic sample close to the BEC transition all atoms in the sample can simultaneously be cooled.

Of the two cooling scenarios the Doppler cavity cooling is the more promising cooling method due to the possibility of self-organization. An interesting scenario to investigate would be to load a BEC into a dipole trap by two adjacent cavity modes such that the potential along the propagation direction is suppressed. Then the atomic sample can then be allowed to heat up to a temperature above the transition temperature for a BEC, and then the cooling beam can be applied to cool the atomic sample below the transition temperature. The cooling rate for a single atom is 3 μK/ms for an intensity of 10^7 mW/cm^2. The lifetime of the BEC in the dipole trap is expected to be in the range of a few hundred ms, and thus it would be desirable to have a sufficient cooling rate to cool the atomic sample back to a BEC with a timescale in the range of ms. The self-organization process can increase the scattering rate into the cavity mode, and this could significantly lower the intensity requirement of the pump beam for a given cooling rate.

The advantage of using a large mode volume cavity for cavity Doppler cooling is the low Doppler temperature due to the small linewidth, however, one has to keep in mind that a small linewidth accounts for a small capture velocity.

An interesting perspective for further development could be to use the cavity for quantum non-demolition measurements on a cold atomic gas. In [92] it is discussed how scattering into a cavity mode can be used to distinguish between a Mott insulator state and the super-fluid state of an atomic gas in an optical lattice. The detection of the detects in an optical lattices by measuring the polarization of the photons in the cavity is suggested in [93]. The study of cold atoms in optical lattice is a very interesting field of research as it offers a parallel to the crystal structures known from solid state physics. The advantage of studying cold atoms in an optical lattice instead of a crystal structure is the much greater control of the experimental parameters.

Appendix A: Laser systems

All the laser beams needed in this experiment are generated by diode lasers. The advantages of diode lasers are a relative low price and high reliability. Laser diodes are easily commercially available for the Rubidium transitions used in this experiment (D2, 780 nm), and have power outputs which are sufficient to saturate the relevant transitions. When the laser diode is operated without additional feedback, the laser diode is said to be in free running mode. This operating mode is not desirable to use in the experiment due to a line width of typically a few MHz, difficult in getting the laser operating on a specific transition and the laser diode is often running multimode in free-running mode. To overcome these problems an external cavity set-up was used [94,95,96].

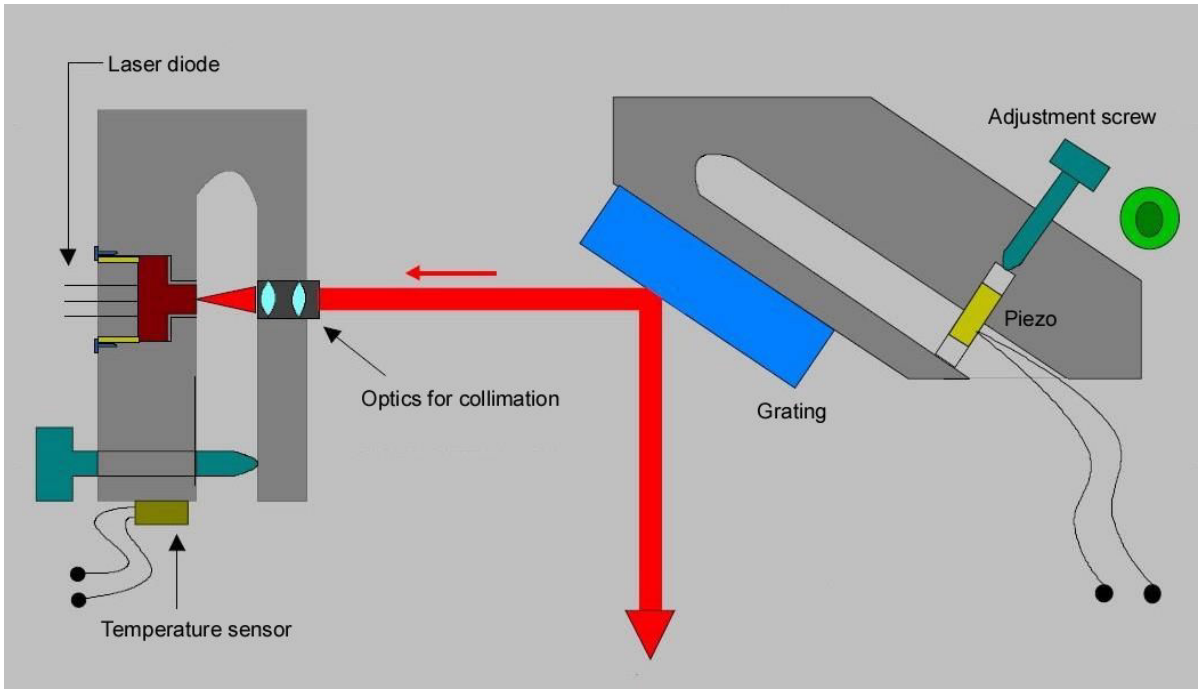

Figure 50: External cavity set-up [71].

The zero order mode of the diffraction grating is the output beam. From Bragg's law, it follows that for a certain wavelength, the incident beam and the first diffraction order coincide in the horizontal plane and the vertical angle of the diffraction grating is adjusted such they also coincide in the vertical plane.

The gain of a laser beam passing one time through the gain medium of the laser diode depends on wavelength. The laser diode itself is a cavity with a free spectral range of the order of 300 GHz. In free-running mode the laser is operating on the longitudinal mode of laser cavity with the highest gain. By varying the temperature of the laser diode and the current through it, the peak of the gain profile can be changed (typical values are: 0.3 nm/K and 4GHz/mA [94]).

The frequency width of the first order that is reflected back into the laser diode is of the order 100 GHz [97]. The external grating and front facet of the laser diode forms an external cavity with a length of the order 3 cm. Then the free spectral range of the external cavity is of the order 5 GHz. The laser will run the external cavity mode, which has the highest gain. By varying the length of the external cavity, it is possible to scan the frequency emitted by the laser diode.

Due to the external cavity, there is a higher light power in the laser cavity at same current compared to free running mode. Thus the threshold power is at a lower current with the external cavity, and this is used to see if the first order is sent back into the laser diode. The criterion for good injection is as low as possible threshold current. The beam is strongly divergent when it exits the end facet of the laser diode. A collimator is used to make a collimated beam. Fine adjustment of the distance between the collimator and the laser diode is done by trying to lower the threshold current. The number of lines on the grating (1800 lines/mm) was chosen such that the angle between the incident beam and the normal of the grating surface is roughly 45°. With this set-up it is possible to move the free-running wavelength ± 5 nm and have a line width in the sub MHz regime. The line width reduction is sufficient for using the laser beam for a MOT as the natural line width of the D2 line is 6.1 MHz [98].

The disadvantage of this method is the higher intra-cavity power due to the external cavity and this lowers the output power with around 25-30%.

A second method to change the wavelength of a diode laser is to inject a laser beam from another laser, which is running on the desired wavelength, into the laser diode. This is called a master slave configuration or injection lock. With this method it is possible to run the laser diode with a higher output power on the desired wavelength than with the previous method.

Appendix B: Pictures of the experiment

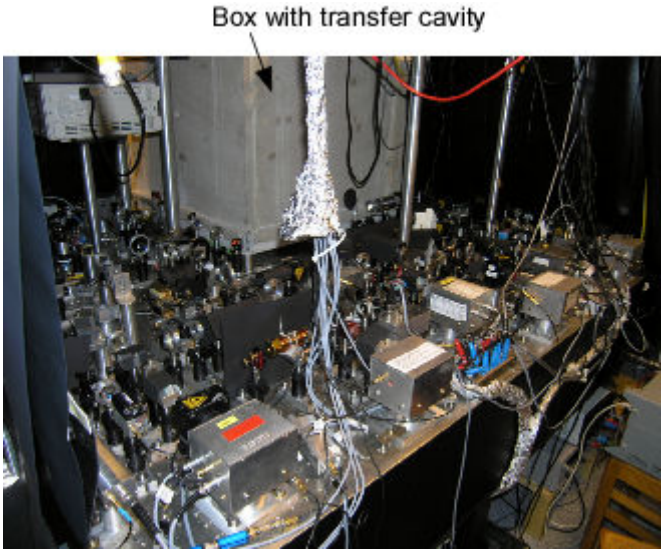

Figure 51: The optical set-up for generating the laser beams for the two MOTs and the imagining.

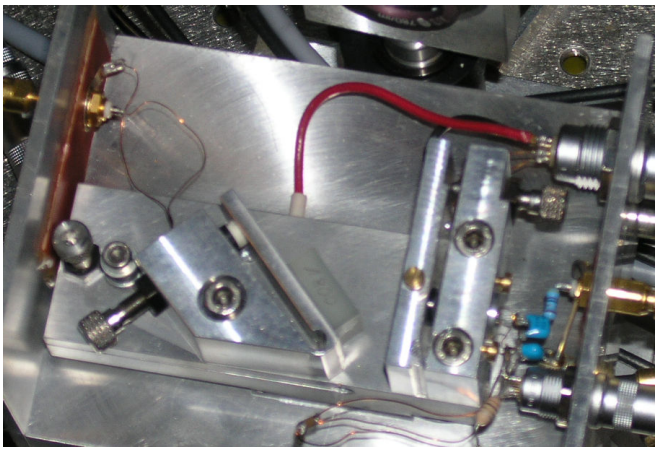

Figure 52: The grating stabilization set-up for the laser diodes.

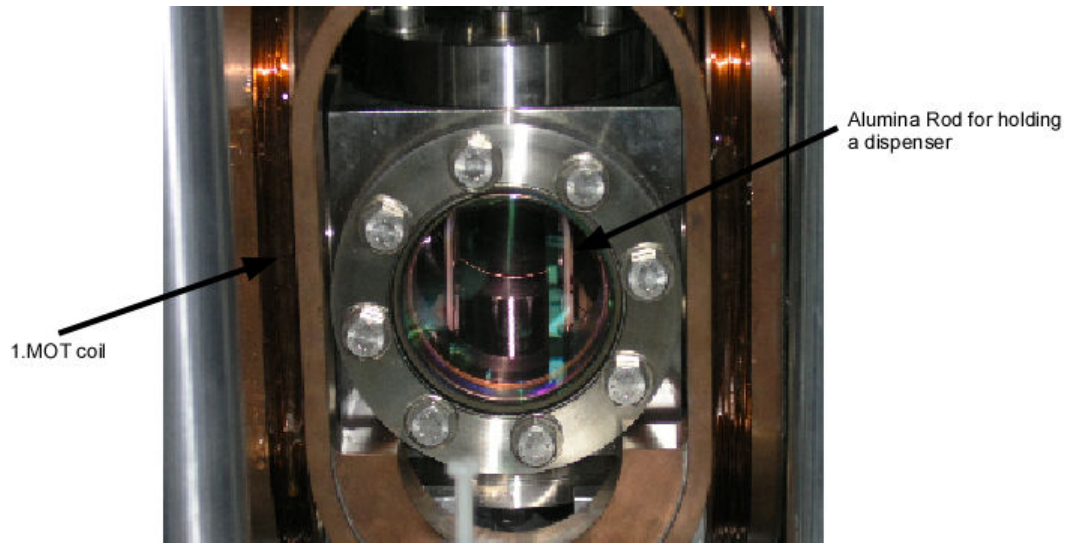

Figure 53: Picture of the first MOT chamber

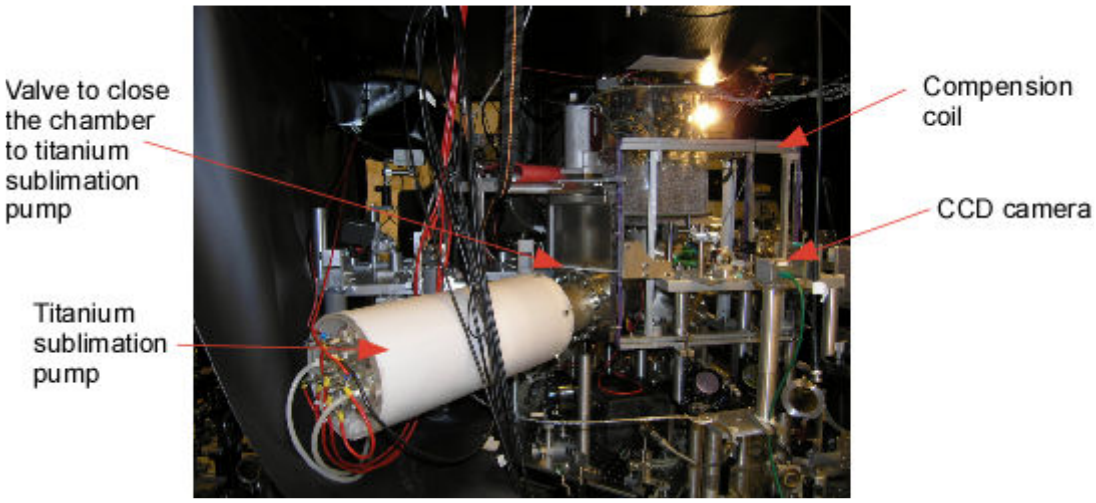

Figure 54 Picture of the experimental chamber

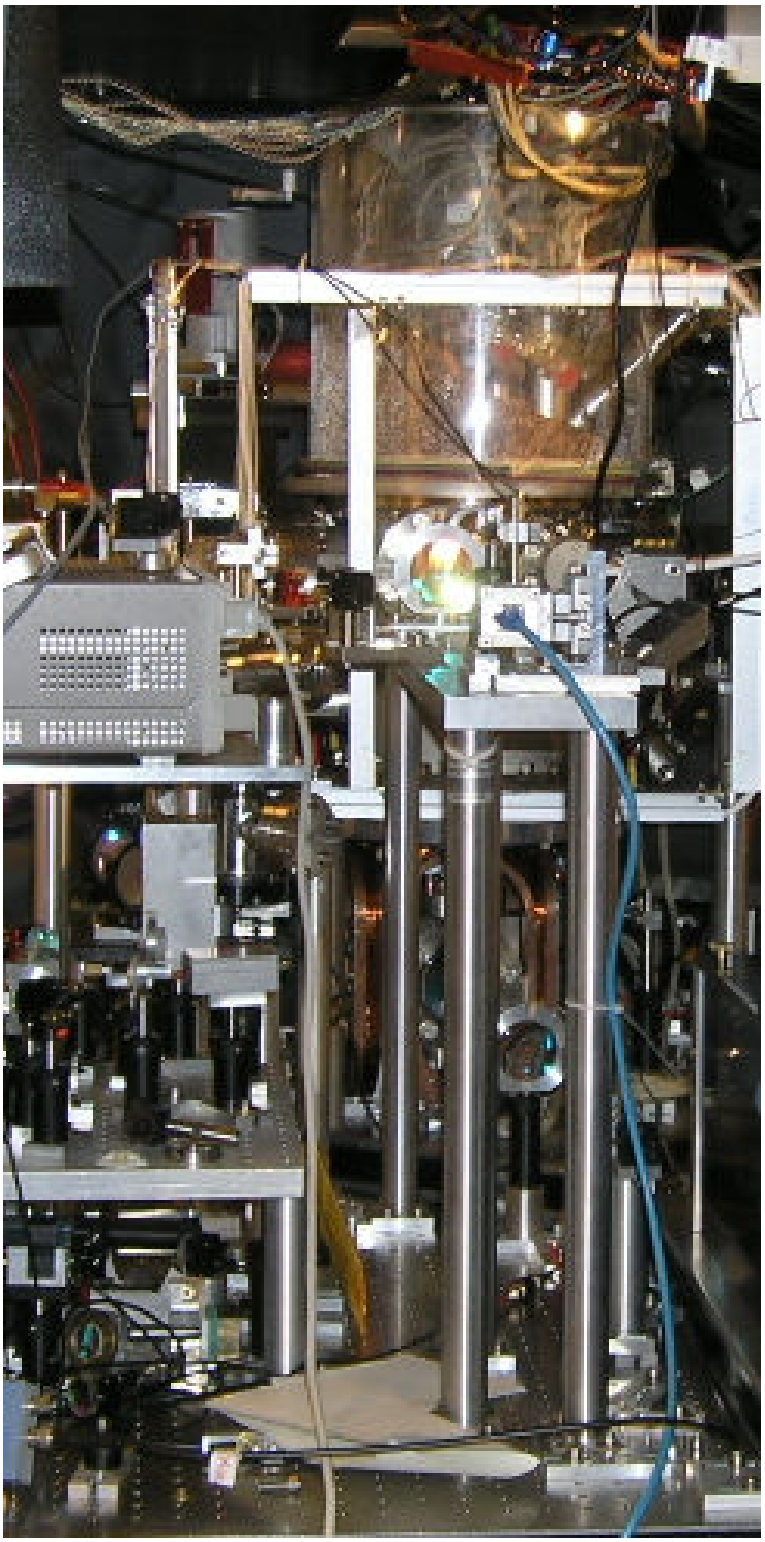

Figure 55: Picture of the experimental chamber

Acknowledgement

During my PhD I have had assistance and help of many different people and I wish to use this space to thank them. I foremost wish to thank my supervisor Professor Andreas Hemmerich for giving me the opportunity to work in experimental quantum optics. I am particular thankful for that he has always taken time to discuss the physical problems and to assist me with the many practical problems in the laboratory.

Dr. Boris Nagorny, I had the pleasure to work with during the first two years of my PhD. After leaving the group for a position at Desy he closely followed the experimental work in the lab, and I fondly recall many discussions about the experiment after the workday in the lab was over. I wish thank him for his many suggestions and corrections for my thesis.

I also wish to thank my other predecessor Dr. Thilo Elsässer for his assistance in setting the phase lock up, that we used for the measurement of the normal mode splitting. I wish to thank Kai Jentson for his work on the AOM lock and constructing the test cavity I used to test the AOM lock, and also thanks to Arne Wickenbrock for designing and constructing his very stable transfer cavity. I also acknowledge M. Wolke and J. Klinner for their work on the experiment.

An experimental physics is not an isolate island in the ocean and without a large group of people to assist the experiment it would never have been constructed. I wish to thank the current and previous members in the group of Professor Hemmerich for providing an interesting environment for experimental physics and for providing a good social atmosphere. I wish the Calcium team and the Lattice team the best of luck to finish their work and look forward coming to their disputations.

When designing and constructing a physics experiment many customs made parts are needed and luckily the institute machine shop lead by Mr. Fleig has done an excellent job of constructing the many parts we have needed. The Desy workshop deserves many thanks for constructing our vacuum chamber. I wish to thank Reinhard Mielck for the countless cables and many other things he has constructed for the experiment, to thank Dieter Barloesius for the optical components he has made, Stephan Garbers for his assistance in making metallic parts for the experiment and Frank Holweg for providing asssistance with and designing many electronic circuits. I wish to thank Silke Frömmig for assisting me by writing many letters in German on my behalf and to assist me with the practical issues of moving to Germany.

While I enjoyed living among the Germans, I enjoyed very much to have the opportunity to meet my fellow Danes, who were also living in Hamburg. These meetings were arrange by the Danish church in Hamburg and I wish to express my thanks for the arrangement and activities they have organized. Kristina Rasmussen deserves many thanks proofreading my thesis and her assistance have significantly improved the language of my thesis.

I am thankful that Prof. Dr. W. Neuhauser agreed to be the second corrector for my thesis and that Prof. Dr. K. Sengstock has agreed to be the corrector of my disputation.

Finally I wish to thank my parents and my brother Asger for their assistance and support through the years.

Bibliography

[1] M. Gross, P.Goy, C. Fabre, S. Haroche and J.M. Raimond, Maser Oscillation and Microwave Superradiance in Small Systems of Rydberg Atoms, Phys. Rev. Lett. 43, 343 (1979).

[2] D. Meschede, H. Walther and G. Müller, One-Atome-Maser, Phys. Rev. Lett. 54, 551 (1985)

[3] P. Maunz, T. Puppe, I. Schuster, N. Syassen, P. W. H. Pinkse and G. Rempe, Cavity Cooling of a Single Atom, Nature 428, 50 (2004)

[4] A. Lambrecht, J. M. Courty, S. Reynaud and E. Giacobino. Cold atoms: A new medium for quantum optics, Appl. Phys. B 60, 129-134 (1995

[5] C. Zimmermann, D. Kruse, C. von Cube, S. Slama ; B. Deh and P. Courteille, Collective Atomic Recoil Lasing, J. of modern optics, vol. 51, n°6-7, pp. 957 (2004)

[6] F. Brennecke, T. Donner, S. Ritter, T. Bourdel, M. Kohl, and T. Esslinger, Cavity QED with a Bose-Einstein Condensate, Nature, 450, 268 (2007)

[7] Y. Colombe , T. Steinmetz , G. Dubois, F. Linke , D. Hunger and J. Reichel, Strong Atom–field Coupling for Bose–Einstein Condensates in an Optical Cavity on a Chip, Nature 450, 272 (2007)

[8] S. Slama, S. Bux, G. Krenz, C. Zimmermann, and Ph.W. Courteille, Superradiant Rayleigh Scattering and Collective Atomic Recoil Lasing in a Ring Cavity, Phys. Rev. Lett. 98, 053603 (2007)

[9] B. Nagorny , Th. Elsässer, and A. Hemmerich, Collective Atomic Motion in an Optical Lattice Formed Inside a High-finesse Cavity, Phys. Rev. Lett. 91, 153003 (2003)

[10] W. Ketterle, D.S. Durfee, and D.M. Stamper-Kurn, Making, probing and understanding Bose-Einstein condensates, Proceedings of the International School of Physics "Enrico Fermi", Course CXL, edited by M. Inguscio, S. Stringari and C.E. Wieman (IOS Press, Amsterdam, 1999) pp. 67-176.

[11] A. Einstein, Sitzungsber. Preuss. Akad. Wiss., Bericht 1 (1925)

[12] M. H. Anderson, J. R. Ensher, M. R. Matthews, C. E. Wieman, and E. A. Cornell, Observation of Bose-Einstein Condensation in a Dilute Atomic Vapor, Science, Vol. 269. no. 5221, pp. 198 – 201 (1995)

[13] K. B. Davis, M. -O. Mewes, M. R. Andrews, N. J. van Druten, D. S. Durfee, D. M. Kurn, and W. Ketterle, Bose-Einstein Condensation in a Gas of Sodium Atoms, Phys. Rev. Lett. 75, 3969 - 3973 (1995)

[14] H.J. Lewandowski, D. M. Harper, D.L. Whitaker and E.A. Cornell, Simplified System for Creating a Bose-Einstein Condensate, Journal of low temperature physics, vol. 132, no5-6, pp. 309-367 (2003)

[15] C.J. Pethick, H. Smith, Bose-Einstein Condensation in Dilute Gases, Cambridge University Press (2002)

[16] F.H. Mies, C.J. Williams, P.S. Julienne, and M. Krauss, Estimating Bounds on Collisional Relaxation Rates of Spin-Polarized /Sup 87/Rb Atoms at Ultracold Temperatures, J. Res. Natl. Inst. Stand. Technol, 101, 521 (1996)

[17] F. Dalfovo, S. Giorgini, L. P. Pitaevskii, and S. Stringari, Theory of Bose-Einstein Condensation in Trapped Gases, Rev. Mod. Phys. 71, 463 (1999)

[18] A. J. Moerdijk, H. M. J. M. Boesten, and B. J. Verhaar, Decay of Trapped Ultracold Alkali Atoms by Recombination, Physical Review A, 53, 916 (1996)

[19] T.walker, D.Sesko and C. Wieman, Collective Behavior of Optically Trapped Neutral Atoms, Phys. Rev. Lett. 64, 408 (1990)

[20] D.W. Sesko, T.G. Walker, and C.E. Wieman, Behavior of Neutral atoms in a Spontaneous Force Trap, J. Opt. Soc. Am B, 8, 946 (1991)

[21] J. Dalibard and C. Cohen-Tannoudjii, Laser Cooling Below the Doppler Limit by Polarization Gradients – Simple Theoretical-models. J. Opt. Soc. Am. B. 6, 2023 (1989)

[22] G. Breit and I. I. Rabi, "Measurement of Nuclear Spin," Physical Review 38, 2082 (1931).

[23] W. H. Wing. Some Problems and Possibilities for Quasistatic Neutral Particle Trapping. In W. D. Phillips, editor, Proceedings of the Workshop on Spectroscopic Applications of Slow Atomic Beams, volume 653. NBS, Gaithersburg (1983)

[24] C. Zener. Non-adiabatic Crossing of Energy Levels. Proceedings of the Royal Society of London Series A, 137, 696 (1932)

[25] J. R. Rubbmark, M. M. Kash, M. G. Littman, and D. Kleppner. Dynamical Effects at Avoided Level Crossing: A Study of the Landau-Zener Effect using Rydberg Atoms. Physical Review A, 23, 3107 ((1981)

[26] W. Petrich, M. H. Anderson, J. R. Ensher, and E. A. Cornell, Stable, Tightly Confining Magnetic Trap for Evaporative Cooling of Neutral Atoms, Phys. Rev. Lett. 74, 3352 (1995)

[27] T. Bergeman, G. Erez, and H. Metcalf, Magnetostatic Trapping Fields for Neutral Atoms, Phys. Rev. A, 35, 1535 (1987)

[28] V. Bagnato, D.E. Pritchard, and. Kleppner, Bose-Einstein Condensation in an External Potential, Phys. Rev. A 35, 4354 (1987)

[29] O. J. Luiten, M. W. Reynolds, and J. T. M. Walraven. Kinetic Theory of the Evaporative Cooling of a Trapped Gas. Physical Review A 53, 381, 1996

[30] W. Ketterle and N.J. van Druten, Evaporative Cooling of Trapped Atoms, Adv. At. Mol. Opt. Phys. 37, 181 (1996)

[31] C. R. Monroe, E. A. Cornell, C. A. Sackett, C. J. Myatt and C. E. Wieman, Measurement of Cs-Cs Elastic Scattering at T = 30 μK, Phys. Rev. Lett. 70, 414 (1993)

[32] P. S. Julienne, F. H. Mies, E. Tiesinga, and C. J. Williams, Collisional Stability of Double Bose Condensates, Phys. Rev. Lett. 78, 1880 (1997)

[33] E. L. Surkov,[1] J. T. M. Walraven,[2] and G. V. Shlyapnikov, Collisionless Motion and Evaporative Cooling of Atoms in Magnetic Traps, Phys. Rev. A 53, 3403 - 3408 (1996)

[34] K. Dieckmann. Bose-Einstein Condensation with High Atom Number in a Deep Magnetic Trap. Ph.D. thesis, University of Amsterdam (2001)

[35] B. Desruelle, V. Boyer, S. G. Murdoch, G. Delannoy, P. Bouyer, and A. Aspect. Interrupted Evaporative Cooling of 87Rb Atoms Trapped in a High Magnetic Field. Phys. Rev. A, 60, 1759 (1999)

[36] E. A. Burt, R. W. Ghrist, C. J. Myatt, M. J. Holland, E. A. Cornell, and C. E. Wieman, Coherence, Correlations, and Collisions: What One Learns about Bose-Einstein Condensates from Their Decay, Phys. Rev. Lett. 79, 337 (1997)

[37] G. Baym and C.J. Pethick, Ground-State Properties of Magnetically Trapped Bose-Condensed Rubidium Gas, Phys. Rev. Lett. 76, 6 (1996)

[38] Y. Castin and R. Dum. Bose-Einstein Condensation in Time Dependent Traps, Phys. Rev. Lett. 77, 5315 (1996)

[39] P. W. Milonni and J. Eberly, Lasers, John Wiley & Sons Inc., (1988)

[40] A. Siegman, Lasers, University Science Books, (1986)

[41] D.Z. Anderson, Alignment of Resonant Optical Cavities, Applied Optics, Vol. 23, Issue 17, pp. 2944 (1984)

[42] E.M. Purcell, Spontaneous Emission Probabilities at Radio Frequencies, Phys. Rev. vol. 69, pp. 681 (1946)

[43] M. Scully and M. Suhail Zubairy, Quantum Optics, Cambridge University Press, (1997)

[44] J. Gérad and Bruno Gayral, Strong Purcell Effect for InAs Quantum Boxes in Three-Dimensional Solid-State Microcavities, Journal of Lightwave Technology, Vol. 17, No. 11, (1999)

[45] The path length of a resonant photon inside the experimental cavity (around 5 km) is much longer than any relevant distances outside of the cavity in the experimental set-up. Therefore one can simply assume the energy of the vacuum mode is completely inside the resonator.

[46] V. Vuletić, H.W. Chan and A.T. Black, Three-dimensional Cavity Doppler Cooling and Cavity Sideband Cooling by Coherent Scattering, Phys. Rev. A, Vol. 64, 033405 (2001)

[47] The free space scattering rate is assumed to be unchanged by the cavity. This is a good approximation when the solid angle by the two mirror surfaces from the position of the focus is small compared to 4π.

[48] R. Grimm, M. Weidemüller und Y.B. Ovchinnikov. Optical Dipole Traps for Neutral Atoms. Adv. At. Mol. Opt. Phys., 42:95, (2000)

[49] E. Merzbacher, Quantum Mechanics, John Wiley & Sons Inc. (1961)

[50] H.J. Metcalf and P. van der Straten, Laser cooling and Trapping, Springer-Verlag New York inc., (1999)

[51] P. Domokos and H. Ritsch, Collective Cooling and Self-Organization of Atoms in a Cavity, Phys. Rev. Lett. 89, 253003 (2002)

[52] R.H. Dicke, Coherence in Spontaneous Radiation process, Phys. Rev. 93, 99 (1954)

[53] A.T. Black, H.W. Chan and V. Vuletić, Observation of Collective Friction Forces due to Spatial Self-Organization of Atoms: From Rayleigh to Bragg Scattering, Phys. Rev. Lett. 99, 203001 (2003)

[54] P. Domokos, P. Horak and H. Ritsch, Semiclassical Theory of Cavity-assisted Atom Cooling, J. Phys. B. At. Mol. Phys. 34 187-198 (2001)

[55] S. Zippilli, G. Morigi and H. Ritsch, Suppression of Bragg Scattering by Collective Interference of Spatially Ordered Atoms with a High-Q Cavity Mode, Phys. Rev. Lett. 93, 123002 (2004)

[56] P. Domokos and H. Ritsch, Mechanical Effects of Light in Optical Resonators, J. Opt. Soc. Am. B.,Vol. 20, No. 5, 1098 (2003)

[57] J.K. Asbóth, P. Domokos, H. Ritsch and A. Vukics, Self-organization of Atoms in a Cavity Field: Threshold, Bistability, and Scaling Laws, Phys. Rev. A 72, 053417 (2005)

[58] S. Zippilli, J.K. Asbóth, G. Morigi and H. Ritsch, Forces and Spatial Ordering of Driven Atoms in a Resonator in the Regime of Fluorescence Suprression, Appl. Phys. B, 79, 969 (2004)

[59] D.J. Wineland and W. M. Itano, Laser Cooling of Atoms, Phys. Rev. A, Vol. 20, 1521 (1979)

[60] A.L. Wells and R. J. Cook, Simple Theory of Sideband Cooling, Phys. Rev. A, Vol. 41, 3916 (1990)

[61] Th. Elsässer, B. Nagorny, and A. Hemmerich, Collective Sideband Cooling in an Optical Ring Cavity, Phys. Rev. A. 67, 051401 (2003)

[62] M.G. Raizen, R.J. Thomsen, R.J. Brecha, H.J. Kimble, and H.J. Carmichael, Normal-Mode Splitting and Linewidth Averaging for Two-State Atoms in an Optical Cavity, Phys. Rev. Lett. 63, 240 (1989)

[63] P. Maunz, T. Puppe, I. Schuster, N. Synassen, P.W.H. Pinkse and G. Rempe, Normal-Mode Spectroscopy of a Single-Bound-Atom-Cavity System, Phys. Rev. Lett. 94, 033002 (2005)

[64] M. Gangl and H.Ritsch, Cold Atoms in a High-Q Ring Cavity, Phys. Rev. A 61, 043405 (2000)

[65] T. Elsässer, Optical Bistability and Collective Behaviour of Atoms Trapped in a High Finesse Cavity, PhD thesis, Hamburg University (2004)

[66] T. W. Hänsch, A. L. Schawlow, and G. W. Series. The Spectrum of Atomic Hydrogen. Scientific American, 240:72 (1979)

[67] W. Demtröder. Laserspektroskopi*e*. Springer Verlag, Heidelberg (1991)

[68] E. Black, An Introduction to Pound-Drever-Hall Laser Frequency Stabilization, Am. J. Phys. 69, 79 (2001)

[69] Application note 7, Rev B, 2001 New focus.

[70] A. Schoof , Entwicklung eines Ultrastabilen Laserdiodensystems bei 657 nm für die Metrologie, Master Thesis, Hamburg University (2001)

[71] B. Nagorny, Dynamik kalter Atome in der Stehwellendipolfalle eines Ringresonators hoher Güte, PhD thesis, Hamburg University (2003)

[72] A. Schoof, J. Grünert, S. Ritter, and A. Hemmerich, Reducing the Linewidth of a Diode Laser below 30 Hz by Stabilization to a Reference Cavity with a Finesse above 10^5, Optics Letters, Vol. 26 Issue 20, pp.1562-1564 (2001)

[73] K. Dieckmann, R. J. C. Spreeuw, M. Weidemüller and J. T. M. Walraven, Two-Dimensional Magneto-optical Trap as a Source of Slow Atoms, Physical Review *A*, 58, 3891 (1998)

[74] C.G. Townsend, N. H. Edwards, C.J. Cooper, K. P. Zetie, C. J. Foot., A. M. Steane, P. Szriftgiser, H. Perrin, and J. Dalibard, Phase-space Density in the Magneto-optical Trap, Phys. Rev. A 52, 1423 (1995)

[75] W. Petrich, M. H. Anderson, J. R. Ensher, and E. A. Cornell, Behavior of Atoms in a Compressed Magneto-Optical Trap, J. Opt. Soc. Am. B 11, 1332 (1994)

[76] H. J. Lewandowski, D. M. Harber, D. L. Whitaker, and E. A. Cornell, Simplified System for Creating a Bose-Einstein Condensate, Journal of low temperature physics, vol. 132, n°5-6, pp. 309 (2003)

[77] Greiner, M., I. Bloch, T.W. Hänsch und T. Esslinger, Magnetic transport of Trapped Cold Atoms over a Large Distance. Physical Review A, 63(3): p. 031401/1, (2001)

[78] T. Esslinger, I. Bloch, and T.W. Hänsch Bose-Einstein Condensation in a Quadrupole-Ioffe-Configuration Trap, Phys. Rev. A 58, 2664 (1998)

[79] T.A. Savard, K.M. O'Hara, and J.E. Thomas, Laser-noise-induced Heating in Far-off Resonance Optical Traps, Phys. Rev. *A*, 56 R1095 (1997)

[80] W. Ketterle, D.S. Durfee, and D.M. Stamper-Kurn, Making, Probing and Understanding Bose-Einstein Condensates, arXiv:cond-mat/9904034v2

[81] T. Bergeman, G. Erez and H. J. Metcalf, Magnetostatic Trapping Fields for Neutral Atoms, Phys. Rev. A 35, 1535 (1987)

[82] To calculate the magnetic field configuration for the coil set-up the computer program Biotsavart from Ripplon Software Inc. was used.

[83] E. Hecht, Optics 3rd edition, Addison Weslay Longman Inc. (1998)

[84] P.W. Milonni and J.H. Eberly, Lasers, John Wiley and sons, New York (1988)

[85] M.A. Joffe, W. Ketterle, A. Martin, and D.E. Pritchard, Transverse Cooling and Deflection of an Atomic Beam Inside a Zeeman Slower, J. Opt. Soc. Am. B, 10 2257 (1993)

[86] J. Klinner, M. Lindholdt, B. Nagorny, and A. Hemmerich, Normal Mode Splitting and Mechanical Effects of an Optical Lattice in a Ring Cavity, Phys. Rev. Lett. 96, 023002 (2006) Phys. Rev. Lett. 96, 023002 (2006)

[87] H. Richter, Phasenstabiles Diodenlasersystem zur Dunkelresonanzspektroskopie an Rb_{85}, Master Thesis, Hamburg University, (2002)

[88] A. Wickenbrock, Aufbau eines Ultrastabilen Hochfinesseresonators, Master Thesis, Hamburg University (2006)

[89] E.A. Donley, T.P. Heavner, F. Levi, M.O. Tataw, and S.R. Jefferts, Double-pass Acousto-optic Modulator System, Review of Scientific Instruments 76, 063112 (2005)

[90] K. Jentson, Master thesis, Hamburg University (2005)

[91] H. Schmaljohann, Spindynamik in Bose-Einstein Kondensaten, PhD thesis, Hamburg University (2004)

[92] I.B. Mekhov, C. Maschler and H.Ritsch, Light Scattering from Ultracold Atoms in Optical Lattices as an Optical Probe of Quantum Statistics, Phys. Rev. A, 76 053618 (2007)

[93] H. Zoubi and H. Ritsch, Exciton-Polariton Scattering as Scattering of Detects in Cold atom Lattices, New J. of Physics 10, 023001 (2008)

[94] L. Ricci, M. Weidemüller, T. Esslinger, A. Hemmerich, C. Zimmermann, V. Vuletic, W. König and T.W. Hänsch, A Compact Grating-stabilized Diode Laser System for Atomic Physics, Opt. Comm. 117, 541 (1995)

[95] J. J. Maki, N. S. Campbell, C. M. Grande, R. P. Knorpp and D. H. McIntyre, Stabilized Diode-laser System with Grating Feedback and Frequency-offset Locking; Opt. Comm. 102, 251 (1993)

[96] K. B. MacAdam, A. Steinbach and C. Wieman, A Narrow-band Tunable Diode Laser System with Grating Feedback, and a Saturated Absorption Spectrometer for Cs and Rb, Am. J. Phys.60, 1098 (1992)

[97] Scientific Lasers 2008/09 TOPTICA Photonics AG, Lochhamer Schlag 19, 82166 Graefelfing Munich

[98] D. A. Steck, "Rubidium 87 D Line Data," available online at http://steck.us/alkalidata (revision 2.1.1, 30 April 2009).